

Politecnico di Torino

Department of Mechanical and Aerospace Engineering

Master of Science in Mechanical Engineering



FCA

FIAT CHRYSLER AUTOMOBILES

Design of a Maraging steel steering knuckle for Additive Manufacturing

Supervisor: *Prof. Giovanni Belingardi*

Co-supervisors: *Prof. Mohamed A. Elbestawi*

Eng. Carlo Carcioffi

Eng. Roberta Sampieri

Candidate:

Gabriele Borsato

Academic Year 2019-2020

Contents

Contents.....	2
List of figures.....	4
1 Introduction.....	7
2 Steering knuckle	9
2.1 Literature review	14
3 Additive Manufacturing.....	16
3.1 General steps for Additive manufacturing process	19
3.2 AM advantages and disadvantages.....	24
3.3 Additive manufacturing for metal parts	28
3.3.1 Laser Direct Energy Deposition.....	28
3.3.2 Selective Laser Melting	30
3.3.3 Electron Beam Melting	35
4 Material	38
4.1 Verification of the tensile resistance of Maraging steel	42
5 Topology optimization.....	47
5.1 Types of optimization.....	48
5.2 Mathematical definition of the problem	49
5.2.1 Penalization.....	51
5.2.2 Homogenization method	52
5.2.3 SIMP method	53
5.2.4 Compliance problem.....	56
5.2.5 Stress-constrained problem.....	57
5.3 Softwares.....	59
5.3.1 Popular structural optimization programmes	59
5.3.2 Abaqus	60
6 Re-design of the suspension mounting	63
6.1 Definition of the design space.....	63
6.2 Adjusting the part.....	68

6.3	Material properties	70
6.4	Assembly	70
6.5	Interactions	71
6.6	Steps	74
6.7	Load	77
6.8	Mesh.....	79
6.9	Preliminary FEA	81
6.10	Topology optimization	88
6.11	Job definition.....	92
6.12	Result of the optimization.....	94
6.13	Verification of the optimized part.....	98
6.14	Printing operation	121
7	Conclusions.....	122
8	References	124

List of figures

Figure 4-1 Steering knuckle of a Maserati Ghibli [4]	9
Figure 4-2 Common wheel hub assembly [7]	10
Figure 4-3 Steering knuckle of a McPherson suspension [10].....	11
Figure 4-4 Alfa Romeo Giulia front suspension components [11].....	12
Figure 5-1	16
Figure 5-2 Google researches of Additive Manufacturing vs Rapid Prototyping [25].....	17
Figure 5-3 Additive manufacturing – Layers [26]	17
Figure 5-4 Graph: AM revenues by industrial sector (Wholers 2017) [32]	18
Figure 5-5 Additive manufacturing steps [33]	19
Figure 5-6 Triangular facets of the STL file [34].....	20
Figure 5-7 Dependence of stair-stepping effect on part orientation [37].....	21
Figure 5-8 Particular geometries that requires a support structure (in orange) [39]	22
Figure 5-9 Complexity vs costs of AM and traditional technologies [40].....	25
Figure 5-10 Comparison of assembly: Conventional vs AM design [41]	25
Figure 5-11 Laser Direct Energy Deposition scheme [43].....	29
Figure 5-12 Powder Bed Fusion process [43]	30
Figure 5-13 Molten area in SLM [45]	32
Figure 5-14 EOS: metal powders list [38]	34
Figure 5-15 Schematic structure of an Electron Beam Melting machine [51]	35
Figure 6-1 Engineering stress-strain graph of heat treated (red) and as-build (blue) MS1 specimens [56]	41
Figure 6-2 Round tension test specimen dimensions [64]	43
Figure 6-3 EOS INT M280 3D printer [65]	44
Figure 6-4 Tensile specimens on the building base	45
Figure 6-5 Tensile specimens.....	46
Figure 7-1 Comparing the application of sizing (a), shape (b) and topology (c) optimization on a struss structure [71].....	48
Figure 7-2 Graphical representation of Pareto optimality in a Multi-objective problem	50
Figure 7-3 Before and after topology optimization [69]	51
Figure 7-4 Density between the value 0 and 1	52
Figure 7-5 Homogenization approach: Microstructures elements as perforated squares (a) or layered rectangles (b)	52
Figure 7-6 SIMP interpolation scheme	54
Figure 7-7 Clamped beam topology optimization: a) model; b) Result with mesh size 1; c) Result with mesh size 0,5; d) Result with mesh size 0.25;	55
Figure 7-8 Abaqus/CAE workspace components.....	62
Figure 7-9 Abaqus modules	62
Figure 8-1 Design space and non-design space	64
Figure 8-2 Brake caliper	65

Figure 8-3 Non-design part (16): bearing housing and ABS sensor housing	65
Figure 8-4 Different views of the space design	67
Figure 8-5 Modified space-design.....	69
Figure 8-6 "Edit constraint" window	71
Figure 8-7 Interactions between reference nodes and non-design surfaces.....	72
Figure 8-8 Interaction node 16	73
Figure 8-9 Interaction node 16bis with node 1 and 2 (Bracking couple)	74
Figure 8-10 "Create a new step" window	75
Figure 8-11 How to create a load on Abaqus	78
Figure 8-12 Boundary condition definition.....	78
Figure 8-13 "Mesh Controls" window.....	79
Figure 8-14 Part seeds options	80
Figure 8-15 Meshed component with some edges' refinement	81
Figure 8-16 Stress on design space: Braking couple	83
Figure 8-17 Stress on design space: Cornering 1	84
Figure 8-18 Stress on design space: Braking 2.....	85
Figure 8-19 Stress on design space: ax + ay 1.....	86
Figure 8-20 Stress on design space: Steering buckling.....	87
Figure 8-21 Non-design cells excluded from the topology optimization	88
Figure 8-22 List of Design variables available for the General optimization approach.....	89
Figure 8-23 Advanced options for topology optimization.....	90
Figure 8-24 Density options for topology optimization.....	90
Figure 8-25 "Optimization Process Manager" window	92
Figure 8-26 Evolution of the optimization (chart)	93
Figure 8-27 Cantilever structures of a discard optimization	94
Figure 8-28 Optimization result ISO 0,3.....	95
Figure 8-29 Extraction option on Abaqus	96
Figure 8-30 Optimized component.....	97
Figure 8-31 Mesh of the optimized component.....	98
Figure 8-32 Stress results: Stabilisation #2	100
Figure 8-33 Stress results: Vertical 1	101
Figure 8-34 Stress results: Vertical 2	102
Figure 8-35 Stress results: Cornering 1	103
Figure 8-36 Stress results: Cornering 2	104
Figure 8-37 Stress results: Cornering 3	105
Figure 8-38 Stress results: Cornering 4	106
Figure 8-39 Stress results: Bump	107
Figure 8-40 Stress results: Rebump	108
Figure 8-41 Stress results: Acceleration	109
Figure 8-42 Stress results: Braking 1.....	110
Figure 8-43 Stress results: Braking 2.....	111

Figure 8-44 Stress results: ax+ay 1.....	112
Figure 8-45 Stress results: ax+ay 2.....	113
Figure 8-46 Stress results: ax+ay 3	114
Figure 8-47 Stress results: ax+ay 4.....	115
Figure 8-48 Stress results: ax+ay 5.....	116
Figure 8-49 Stress results: ax+ay 6.....	117
Figure 8-50 Stress results: ax+ay 6.....	118
Figure 8-51 Stress results: Buckling steering	119
Figure 8-52 Stress results: Braking torque.....	120
Figure 8-53 Support removal process on the optimized component	121

1 Introduction

This thesis work is the product of a project in collaboration between the Politecnico di Torino, the McMaster University in Hamilton (Canada) and FCA (Fiat Chrysler Automobiles), combining the academic research knowledge with the industrial technological development. The project involved the first two months at the FCA Product Development EMEA AM Centre following six months, from September 2019 at the McMaster University, with the research team called Additive Manufacturing Group (AMG).

The purpose of this work is to analyze and redesign the steering knuckle of a new Maserati sport-car, in order to create a new component with the same performances and resistance of the original one, but with a lower weight, by manufacturing the component with the Additive Manufacturing technology and by exploiting the potential of Topology Optimization.

The research of always higher performances in the automotive field and the concurrent necessity of reduction of the emission, is forcing the car-industry to move forward a reduction of weight of the vehicles. The steering knuckle is a relative heavy component and a reduction of its weight, would guarantee not only a reduction of the total car's weight, but in particular a lightening of the unsprung masses of the vehicle, improving the comfort and for a high-performance automobile also the handling and the maneuverability.

Consequently, the researchers are looking for new and more efficient ways of producing the components, which is why the traditional productive processes in some market niches are being progressively replaced by breakthrough techniques. One of the most flourishing technology is the Additive Manufacturing, which allow to print complex shapes (that cannot be created with any other manufacturing methods) with a layer after by addition of material. Nowadays it is possible to print not only prototypes, but also end-usable components, made in several materials including metals. The Direct Metal Laser Sintering is the technology, developed by EOS, which has been used to "print" this metallic large size component.

Differently from the original steering knuckle, which was made with an aluminum alloy, the redesigned component has been fabricated with Maraging steel, which is a high strength steel that despite having three times the density of aluminum, it has almost the triple of the yield strength and definitely a lower cost. It has been chosen to use this particular metal, to verify how far can the AM technology can go, even if a heavier metal is used. Some samples have been produced to verify the mechanical properties of the material and to compare the results to previous researches.

In order to achieve the best possible result by the 3D printing technology, it is necessary to create the lightest possible design for the new component. To do so, it has been taken advantage of the Topology Optimization methods, which consent to optimize to the maximum the geometry of a part, verifying in which area it is possible to remove material and in which area it is necessary to

keep the material so that the component is able to sustain the applied loads. The part has been tested with a wide range of loading conditions, in order to guarantee the correct functioning and safety in all the possible most demanding and critical vehicle situations. Are included a set of fatigue loading conditions, which interest the effect of bumps, braking, and accelerations in both x-y directions. Moreover, it has been studied also the effect of the braking torque caused by the braking caliper and the buckling due to the steering.

In the thesis the most common algorithms for Topology Optimization are presented, with a deeper analysis of the algorithm used for the project with the software Abaqus Tosca. Moreover, considering the reduced number of published papers that treats the topology optimization package of Abaqus Tosca, a detailed description of the optimal settings for the Topology Optimisation and Finite Elements Analysis, while using that particular software, is presented.

2 Steering knuckle

In the last years, due to always more strict regulations, the reduction of the emissions of the vehicles has become one of the main objectives in the automotive industry [1]. In order to reach the prescribed targets, the automotive industry is continuously pushing forward the improvements for internal combustion engines, or moving towards different propulsion systems (electric) [2].

It has been observed that a key factor in the fuel consumption of a vehicle is its weight [3], so even if the weight of the vehicles is generally increasing due to the highest number of accessories and safety equipment, a higher fuel efficiency can be easily achieved by reducing the weight of the car's components.

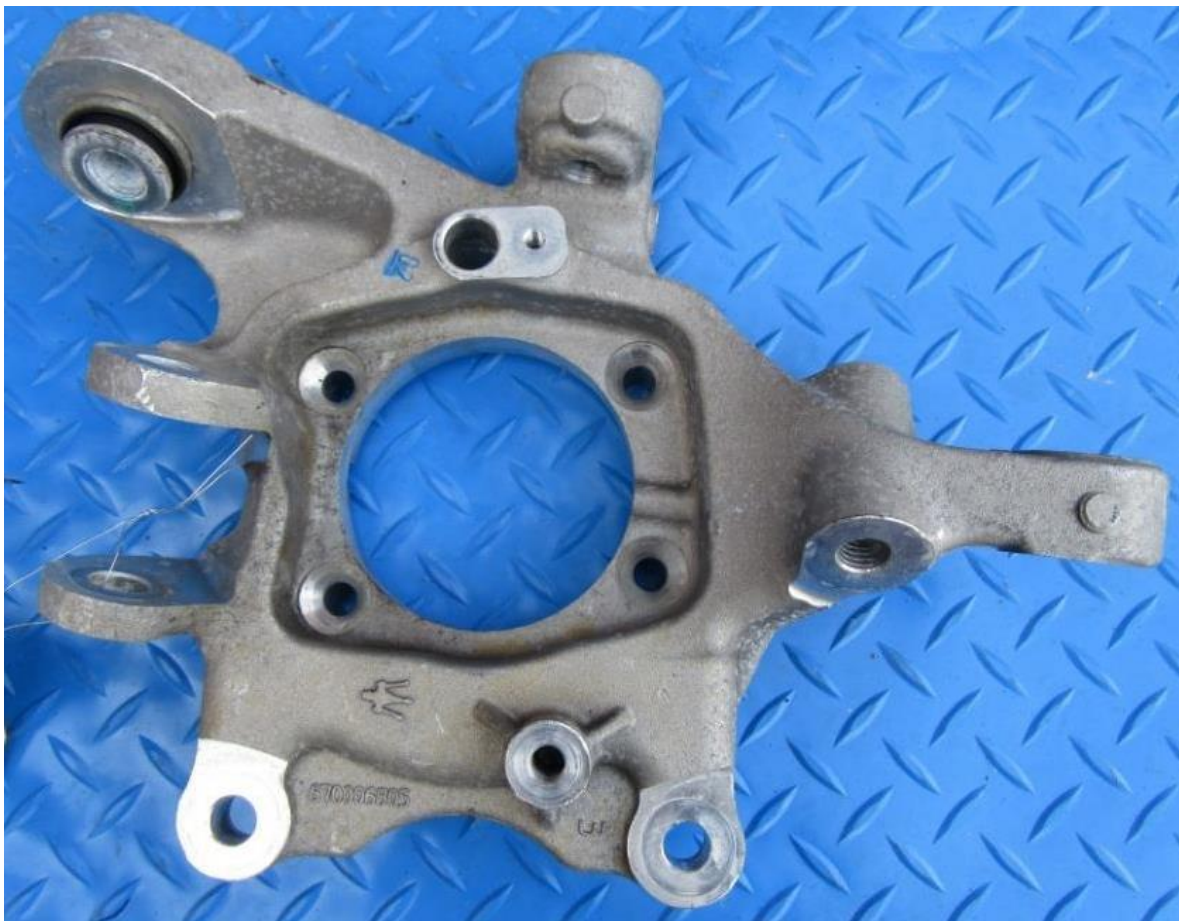


Figure 2-1 Steering knuckle of a Maserati Ghibli [4]

The steering knuckle is a fundamental component of a vehicle, being the connecting element of the suspension, steering and braking systems. This joint, allows to steer the front wheels of the vehicle thanks to its connection with the steering tie rod. The tie rod transmits the force coming from the steering gears, which can have different designs, based for example on the rack and

pinion mechanism, recirculating ball mechanism (with screw and nuts) or also the worm and sector mechanism.

Depending on the suspension system and its application, the steering knuckle can have really different shapes and dimensions. In general, they can be divided into two different categories in function of the wheel's assembly. One has the hub for the wheel's bearing, while the other comes with a spindle [5]. For this thesis work, the steering knuckle has the first configuration.

Similarly to the component shown in Figure 2-1, in the centre of the component the housing for the wheel hub assembly is present, which is assembled to the steering knuckle by means of a set of bolts. Within the wheel hub a set of sensors (ABS and traction control), seals and a 3rd generation bearing, which allows a rotation of the wheel with low frictions [6], are assembled. The wheel and the disk brake rotor are directly connected to this component with a set of threaded studs (the black ones in Figure 2-2).



Figure 2-2 Common wheel hub assembly [7]

The steering knuckle is an important part of the braking system also because it holds the brake caliper, normally connected with two bolts. The brake caliper pushes the brake friction pads on the disk brake rotor, thus reducing the rotational speed of the wheel. When braking, the steering knuckle is subjected to a torque, which is equal to the braking force multiplied by the effective radius that connects the caliper with the wheel center.

In addition to the tie rod, wheel hub and braking caliper, the steering knuckle is connected also to the suspension arms, which connect the knuckle with the rest of the vehicle's body. The suspension system has not only the function of linking the chassis with the wheel, but also to guide the wheel movements with respect to the vehicle body, according to the desired

suspension kinematics, and to control the related forces. It has great importance in ensuring stability of the vehicle while guaranteeing a certain comfort for the passengers.

In first half of the 20th century, the cars suspensions were produced with simple models, based on rigid axle that connected the two front wheels (and also the rear wheels) with a beam, with the motion of one affecting the other one. This design for the front, because of the presence of the steering system, had several problems related to bump steer, roll steer and spring wind-up. Due to the continuous growth of the automobile speed, these issues became always more challenging. The use of independent front suspension has been the solution, which allowed a higher comfort, thanks to the use of less rigid springs while simultaneously providing a much accurate steering [8]. Nowadays almost all the front suspension systems are independent.

The suspension constraints all the motions of the wheel, except for its vertical motion in respect of the vehicle body and a rotation around the spindle axis. Further due to the steering system, a deflection of the steering knuckle around the suspension steering axes is also allowed, whose maximum rotation angle can vary with the vehicle model [9]. The only degree of freedom that the wheel has in respect of the knuckle is the rotation along its spin axis, so also for the knuckle the only permitted motions are the steering rotation and a vertical displacement in respect of the car body. Thus, the suspension restrains the motion of the knuckle in five directions. This restriction can be obtained with several methods and in the history of the automotive a large variety of designs has been implemented.

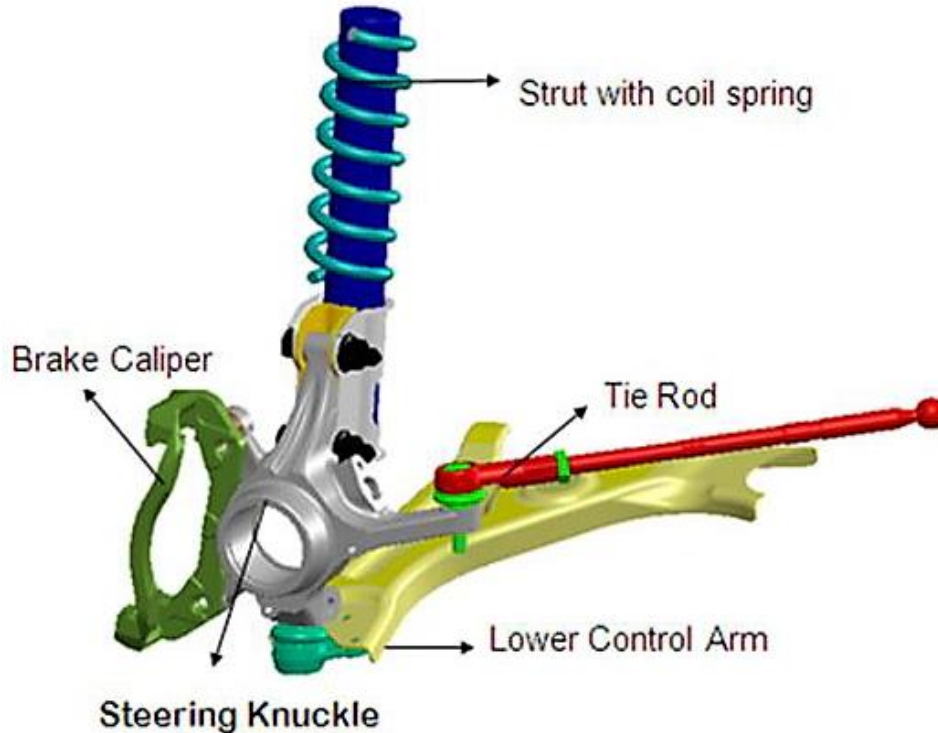


Figure 2-3 Steering knuckle of a McPherson suspension [10]

Nowadays, the most adopted suspension model for race car is the double wishbone suspension, which consists of two A-arms and the tie rod for steering. Each A-arm constrains 2 degrees of freedom and the tie rod just one, leaving only one DOF to the knuckle. The spring and the damper are commonly connected to the upper wishbone. Another quite common model is the MacPherson Structure suspension (that can be seen in Figure 2-3), which is made by the MacPherson Structure itself that restrains two dofs, an A-arm and the tie rod [9].

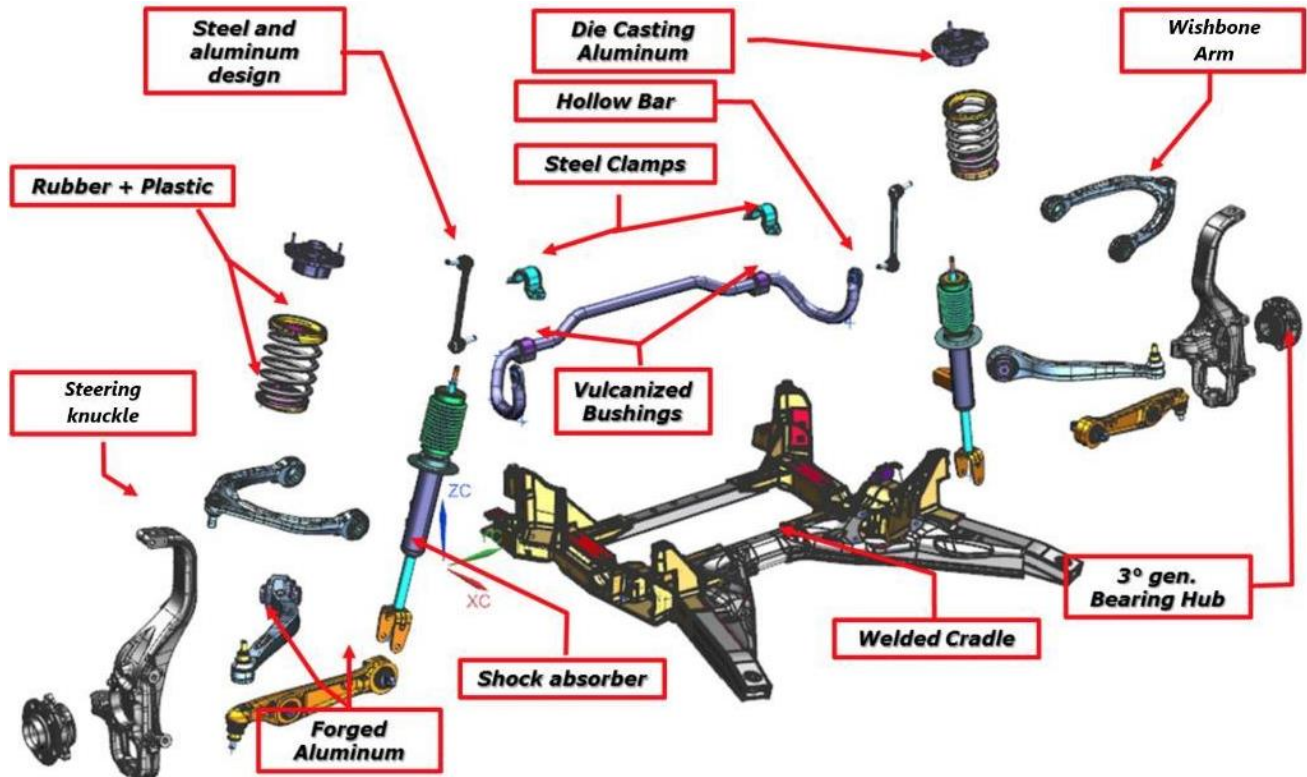


Figure 2-4 Alfa Romeo Giulia front suspension components [11]

The steering knuckle that has been redesigned for this thesis work, is part of a different model of suspension system, having three links, instead of two, as in the models previously presented. The suspensions that present more than two links are generally defined multilink suspensions. As the name suggests, the steering knuckle is connected by some arms, whose maximum number is normally four (five links if it is included also the tie rod). These longitudinal arms can have different lengths and orientation and allow to connect the steering knuckle to different areas of the car's body. In this system, the wishbone arm is divided into two different simpler links [8]. With the five-link suspension, each connecting arm, restrain one degree of freedom.

In the thesis case study, the steering knuckle has four connecting elements (including the steering arm link). The upper linkage is still connected to an A-arm wishbone, which restrains two dofs, while the lower wishbone is substituted by two single arms, each one restraining one dof.

Each arm is connected with the steering knuckle with a ball joint, which has a similar shape and functioning of the human hip joint. The ball joint forces the arm to be subjected to tension-compression stresses, rather than bending [12].

The advantages of this multilink suspension (compared with the other two models presented) are the flexibility and lightness, which allow higher comfort and handling. On the other hand, it is more expensive, due to the higher complexity and larger number of components.

The steering knuckle, being a structural component, is subjected to really high forces, caused by accelerations and decelerations, braking torques, bumps and steering [5]. Being subjected to time-varying loading conditions, its most common failure is generally caused by fatigue [13]. In several cases, it has been observed that the most critical area, where the rupture is more likely to occur, is on the connecting element of the tie rod (which is commonly coupled with a spherical joint, like the other arms). The failure of the knuckle part that connects the tie rod, can be caused both by a fatigue rupture or by a buckling effect. In order to guarantee the safety of the vehicle's users it is important that this component does not fail. A failure may cause a loss of the control of the vehicle, causing a car accident.

When a race car is being designed, it is not sufficient to consider the effect of accelerations, brake bumps and steering on the suspension system but also the effect of lateral forces must be included. It results that considering the high performances requested to the vehicle, it is important to verify the resistance of the components also to lateral accelerations. Considering the combination of the lateral and longitudinal accelerations, it is common to define a "*g-g*" diagram. This diagram is given by the records of the tangential and normal accelerations of the accelerometers placed on a car for the drive tests [9]. In the diagram both positive and negative accelerations are considered, so also the decelerations must be verified. Due to the combination of the two different accelerations, higher loading conditions are reached, so the suspension system must be able to resist to the generated stress. It is not possible to consider all the possible combination of accelerations, so it is necessary to select the most demanding between themselves, providing the largest possible "*g-g*" area of maneuvering for the vehicle.

A reduction in the weight of the steering knuckle is convenient not only for lowering the consumption, but also for the overall handling of the car. When analyzing the vehicle dynamics, it is convenient to divide its total mass into sprung mass and unsprung mass. The sprung mass includes all the part of the vehicle that are held up by the suspensions, while the unsprung mass embrace all the parts underneath the suspensions, like the wheels and their hubs, brake calipers and rotor disks, and all the suspension's components that are not directly constrained on the chassis [14]. The steering knuckle is part of this last group, and generally (depending also on the suspension design), it has a significant mass.

The ratio between the sprung mass and the unsprung mass is commonly computed to verify the comfort level of a vehicle. If this value is over 5, the vehicle can be considered comfortable also on a rough road [15]. This parameter is not really useful for race cars, where the main purpose is not to guarantee a relaxing and smooth ride but a rapid and precise maneuverability. The

unsprung mass is generally around only the 10% of the total mass, but its influence especially for sports car is not negligible [16]. The lighter are the unsprung masses, the quicker will be their response to a variation in the road surface [17]. An optimal grip condition of the tyres with the pavement allows to transfer efficiently the torque generated and preventing any wheel spin. Another important advantage that this weight reduction provides is the lower stress on the suspension connection with the chassis [15].

In order to reduce the weight of the unsprung masses, it is possible to use lighter alloys and modify the geometry of the components by reducing their mass, without decreasing the resistance, so that the same performance and safety level can be guaranteed. To do so, in this thesis project has been used the topology optimization tool, which allows to distribute the material only where it is necessary, (as described in Chapter 5) and manufacturing the optimized component with the additive manufacturing technology, which allows to print really complex shapes, characterized by lower weight.

2.1 Literature review

As previously suggested, being the steering knuckle a relative heavy component, several other researches had the objective of reducing the weight of this component. The vast majority of these researches has been certainly done by automotive companies, but their discoveries and advancements are commonly not published. Consequently, in this paragraph all the mentioned researches come from the academic field.

Dumbre P. et al. [5] used Hypermesh Optistruct to make a topology optimization of a steering knuckle, with a single loading condition. The weight of the component, made in ductile iron, has been reduced of the 11%, while keeping the stress under the limits. The new design has been validated performing a second a linear static analysis and a mode analysis.

Pujari D. et al. [18] have shown a procedure to define the reduction of volume of a steering knuckle. Their focus was on the preliminary FEA, which should precede the topology optimization to verify the loading condition on the pre-existing part.

Srivastava S. et al. [19] did a similar study using the software Ansys and analysing different loading conditions, combined in one single load case. They made both a preliminary FEA and a topology optimization analysis that produced a reduction of weight of 19%, while keeping the same material of the original part (SG iron).

Sivananth V. et al. [20] analyzed the fatigue life of a McPherson steering knuckle considering three different loading conditions. The steering arm region of the knuckle, being the region of the fatigue failure, has been optimized with three different materials ductile iron, LM 6 aluminum alloy and metal matrix composites (MMC) to verify which material guarantees the longer fatigue life. They observed that using the titanium carbide-reinforced composite material, it is possible to have a longer life of the component, with a weight reduction of 60% in respect of the iron component.

Tagade P. [21] made differently from other cited studies, a shape optimization rather than a topology optimization. Shape optimization allowed to obtain a refined design of the steering

knuckle, reducing the weight with constraints on the stress. Not only the shape of the part has been modified, but also the material (from cast iron to aluminium 2011 t-3 alloy). This allowed a weight reduction of 67% (mainly due to the variation of material). Despite the lower stress resistance of aluminum alloy, the stresses are under the prescribed limit also for the optimized knuckle.

Differently from most of previous researches, in the present project the design space has been taken as large as possible, considering all the different external boundary conditions that limit this volume. Due to this, and the higher complexity of the part (not to mention the larger dimension), the number of finite elements for the optimization is rather high. This cause principally a longer time for the execution of the topology optimization. Another contributing factor to this long computational time, is the high number of case studies that must be considered for the simulations.

All previously mentioned researches did not consider additive manufacturing as an alternative for the construction of the optimized component. Due to this, the redesigns were not so different from the original one, and the highest variation in the weight is commonly due to the use of a lighter material. On the other hand, for this project it has been chosen to manufacture the component with Selective Laser Melting (SLM) technology which guarantees greater freedom in terms of manufacturing constraints, which commonly represent an important obstacle in the alteration of a component geometry for the traditional manufacturing techniques.

A similar project to this thesis work has been developed by Sai Nithin Reddy K. et al. [22] who redesigned a steering knuckle made in titanium alloy (Ti-6Al-4V) for a SAE Formula Student vehicle, which has been printed with DMLS technology. Differently from other researches, they took a large design space (a right parallelepiped) where the voids and non-design volumes were excluded by the optimization. The component has been designed considering 4 different loading conditions: rear and forward braking, and inside and outside cornering. A first topology optimization has been done with a considerable coarse mesh, using the software TopOpt, which is not commonly used for complex industrial researches, but for simpler academic projects. The result of this optimization has been used to redesign the component on SolidWorks. Starting from this CAD model, a second topology optimization has been done, by using the more advanced OptiStruct software, with the objective of minimizing the compliance of the structure with a reduction of volume of 20% as constraint. The re-optimized component has been reconstructed on the CAD software with the application of Design for Additive Manufacturing (DfAM) rules that allowed to decrease the material used for supports (reduced of the 91% in respect of the original component). This considerable reduction in the use of support structures, allowed a contraction of the building costs, but at the same time the volume of the component has been increased.

3 Additive Manufacturing

Additive Manufacturing (AM) is a generic term, used to identify several fabricating technics that have in common the construction of a component by an addition of material layer by layer. Popularly known even as *3D Printing*, this latter in reality has some differences with AM because of its field of application: while 3D Printing refers to a domestic or researching application, AM is more related to the industry, so to the production for commercialization.

AM technology is facing a tremendous and continuous evolution, and it is thought that in the future it may completely revolutionize the industrial processes [23].

In the past, this manufacturing method was defined as *Rapid Prototyping (RP)* which is the process of rapidly create a pre-series component during the development of a project, before starting its commercialization. The prototype allows to verify the conceptual and functional validity of the object, and results in prompt feedbacks. The quicker will be the validation, the sooner the product will be released. The advantage of rapid prototyping is that it allows to obtain a physical prototype directly from a Computer Aided Design (CAD) 3D model, without the need of complex fabrication technics, but just building up in few hours, layer after layer, nearly any possible structure. While in the past, the application of the additive technology was principally used for the creation of prototypes, nowadays it is possible to obtain directly end-usable parts thanks to the continuous improvements in the processes. So, it resulted that the term Rapid prototyping wasn't anymore adapted to correctly describe this field, and a technical Committee with the ASTM International decided to adopt the more proper Additive Manufacturing as standard terminology [24].

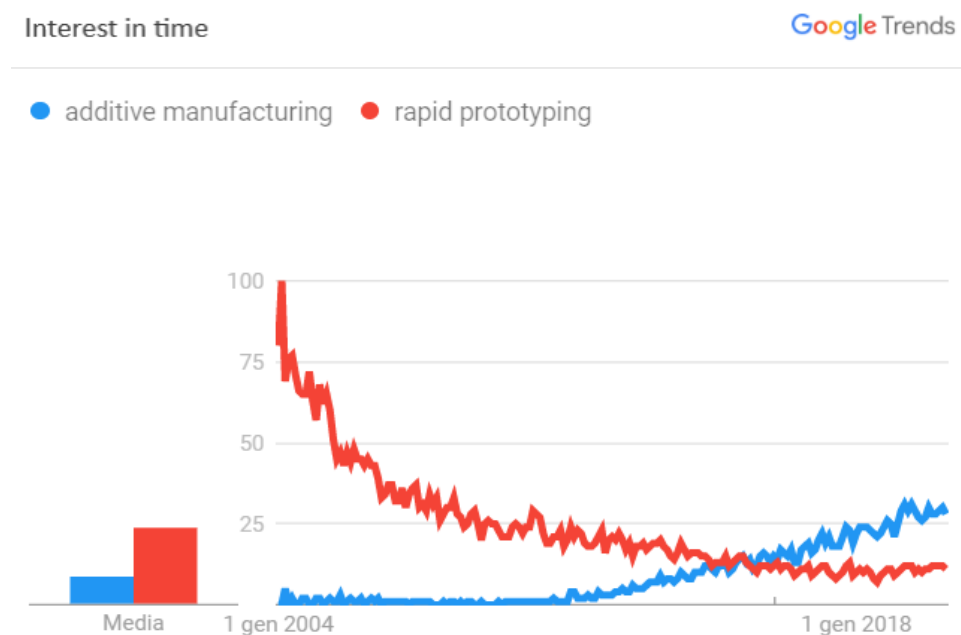


Figure 3-1

Figure 3-2 Google researches of Additive Manufacturing vs Rapid Prototyping [25]

As previously said, the basic concept for AM is the construction by addition of material layers where each layer is a cross-section area of the whole component. The thinner is the layer, the more precise the final part will be; the thickness of the layer may vary considerably depending on the technology and the material that is used. Besides the material, the different technologies may differ for the way the layer are deposited and bonded with the previous layer, the printing speed, the dimension of the final component, the post-processing needed and of course the process cost. All these aspects included the mechanical properties can cover a really wide range having parts which can be made in polymeric, ceramic, organic and metallic materials.

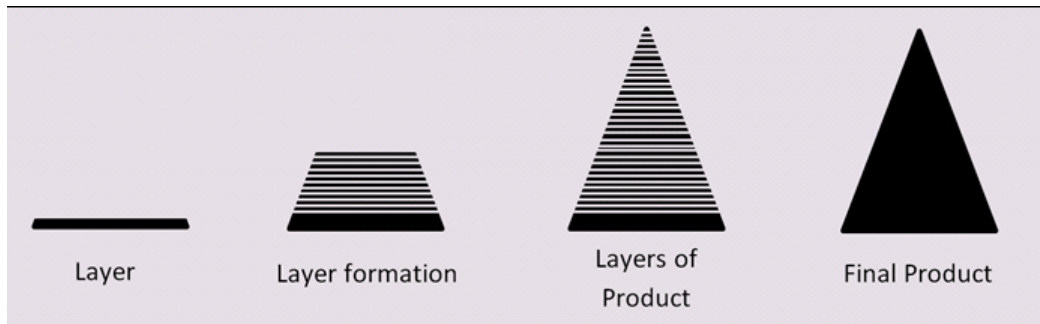


Figure 3-3 Additive manufacturing – Layers [26]

The first developments of this technology dates to the 1984, several studies were conducted simultaneously in different companies in France, Japan and USA. In the USA, the *3D Systems* company founded by Charles Hull, created the first additive machine, based on the Stereolithography technology [27]. In the following years, other companies emerged, even if most of them are not still in the market. Nowadays, the most successful companies are the pioneer *3D Systems*, but even *Stratasys* and *ZCorp* that is mainly focused on low-cost machines. In Europe, the German *EOS* is one of the most advanced in the powder bed fusion systems where a laser is used to melt the material (which can be a polymer or a metal). Some other companies are spread in the European continent like *Arcam*, *Strataconception* and *Materialise* that are smaller than EOS but are specialized in a specific sector. In Asia, several big companies like *Sony* and *Kira* have invested in this field but there have been also famous start-ups like the Japanese *Autostrade*, even if most of the commercialized machines are produced by American or European companies.

Thanks to its high flexibility, and the large benefits that it brings in term of savings in both time and cost, nowadays, AM is applied in several industries, not for a mass production but for those sectors that require rapid prototypes or the construction of few components with specific properties:

- **Aerospace** companies have been the first to invest in additive manufacturing, moving rapidly from prototypes to end-usable parts. For this industry, the number of components to be manufactured is generally not enormous, so it matches with the small-scale

production of AM. The combination of high strength with the lowest weight components, is ideal in order to reduce to the minimum the consumption of propellant. Moreover, considering the high cost materials that are used to build aerospace components, the limited waste of material that involves AM processes is another important advantage.

- Also in the **Automotive** field, there is a growing demand for components always more complex and lighter, while keeping the same stress resistance levels in order to guarantee the safety of the users. Several companies are already producing end-usable additive manufactured parts, but most of the parts are made in polymeric materials. Due to the still high cost of metallic parts, at the present it is not possible a wide application in low-cost cars, metal parts indeed are being produced mainly in the luxury car industry or for race cars [28].
- In the **biomedical** industry, AM allows to construct rapidly, prosthesis and dental plants whose production with other methods is more complex and expensive [29]. For this kind of products, the customization is essential in order to guarantee a precise adaptation to the morphology of the body. In addition to metallic prosthesis, in these years some companies are trying also to recreate organs, for instance *Bioprinting* managed to print a human liver [30].
- In **architecture**, AM is used to create easily miniature urbanistic model prototypes. Moreover, some special machines have been created that allow to create real dimension houses, with really few instruments [31].
- There are also other industries where AM is spreading, like the electronics, fashion and design, allowing to obtain always more particular and sophisticated shapes.

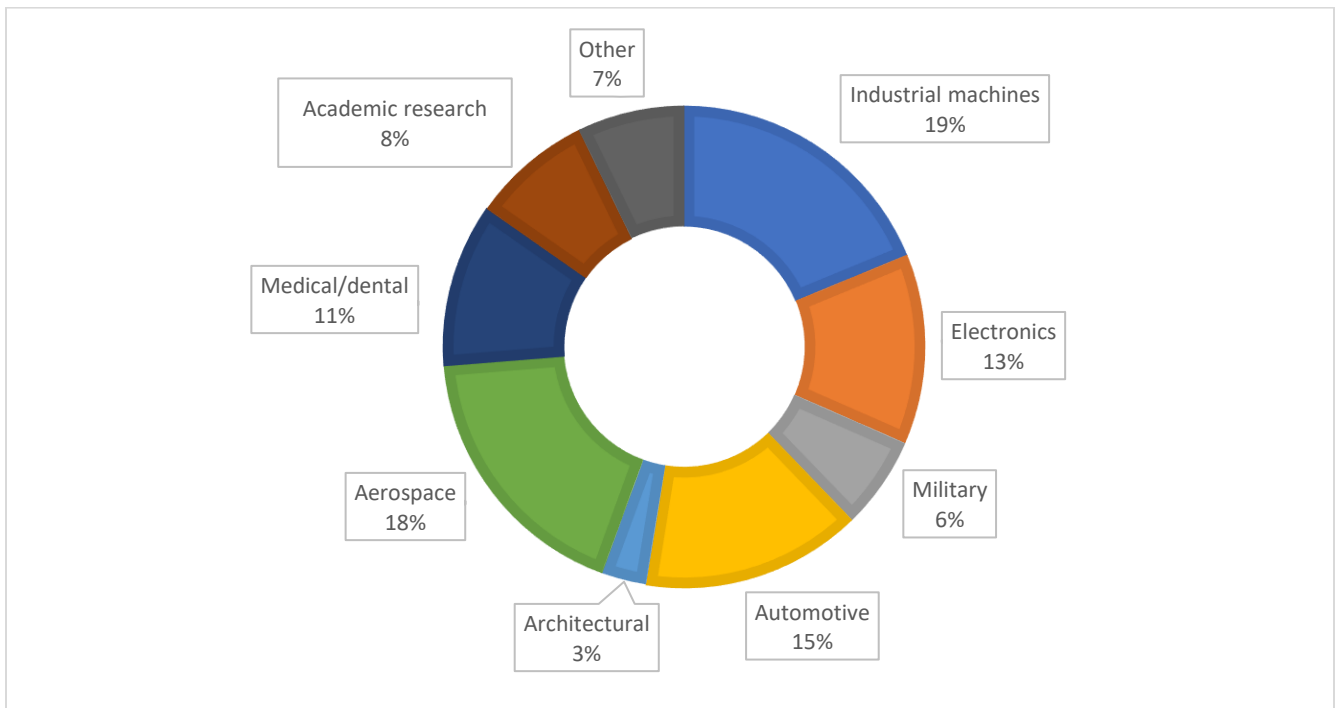


Figure 3-4 Graph: AM revenues by industrial sector (Wholers 2017) [32]

3.1 General steps for Additive manufacturing process

The whole process to produce parts with this approach, can be generally divided in 7 steps even though some steps may vary depending on the technology adopted.

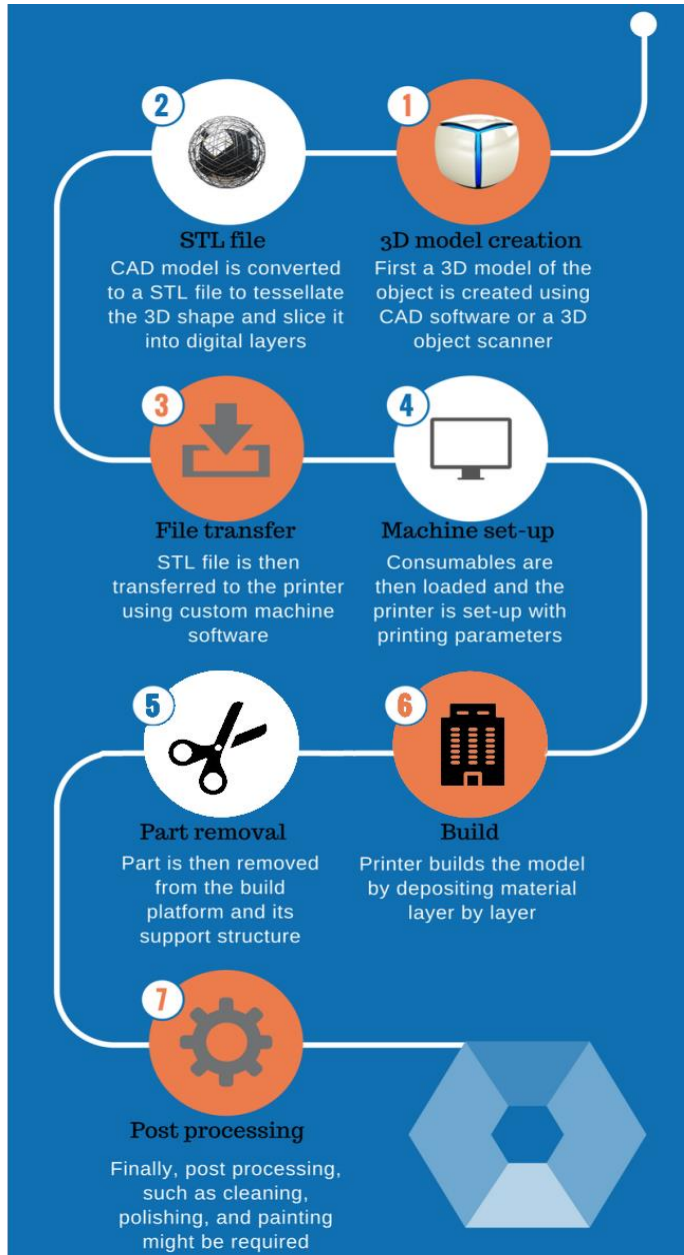


Figure 3-5 Additive manufacturing steps [33]

- 1) **CAD Design:** The starting point for the design of a new component, is a digital definition of the geometry that fully describes its external surfaces. In fact, AM developments is strictly link to the spreading of CAD softwares, because without them it would be missed the starting point of the process. One issue of the CAD models, which was much more

common in the past, is the presence of some undetectable small gaps on the surface of the model, which cause the part to be not mathematically closed. This problem depending on the technology, may create some errors in the fabrication of the part. The new programs are generally able to detect these errors and can be solved without any trouble.

- 2) **Conversion to STL file:** For all the most famous AM companies, the STL file format has become a standard, so every machine can accept this type of file. The abbreviation STL comes from **ST**ereo**L**itography, the first AM technology that was developed (by 3D Systems) that made this file format public and allowed all the CAD software to include it between the various possible outputs. The file describes the component in a simple way as a set of closed surfaces partitioned with triangular facets. The orientation of these triangles can approximate even curve surfaces. Clearly, the smaller are the triangles, the more precise will be the STL file in respect of the CAD model. The STL file contains only the data regarding these triangles, the coordinates of the vertices and the surface normal vectors. Due to this limitation, it has been even developed a new file format called AMF, which include further information of the part, like the units, material color and other information.

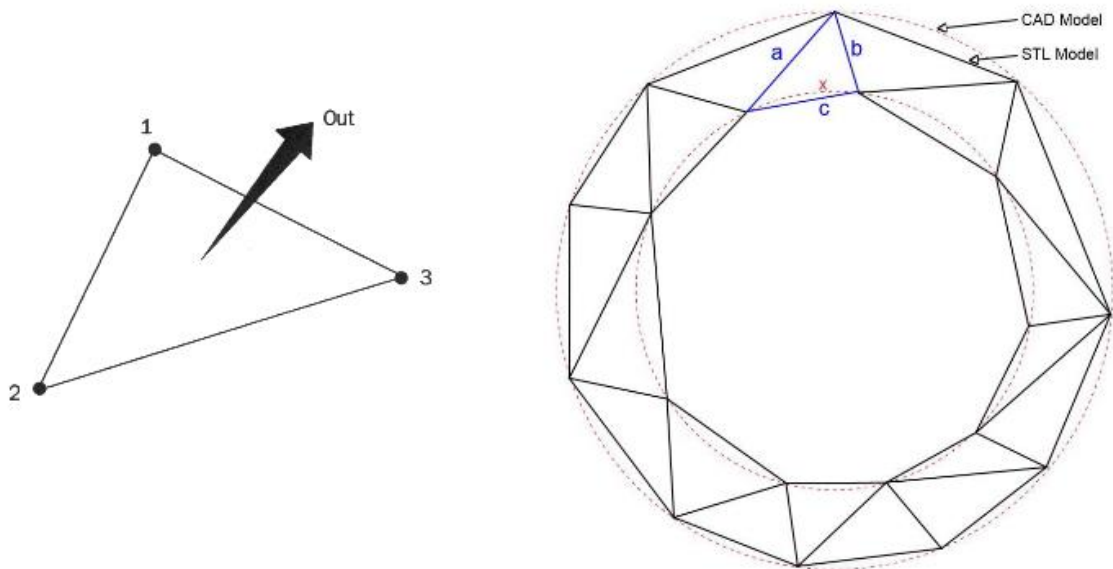


Figure 3-6 Triangular facets of the STL file [34]

The STL file may sometimes have some defects: the most common are gaps between the triangles, inverted normal, intersection of triangles and internal walls.

In a real complex area, it may happen that the vertices of the triangles do not overlap, causing the presence of gaps on the surface. Considering the inverted normal, it is fundamental that the vector is oriented correctly, in order to properly define the internal and external area. Some of these defects can be solved or at least detected by specific

software like Magics (Materialise) [35], preventing the part from being printed with these issues that can cause failures of the printing operation or of the part.

- 3) **Transfer the STL file to the machine:** The STL file, after the fixture of the possible errors, cannot be sent directly to the machine to be printed, because some other options should be defined with the AM machine software. There are several properties that depends on these aspects and it must be found a balance between them. Commonly, the variables involved are the dimensional and shape accuracy, the surface quality, the building time and cost, the component warping, the supporting elements, the stability of the part during the building procedure, and the utilization of the building area. Regarding this last factor, the position of the parts on the building base is crucial, in order to build simultaneously more than one component from one single print. In fact, it is convenient to build the largest number of parts, in order to reduce the total time of production, which is highly influenced by the time for the setup and for the final operations. Not only the positioning, but even the orientation of the part is a crucial decision [36], as the orientation may considerably influence the surface finishing, as it can be seen in Figure 3-7 Dependence of stair-stepping effect on part orientation Figure 3-7.

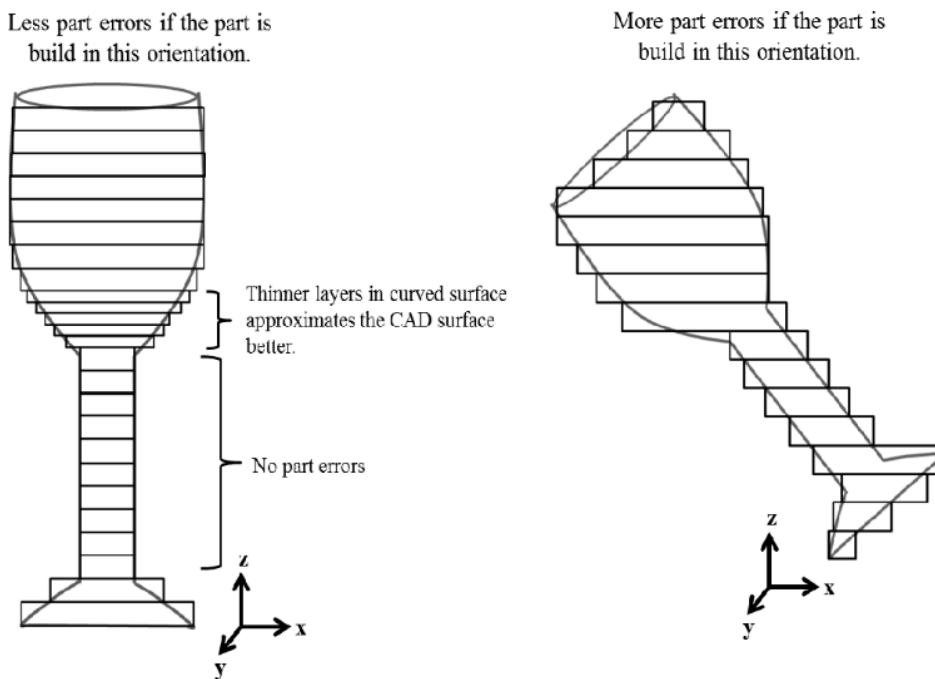


Figure 3-7 Dependence of stair-stepping effect on part orientation [37]

Moreover, the building orientation has an influence on the resistance of the part. In fact, it has been proven that the part resistance along the building direction (z axis) is lower than the in other direction, because of possible imperfections in the bonding between the consecutive layers [38]. Stair stepping is typical for AM parts, but this superficial effect

may be reduced both thanks to a correct orientation and by reducing the layer thickness (that normally has a fixed height).

Even greater importance has the supports generation, which are needed for the majority of the processes. Commonly the supports are automatically defined by the software (*Magics* or similar), but the operator can modify them. It is preferred to minimize the use of supports structures, because they must be removed manually, they need time to be built and they are a waste of material (because of the difficulty in recycling the printed material), without forgetting even the energy necessary to be build them. Furthermore, the support structures beyond their principal function of increasing the rigidity of the part under construction, they bring also other advantages:

- In the case of unsupported geometries (like the examples in Figure 3-8 Particular geometries that requires a support structure (in orange) Figure 3-8), it is necessary to have supports in order to prevent any deformations due to gravity. Moreover, they are used for unbalanced structures that may risk collapsing in the absence of a solid base;

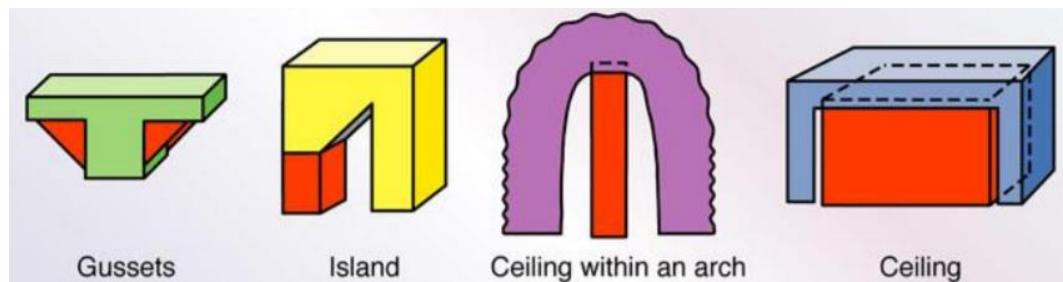


Figure 3-8 Particular geometries that requires a support structure (in orange) [39]

- Generally, the part is not built directly on the building plate, because this part can be reused and detaching the part directly from the building plate may be more challenging and time consuming. So, it is common to start the fabrication of the initial layer on a supporting structure that guarantee a quicker post-processing operation;
 - Especially in those processes that involve the fusion of the building material, in which high thermal stresses are generated, the supports allow to reduce the temperature gradients on the part, which are cause both of distortion and residual stresses. The generated heat is diffused by the support structure to the rest of the volume and to the building base.
- 4) **Machine settings:** For each printing there may be some options that must be defined. Depending on the technology or the machine employed, these adjustments could be

different. These settings must to be tuned in order to obtain an optimal result from the process. They can change depending on the material that is used but can also be varied in function of the final result that is to be achieved. In fact, for a prototype it is acceptable a lower accuracy and surface finishing of the part, if it can be printed in a shorter time. On the other hand, for an end-usable part, it is more convenient to use more power and have a longer process but with a better result in terms of accuracy and strength.

In advanced machines it is common to save different setups for each material, in order to reduce this lead time. Generally, the parameters that can be changed regards the speed and the accuracy of the operation, by changing the layer thickness, increasing the laser velocity (or number of drops/second depending on the technology) or even its power, producing a completely different result.

Moreover, there are some activities that an operator should perform for preparing the machine (outside the software environment), like loading the building material if necessary, inserting the building plate (if the technology requires one) and correcting its position.

- 5) **Building operation:** Once every setup operation has been pursued, the machine can start building the component. The software will initially analyze the STL file, by slicing it into the layers. In this way the construction will be made as a sequence of 2D layers, that in the end will provide the final 3D component. The building operation is made automatically and it is not necessary the supervision of an operator, except for checking that power or software errors have occurred or that the machine has run out of material. Depending on the process, the layer creation, the deposition of material and the adjustment of the building base after each step may change considerably.
- 6) **Support removal and cleaning:** Once the building is completed, before removing the part from the machine, it may be necessary some time for safety reasons, waiting for example that the temperature inside the chamber is lowered or that there are no parts that are moving. In this phase it is required a direct interaction of an operator with the machine and the part itself. This step needs some expertise regarding the operations of removal of the part and all the eventual post-treatment that may take a long. Firstly, the part (and eventually even the chamber) must be cleaned from the excessive building material that surrounds the part. Then the part should be detached by the building plate and all the supporting elements removed. This phase, depending on the building material can be done easily if the supporting elements can be melted (for example if they are made with wax), or on the other hand it can be complex and time consuming with the manual removal of the supporting elements. For hard materials (like steels or other metals) it can be used a milling machine or a wire Electrical Discharge Machine (EDM).
- 7) **Post-processing:** Even this final step, depends heavily on the AM technology used and even on the specific requirements for the component. Sometimes almost no further

treatment may be needed, having a component ready for the use. Weak or fragile parts may require a heat treatment or post-curing for enhancing their mechanical properties. This can be achieved even by an infiltration of a second material or thanks to a surface coating (plating or vacuum metallization). Then for improving the surface finishing a part can be polished, blasted or painted. Finally, the parts may be assembled with other components.

3.2 AM advantages and disadvantages

The design for conventional manufacturing method, has the objective of defining the best layout of a component, with a significant focus on the numerous constraints that characterize not only the manufacturing processes that are necessary to obtain the final part and that can be a large number and quite complex, but even on the assembly procedure which should be simplified, possibly also reduce the number of parts to be assembled. Additive manufacturing has many limitations too, but these are different from the one that designers are used to face and must be analyzed separately. At the same time, it offers a wide range of benefits over the traditional fabrication methods. Considering the continuous developments of this technology, the advantages can still increase, thanks to improvements of both the quality and rapidity of the processes, but even the costs that will gradually decrease. This will lead to a wider application of this manufacturing method also in those businesses where, at the present days, it is still inconvenient. The main advantages of AM in respect of traditional manufacturing methods are listed below:

- **Mass customization:** One of the principal advantages of AM is the possibility of the customization of the parts, which allows to produce components adapted to the needs and requirements of each user. For example, in the field of the biomedical engineering, the production of a hearing-aid device specifically designed for the exact morphology of the ear, making it more comfortable. This advantage can be made without almost any extra efforts except for the creation of the exact design, not affecting the time or the cost for the construction.
- **Design freedom:** What differentiate principally the AM components from other fabrication methods (like molding or machining), is the nearly total absence of constraints. Thanks to this, it is possible to create almost any shape, as the complex three-dimensional construction is divided into simple 2D geometries. It follows that lighter components can be obtained, even including extremely complex geometries with hollow shapes, undercuts or lattice structures. This higher complexity comes without almost any additional costs, because time and cost for AM technologies are mainly proportional to the volume of the component, not to its shape.

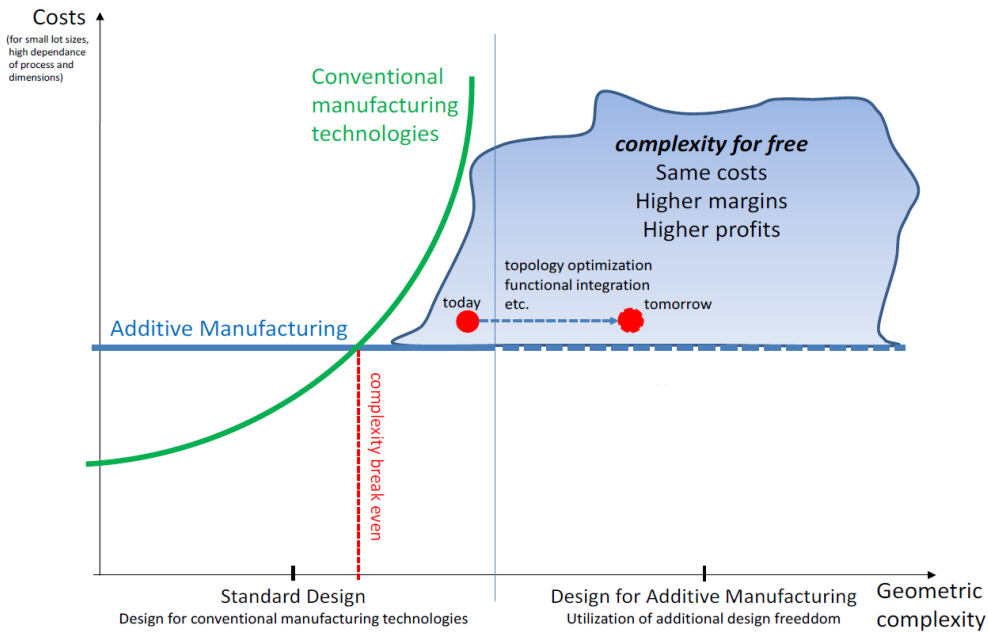


Figure 3-9 Complexity vs costs of AM and traditional technologies [40]

- Assemblies and integrated design:** Multiple components can be built simultaneously in the same printing operation, by leaving a small clearance between the surfaces of two different components, it is possible to obtain pre-assembled kinematic joints. Moreover, having the ability of producing complex shapes, it is possible to reduce the total number of components needed by integrating them in a one-piece assembly. This avoids the need of further assembly processes.

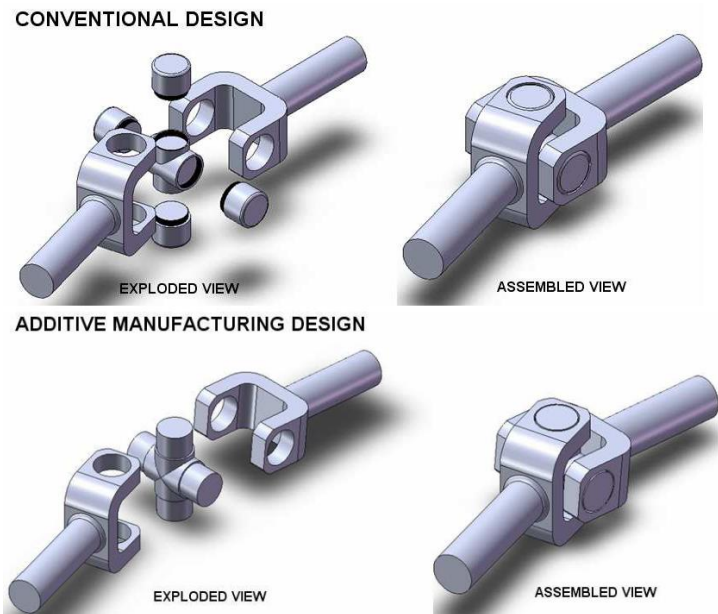


Figure 3-10 Comparison of assembly: Conventional vs AM design [41]

- **Process simplification:** For Additive manufacturing, the production of the component happens in only one step, while with traditional methods, it may require many processes. This greatly simplifies the production phase, even because the activities of the operators are quite limited being the process automated. Only the setup and post-processing need the operation of a worker, but it is valid also for conventional manufacturing methods.
- **One machine:** With a single machine, it is possible to create infinite shapes, without provide any changes on the machine, except for the CAD file and the specific optimal settings for obtaining the best result with each material. On the other hand, for conventional methods, it may take a long time and a large effort to modify the whole fabrication line to produce a different component.
- **Sustainable process:** All the differences that differentiate AM from conventional manufacturing methods, make AM a eco-friendlier process as demonstrated in several studies [29] [42]. The main advantages are the fewer raw material used to produce the part (the material is deposited only where needed and there is few production scrap), thanks also to the recyclability of the material (for most of the AM processes). In addition to the lower wastes, the component being more optimized tend to be lighter, so even the part itself needs less material. This influence not only the manufacturing process but also the consequent use of the part (a reduction of weight in a mean of transport, results in fuel savings and lower pollutant emission). It simplifies the whole plant, reducing the need for tooling and inventory making leaner and simplified the whole supply chain (with reduced lead time), and lowering the number of transportation processes and their carbon footprint. This is also link to the fact that it is not necessary to have huge producing plants, but the production may be distributed in multiple small factories spread in the territories.
- **Multimaterial components:** With some of the processes it is possible to combine in a single printing of a part, the use of different materials. This is easier for those methods in which the material is extruded or deposited by a nozzle. Depositing material where it is needed, different properties can be obtained in different region of same component. For example, in the areas of a turbine's blade subjected to high loads it may be necessary a material with high strength and stiffness while in internal parts the material could have high heat conductivity to reduce the temperature of the component.

As it can be clearly understood, AM has a large number of benefits that make it advantageous for several aspects. On the other side, it also has several limitations and drawbacks:

- **Limited build velocity:** If compared to a CNC machine, the AM can be considered quite slower, in fact the addition of material for any AM process is lower then the subtraction rate of CNC machines. To have a fair comparison it should not be considered only the construction time, but even the time necessary to setup the machines. While AM machines carry out the construction autonomously, CNC machines require a precise and complicated planning, especially for complex shapes. Moreover, traditional machines

may require, to obtain particular geometries, special tools, mould or jigs. It is clear that for a mass-production, an automated manufacturing plant precludes any comparison with AM technology, which is convenient only in small-scale production.

- **Limited building space:** One of the principal limitations that AM machines still have is the small building area. In fact, some of the most advanced methods that allow to produce end-usable components have some building chambers that do not allow to construct big components. This kind of problem has been encountered also in the project of this thesis, as the component that should have been printed, is larger than the chamber of the machine that is available at the university's laboratory.
- **Superficial finishing:** As previously said, the external surface of a printed part, is characterized by a step-scaling structure, due to the layering process. Because of the resulting superficial roughness, it may be necessary a post-processing operation to overcome this problem. With CNC, the part is produced with higher accuracy and this passage could be already integrated in the several steps of the operation or may even not be necessary.
- **Imperfections:** Another aspect that should be considered are the imperfections in the printed part, which can be micro-cracks or even voids inside the printed part. The presence of this defects is mainly related to the settings defined for the printing operation and can be considerably reduced using the optimal setup. Moreover, along the printing direction, the resistance of the part may be slightly lower, due to a not perfect bondage between two consecutive layers.
- **Materials:** The available materials are still limited, especially for the metals. For the polymers there is a wider selection but due to their low mechanical properties, they have huge limitations on their field of application. Moreover, the cost of the materials is still high, so that the production of a component may be less advantageous to be constructed with AM. An additive manufactured component becomes convenient, when its complexity makes it too demanding to be constructed in other ways.
- **Cost of machines:** Not only the materials, but even the machines, especially for constructing metallic parts have high prices. It is expected that in the future the price will decrease, even if this reduction may be lessened by the contemporary increase of the machines' performances.

3.3 Additive manufacturing for metal parts

The production of metal components, at the current state of the art, can be made with three different methods and all of them use the material in the form of powder, while as energy source a laser or an electron beam. For all these processes the energy is concentrated in a real restricted area in order to fuse the material with the highest energy density possible (laser power over 100 W, depending also on the metal to be fused). The more effective will be the concentration, the lower will be the energy required to melt the powder. In order to ensure that enough energy has reached the metal powder particles, the laser speed is slower than when dealing with a polymeric material.

Due to the high temperature that are reached, these machines require heat shields and proper insulations. Moreover, adopting some delicate components like the laser, their maintenance is crucial and needs expertise, also considering the complexity and the cost of the machines. The surrounding environment, must be kept clean and with a low noise, preventing that any vibration could cause a performance degradation.

The accuracy of the machines that produce metallic parts is the best for all the AM field, with high accuracy and density of the part (also over 99%). The surface roughness is of the order of a hundred of microns, but this depends both on the process and on the printing parameters. It is probable that the part may require a post-processing treatment to improve its surface finishing.

3.3.1 Laser Direct Energy Deposition

The *Direct Energy Deposition* (DED) process is the most different between the three methods, as the other two, being both based on a *Powder Bed Fusion* (PBF) technology are quite similar. The DED approach employs as energy source a laser (or a beam), which melts the powder while it is being deposited. Even if this method works even with other raw materials like polymers and ceramics, metal powders are the most used materials.

There are several Companies that produce machines based on this technology: *POM* (USA), *Optomec* (USA), *Huffman* (USA), *Accufusion* (Canada), *Irepa Laser* (France), *Trumpf* (Germany). All these shares the same basic building method but they have many differences related to the laser (type, energy and diameter), delivery method, inert gas used and moving method.

As it can be seen in Figure 3-11, the deposition head is mainly composed by a laser optic, a set of powder nozzles and inert gas nozzles.

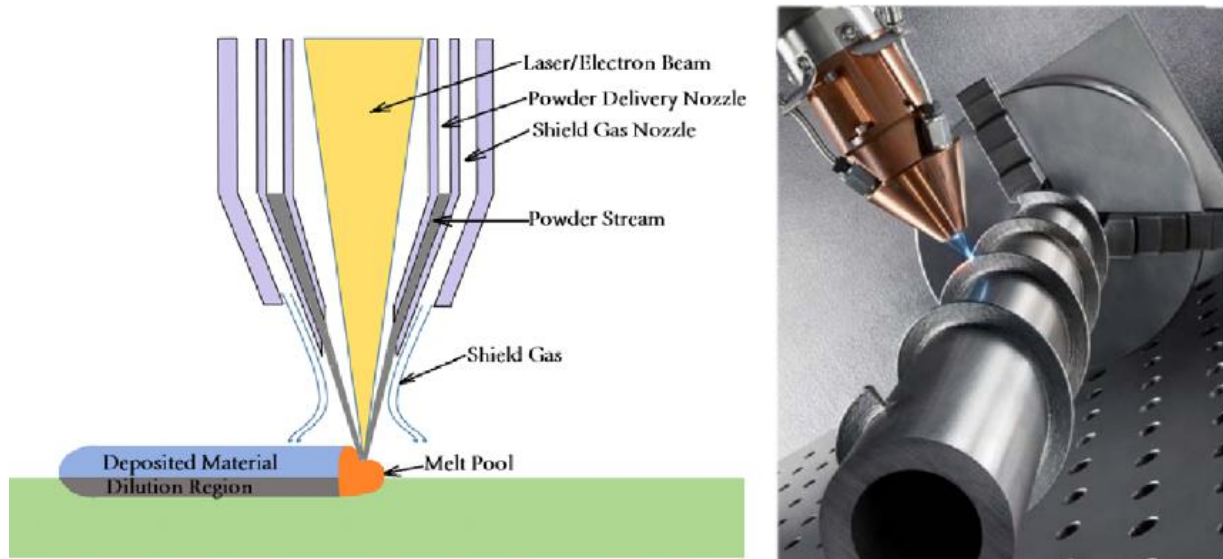


Figure 3-11 Laser Direct Energy Deposition scheme [43]

During fabrication, there can be a double motion of the substrate (the area where the material is being printed) and of the deposition head. Thanks to these relative movements, a 3D object can be obtained with a quicker process. With this motion, the laser creates a thin line of solidified metal welded to the layer below. A complete layer is generated only after a series of consecutive overlapping lines. After each layer is formed, the deposition head moves upward by one layer thickness. For this technology, it is strongly required the construction of support structures, to obtain the prescribed shape and prevent any distortion. Moreover, DED can be used also to build on already existing components, for example to reconstruct a broken part or to create a coat. This printing tool, in fact, has also been inserted in CNC milling machines for maintenance usage.

Thanks to the high kinetic energy, which overcomes the gravity effect on the powder particles, it is possible to print also not vertically (this is implemented in complex 4 or 5 axis machines). The laser creates a molten area of small dimension (0,25-1 mm), and the powder is not molten directly by the laser, but it melts as it enters inside the molten pool and it solidifies afterwards when the laser has moved beyond. Due to the small dimension of the fused pool, the molten metal is subjected to a rapid air quenching (with cooling rates around the 10^4 °C/s). These allow to obtain particular microstructures with grains that are not realizable with the Powder Bed Fusion methods.

3.3.2 Selective Laser Melting

In this thesis work, it has been used this technology to print some tensile samples to verify the resistance of the material, so a more thorough analysis is given of this method in respect of the other two.

The Selective Laser Melting (SLM), also called Selective Laser Sintering (SLS), is with the Electron Beam Melting (EBM) a Powder Bed Fusion technology.

There are several companies that produce machines based on the PBF technology, like: *EOS* (Germany), *Concept Laser*, (Germany), *Renishaw* (UK), *Realizer* (Germany), *Phenix* (France), *SLM Solutions* (Germany), *Matsuura* (Japan), *Arcam* (Sweden) that is the onliest that uses as heat source an electron beam. All these companies produce metallic parts, while EOS and Phenix produce also ceramic parts and finally *3D Systems* (USA) is the onliest that uses polymeric powders (principally due to a patent limitation). Between all these companies, the leader in the production of these machines is certainly the German EOS, which defines its SLM process as Direct Metal Laser Sintering (DMLS).

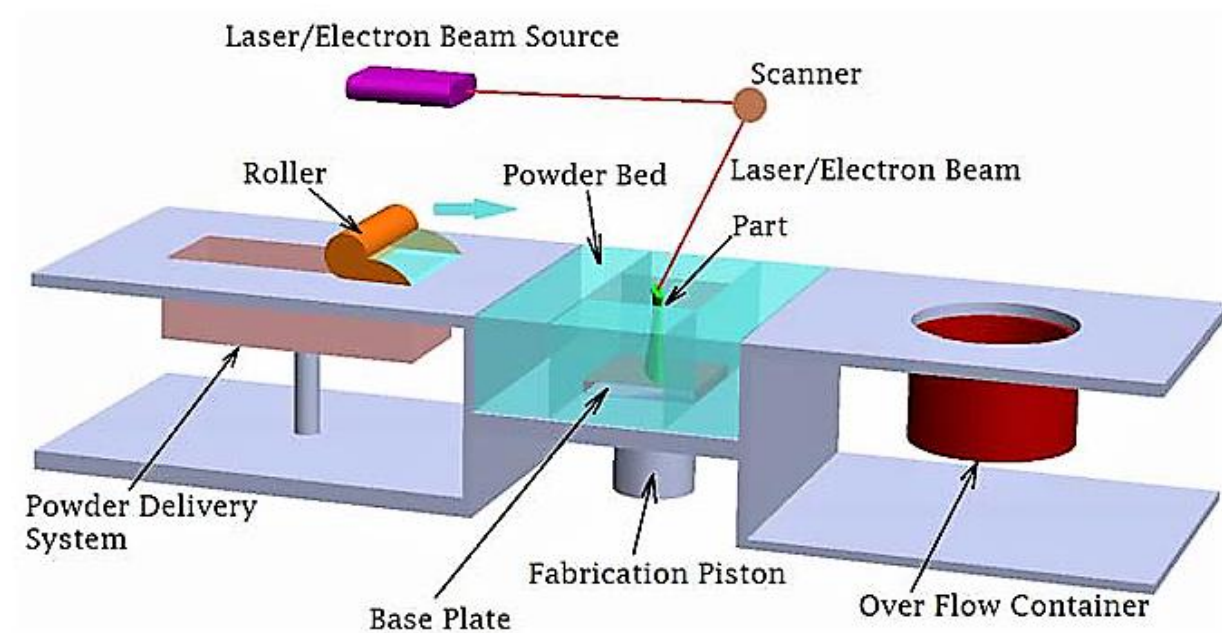


Figure 3-12 Powder Bed Fusion process [43]

Each company has its particular characteristics for its machines, but they all share some fundamental concepts of the PBF methods:

- A mechanism (for example a counter rotating levelling roller) is used to spread precise thin layers of powder on the building area.

- The process happens in a chamber with an inert atmosphere (with nitrogen or argon) or a partial vacuum that works as a shield for the material, in order to prevent or reduce the metal's oxidation.
- The distributed powder on the building area is kept at a high temperature (under the melting point or glass transition temperature of the material) thanks to a series of infrared heaters that are placed on the top of the chamber. This preheating allows to reduce to the minimum the energy consumption of the laser and to prevent distortions of the part during the print, caused by thermal expansion of the fused area and contraction of colder zones. Moreover, the powder is pre-heated also before being spread in the chamber, because the process is really rapid and the infrared in the chamber cannot bring instantaneously the temperature to high values.
- One or more heating sources (lasers or electron beams) are used to melt powder particles. A system (like a scanner or a set of galvanometers) moves the point where the thermal energy is concentrated, in order to selectively induce the melting only where required. The non-molten powder works as secondary support for the molten metal, because the built supports are anyway needed to keep the part in the correct position.
- Once the construction of a layer is completed, the piston under the base plate moves downward of a layer thickness, while the piston of the powder delivery system moves upward. After the roller (or a different instrument) spreads a new layer, the process can restart.
- The whole manufacturing process will finish when all the layers are built. After the printing operation is finished, the part cannot be extracted immediately, instead it is necessary to wait some time that the inert gas is extracted from the chamber with a fan and more importantly that the temperature in the chamber is lowered. This must be done for safety requirements, but principally to prevent that the hot powder in direct contact with the oxygen of the air (at room temperature) is rapidly degraded and that the part due to the rapid variation of temperature is subjected to any deformations.

The SLM methodology was first developed with polymeric materials, while the use of metal powders initially faced several criticalities related to the high conductivity of metals, the rapid oxidation and most of all the high reflectivity when hit by the laser. In order to overcome especially this last issue, the CO₂ laser used with polymers was substituted by other kind of lasers like the Nd-YAG and the fiber lasers [27]. These heat sources work at different wavelengths and led to a higher absorptivity of the emitted energy. The fiber laser is nowadays the most used because of its lower cost and general higher energy efficiency and beam quality. This laser's power can range between 200 W and 1000W and has a focus of around 0.1 mm. The energy required to melt the metal is influenced by the laser power, spot size, scan speed, and bed temperature. The longer the laser reaches a fixed area, the deeper the fusion depth and the larger the melt pool diameter will be. The energy density of the laser can be computed as shown in other researches with the following formula [44]:

$$E = \frac{P}{v \cdot d \cdot \Delta z} \left[\frac{J}{mm^3} \right]$$

Where P is the laser's power [W], v is scanning speed [mm/s], d is the diameter of the laser [mm] and Δz is the layer's thickness [mm].

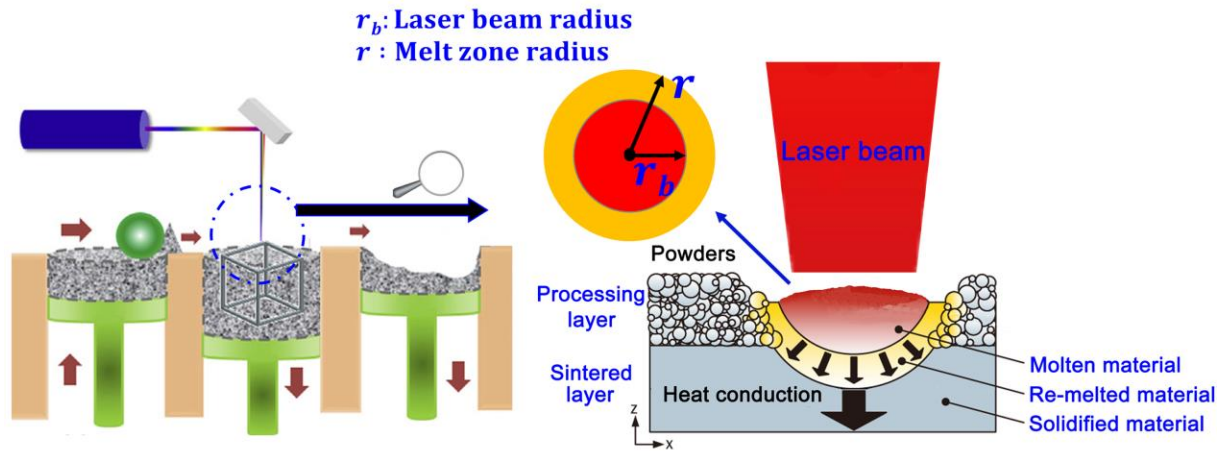


Figure 3-13 Molten area in SLM [45]

It must be assured that for each point reached by the laser, the melted zone is deep enough, so that a correct bondage with the underneath layer is obtained. Commonly the layers have a thickness between 0.02 and 0.1 mm. The focus point of the laser is defined by a series of lenses and scanning galvanometers “mirrors” that can move and rotate to define the correct position on the building area.

This technology allows to obtain high quality end-usable components with almost no porosity and consequently a density over 99%. The final part properties can considerably change in function of all the that process parameters that can be defined, like the layer thickness, the hatch spacing, the laser power, the scanning speed, etc. Each producer suggests some predefined settings for each material. Varying these parameters, the quality of the part can degenerate, but it has also been proved that optimal results have been obtained by slight variations of the standard setup [46] [47].

A large amount of the powder that is distributed on the powder bed is not molten, as it is not part of the component. In order to prevent a large waste of this unused powder a recycling methodology must be adopted. However, it should be considered that even if this powder has not been melted, it has been subjected to high temperatures and this thermal history may influence the properties of the material. Actually, it has been demonstrated in several studies that the decay of reused powders' properties is limited and the reduction of the tensile strength is really small (if not null in some cases) [48] [49].

This technology requires the use of support structure, in order to prevent a deformation (with warping and curling) of the part while the material is still fused, especially if are present some overhang structures. Due to the presence of a bed of powder, the supports can only be of the same material on the component. So, at the end of the process they will have to be removed

with a caliper or, for hard materials with a wire EDM or a milling machine. This post-process can be time consuming and expensive. The supports can be avoided for small internal channels (where the removal of the support structures would be almost impossible), and the non-melted powder takes the role of support. In this case, it must be considered the possible compression of the underneath powder, which may cause an error in the printing.

The SLM (but in general all PBF methods), differently from other processes allows to treat several material powders. It can be theoretically assumed that if the metal can be welded then it can also be used for this process. In reality, there are some issues with the use of several materials, related for example to the quality of the printed part, which may present a low uniformity in the microstructure and the presence of several defects like micro-cracks. Especially pure metals are not used with AM because of their problem related to oxidation and corrosion and the typical lower mechanical properties in respect of alloys.

The number of metal powders that are nowadays available is not really vast, but more materials will be implemented in the future. In the next Figure 3-14 are listed all the powders available from EOS, which are several types of steels like stainless steels or Maraging steel (that is the material chosen for this thesis work), nickel-based alloys (like Inconel) and titanium alloys (used in particular for the Aerospace industry), different aluminum alloys and cobalt-chrome.

Product class	Product name	Material type*	Product class	Product name	Material type*
Steels	EOS MaragingSteel MS1	18Ni300, M300	Cobalt chrome	EOS CobaltChrome MP1	UNS R31537, ISO 5832-4, ASTM F75, ISO 5832-12, ASTM F1537
	EOS ToolSteel 1.2709**	EN 1.2709		EOS CobaltChrome SP2	*Type 4* CoCr dental material as per ISO 22674
	EOS ToolSteel H13**	ASTM A681		EOS CobaltChrome RPD	*Type 5* CoCr dental material as per ISO 22674
	EOS CaseHardeningSteel 20MnCr5**	EN 10084	Coppers	EOS Copper Cu	High purity copper
	EOS StainlessSteel GP1	Stainless steel 17-4 / 1.4542		EOS CopperAlloy CuCrZr	C18150, CW106C
	EOS StainlessSteel PH1	1.4540, UNS S15500	Titanium	EOS Titanium Ti64	Ti6Al4V, ISO5832-3, ASTM F1472, ASTM F2924, ASTM F3302
	EOS StainlessSteel 316L	1.4441, UNS S31673, F138		EOS Titanium Ti64 Grade 5	Ti6Al4V ELI, ASTM F136, ASTM F3001, ASTM F3302
	EOS StainlessSteel 316L VPro	1.4404, UNS S31603		EOS Titanium Ti64 ELI	Ti6Al4V ELI, ASTM F136, ASTM F3001, ASTM F3302
	EOS StainlessSteel CX	Precipitation hardening tool steel	Aluminium	EOS Titanium TiCP	ASTM F67, ISO 5822-2
	EOS StainlessSteel 17-4PH	1.4542, UNS17400, A564M		EOS Aluminium AlSi10Mg	AlSi10Mg
Nickel alloys	EOS NickelAlloy IN718	UNS N07718, AMS 5662, AMS 5664, 2.4668, NiCr19Fe19NbMo3	EOS Aluminium AlF357	AlSi7Mg0,6, SAE AMS 4289	
	EOS NickelAlloy IN625	UNS N06625, AMS 5666, AMS 5599, 2.4856, NiCr22Mo9Nb	Refractive Metals	EOS Tungsten W1	Pure tungsten
	EOS NickelAlloy IN939**	Inconel™ 939			
	EOS NickelAlloy HX	UNS N06002, AMS 5390			

Figure 3-14 EOS: metal powders list [38]

3.3.3 Electron Beam Melting

Electron Beam Melting is a PBF process, which has been developed in Sweden in 1997, and the onliest company that produce industrial machines based on this process is the Swedish Arcam AB (which has been acquired in 2017 by General Electric [50]).

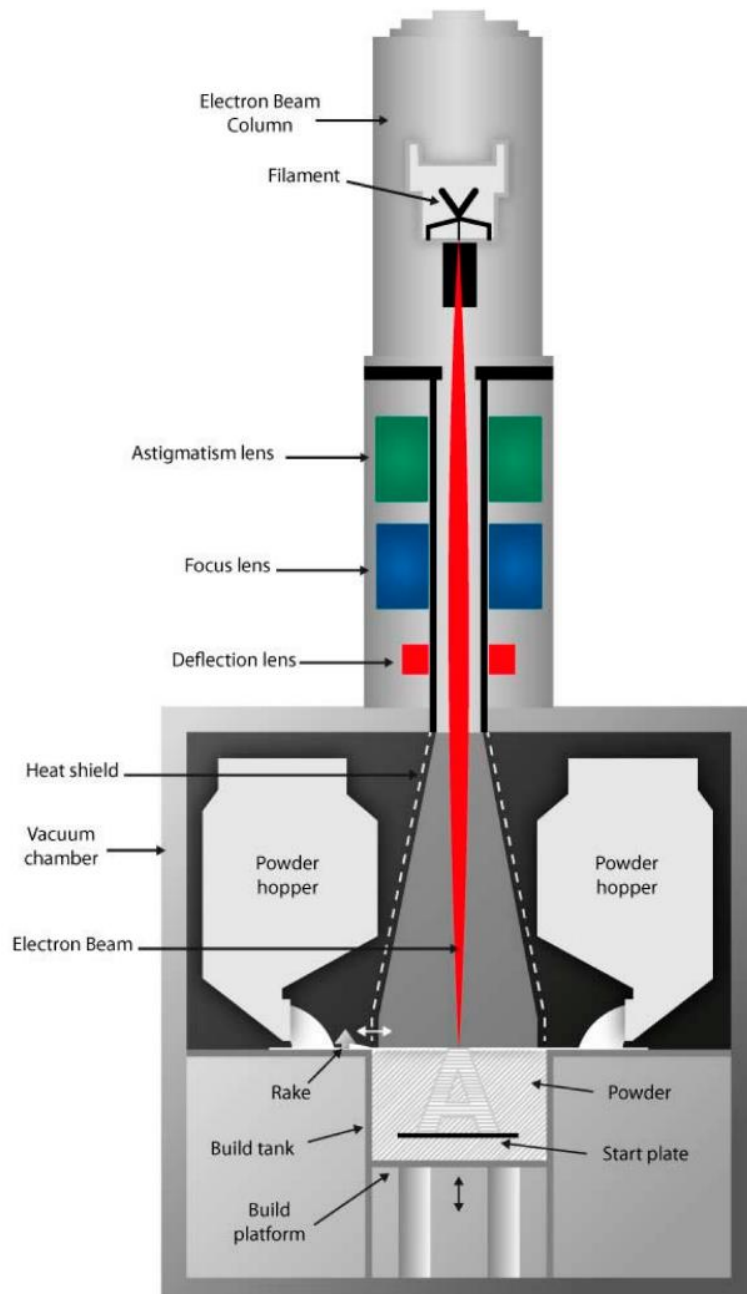


Figure 3-15 Schematic structure of an Electron Beam Melting machine [51]

Being a PBF process, it has numerous similarities with SLM, but in contrast with the latter, EBM machines use an electron beam as energy source to melt the metal powder. The electrons composing the beam are emitted by a filament that reaches a temperature over 2500 °C, which is heated up thanks to an electrical current. An anode accelerates the electrons that are afterward focused into the beam by a set of magnetic field lens. A second magnetic field has the function of control the deflection of the beam. The electrons move with high velocity, so that when they reach the powder bed, their kinetic energy is transformed in thermal energy, allowing the fusion of the particles. The electrons' energy is controlled by varying the electrical current of the emitting filament.

The melting energy source is not the only difference. In fact, while for SLM the chamber is filled with an inert gas, for EBM the chamber is under a high vacuum, in order to improve the quality of the electrons beam which lead to higher building rates (thanks to a deeper penetration of the beam), quick scanning speeds, less contamination of the part by the inert gas (which in SLM may be cause of porosity) allowing to reach densities over the 99,8% [51].

The EBM's scanning method, instead of being done with moving galvanometers, is realised with fixed deflection coils which make the process more trustworthy (not having any moving parts) and tremendously faster due to the limited inertia of the SLM's galvanometers.

Another difference is linked to the energy absorption, in fact the SLM's laser hits powder particles with photons, while in EBM with electrons, the system is based on a conductivity rather than absorptivity energy absorption method. So, the conductivity of the material must be higher in order to enhance the process (and consequently the EBM method can be used only with metallic powders). Moreover, due to the absorption of all the electrons there is a risk that the powder bed becomes too negatively charged. This may cause two issues, firstly the powder particles may reject the incoming electrons and much more problematic is the risk of a small explosion that will raise all the powder in the chamber. In order to prevent this high negativity, the electron beam has a larger radius than the laser so that a larger melting pool is created, this leads to a worse resolution and accuracy of the part in respect of SLM.

From the energy consumption point of view, EBM is more efficient, in fact most of the consumed electrical energy is released in the electron beam and higher energy beams (around 2kW) can be reached with medium consumption. On the other hand, for SLM less than the 20% of the consumed energy is transferred into the laser and the lasers with the same power have much higher costs than electron beam guns. This was valid especially in the past, because nowadays the utilization of fiber lasers has almost eliminated this difference, because these lasers are really energy efficient and have a simple and cheap architecture.

For the EBM technology, the powder bed heating system of the SLM is not necessary because by defocusing the beam, it is possible to rapidly warm up the whole powder bed. To improve the whole process and also to reduce the residual stresses, the powder bed is kept at a higher temperature in EBM. The combination of this higher bed temperature with the larger melting

area generated by the e-beam, produces a microstructure with larger grain sizes and indistinguishable laser scan lines (more similar to a cast product).

Also EBM requires the use of supports, which in this case have the additional function of electrical conductor, in order to discharge the electron charge. A difference with SLM is that for EBM the mass of the supports needed is much lower [27].

4 Material

The metal used by Maserati to produce the pre-existing steering knuckle for this specific vehicle is an aluminum alloy. For this thesis work instead it has been requested to redesign a new component, using a steel, in particular a Maraging steel, defined for the US and European classifications respectively as 18 Ni Maraging 300 and X3NiCoMoTi 18-9-5 [38]. In parallel with this thesis, there is a second research study in which the same component has been redesigned for the same AM technology, but in this case with the AlSi10Mg aluminum alloy, instead of the Maraging steel. This has been done, because in addition to the comparison of the steel's component with the original wrought component, the study focused also on the differences between the two components obtained by the SLM technology. In fact, it is interesting to find which is the potential of the steel if confronted with the most popular aluminum powder.

The material considered for this thesis, defined Maraging Steel MS1 by its producer EOS, is optimized for the production with the Direct Metal Laser Sintering (DMLS) technology, applied in their machines of the M-series [38]. The precise chemical composition is reported in Table 4-1.

Maraging steels are Iron-Nickel based alloys with the almost total absence of carbon and with several alloying elements like cobalt, molybdenum, titanium and aluminum. These steels combine good yield and tensile strength, fatigue limit, toughness, ductility, hardness and wear resistance. Moreover, they are characterized by high weldability and low reflectivity, which are two fundamental requirements for the Selective Laser Sintering technology, considering that the whole printing process is based on the melting powder particles that must fuse together. The main applications of this material are the aerospace and aircraft industry, machinery and tooling industries.

Alloying element	Fe	Ni	Co	Mo	Ti	Al	Cr, Cu	C	Mn, Si	P, S
wt %	(balance)	17-19	8.5-9.5	4.5-5.2	0.6-0.8	0.05-0.15	≤0.5	≤0.03	≤0.1	≤0.01

Table 4-1 Chemical composition of 18 Ni Maraging 300 [38]

This metal is part of a special category of high-strength steel that is distinguished from the common steel because of the absence of carbon, which is considered an impurity. In fact, the hardening is not linked to a metallurgical reaction that involves that element, instead the centered cubic martensitic element is strengthened by the precipitation of intermetallic compounds at around 480 °C [52].

Thanks to the low carbon content the risk of quench cracking, which may cause an unexpected rupture during the usage, is considerably reduced. Moreover, being free of carbides and having a high nickel content maraging steel is characterized by a high corrosion resistance [53]. The name *Maraging* comes from the ageing of the martensite, which is easily obtained, thanks to the high percentage of Nickel.

With Maraging steel powder is possible to obtain components with a density over the 99%, with an achievable accuracy of $\pm 50 \mu\text{m}$. The approximate surface roughness expected for the part is equal to $R_a=12\div 18 \mu\text{m}$ [38], where R_a is the average roughness of the surface [54]. It must be underlined that that the surface finishing is highly influenced by the stair-stepping effect, so that the roughness for a curve surface is much higher due to this issue. In fact, the value reported on the EOS datasheet refers to a mean roughness of a flat (horizontal or vertical) surface.

The metal powder particles are commonly spherical with a diameter in the range between 12 and 22 μm [46]. The density of the material is around 8 g/cm^3 .

The principal mechanical properties of the as built and the heat-treated material at 20°C, as declared by the producer EOS, are provided in the following Table 4-2 [38]:

	As built	After age hardening [2]
Tensile strength [6]		min. 1930 MPa min. 280 ksi
└ in horizontal direction (XY)	typ. 1200 ± 100 MPa typ. 175 ± 15 ksi	typ. 2050 ± 100 MPa typ. 297 ± 15 ksi
- in vertical direction (Z)	typ. 1100 ± 100 MPa typ. 160 ± 15 ksi	
Yield strength (Rp 0.2 %) [6]		min. 1862 MPa min. 270 ksi
- in horizontal direction (XY)	typ. 1050 ± 100 MPa typ. 152 ± 15 ksi	typ. 1990 ± 100 MPa typ. 289 ± 15 ksi
- in vertical direction (Z)	typ. 870 ± 100 MPa typ. 125 ± 15 ksi	
Elongation at break [6]		min. 2 %
- in horizontal direction (XY)	typ. (13 ± 4) %	
- in vertical direction (Z)	typ. (12 ± 4) %	typ. (4 ± 2) %
Modulus of elasticity [6]		
- in horizontal direction (XY)	typ. 160 ± 30 GPa typ. 23 ± 5 Msi	typ. 180 ± 20 GPa typ. 26 ± 3 Msi
- in vertical direction (Z)	typ. 150 ± 30 GPa typ. 22 ± 5 Msi	
Hardness [7]	typ. 33 - 37 HRC	typ. 50 - 56 HRC
Ductility (Notched Charpy impact test)	typ. 45 ± 10 J	typ. 11 ± 4 J

[6] Tensile testing according to ISO 6892-1:2009 (B) Annex D, proportional test pieces, diameter of the neck area 5mm (0.2 inch), original gauge length 25mm (1 inch).

[7] Rockwell C (HRC) hardness measurement according to EN ISO 6508-1 on polished surface. Note that measured hardness can vary significantly depending on how the specimen has been prepared.

Table 4-2 Mechanical properties at 20°C for the as built and age hardened Maraging steel [38]

As it is shown in EOS datasheet, the material's resistance is dependant on the building direction. In fact, due to any possible defects in the weld between two consecutive layers the mechanical properties are lower along the vertical direction (Z). While for X and Y directions there are not any differences.

Several studies have been carried out to verify these values, analyzing the effect of the building orientation on the tensile and fatigue limit. Regarding the tensile tests, in different experimental researches it has been observed that contrary to what is reported in the EOS datasheet, there is

not considerable difference between the samples printed at 0° and 90° [55] [56]. Also for what concerns the fatigue solicitations, it has been observed by Croccolo *et al.* [57] it has been observed that the building orientation does not particularly influence the material performances. Moreover, they found that the fatigue limit can be estimated to be around the 50% of the ultimate strength. This data is really important for this research also because differently from other materials, the fatigue limit is not shown between the information that EOS has published for Maraging steel. In general, the mechanical properties seem to be more uniform whichever is the building direction for samples that have been subjected to a heat treatment, while the as-manufactured specimens have slightly differences, even if not as large as presented in EOS datasheet.

Being the low-carbon body-centered cubic (BCC) martensite structure relatively soft, it is common to subject the component to an ageing heat treatment that allows the precipitation of the intermetallic precipitates like Ni₃Mo, Ni₃Ti and Fe₂Mo phases, which allows to strongly enhance the mechanical properties of the material. For example, the hardness is increased from around 35 HRC (for the as-fabricated material) over 50 HRC [58]. In this way the hardness of the printed component is comparable to the hardness of components of the material, obtained with wrought technology. It must be considered that with higher brittleness the elongation of the samples is definitely reduced, with values that go from a 12,5% of elongation to around 2,5% [59] [58]. The ASM suggests a heat treatment between 470°C and 510°C for 3 to 8 hours [60]. Moreover, thanks to the precipitated particles that obstruct the movement of the material, it can be reached an ultimate tensile strength over 2000 MPa [58].

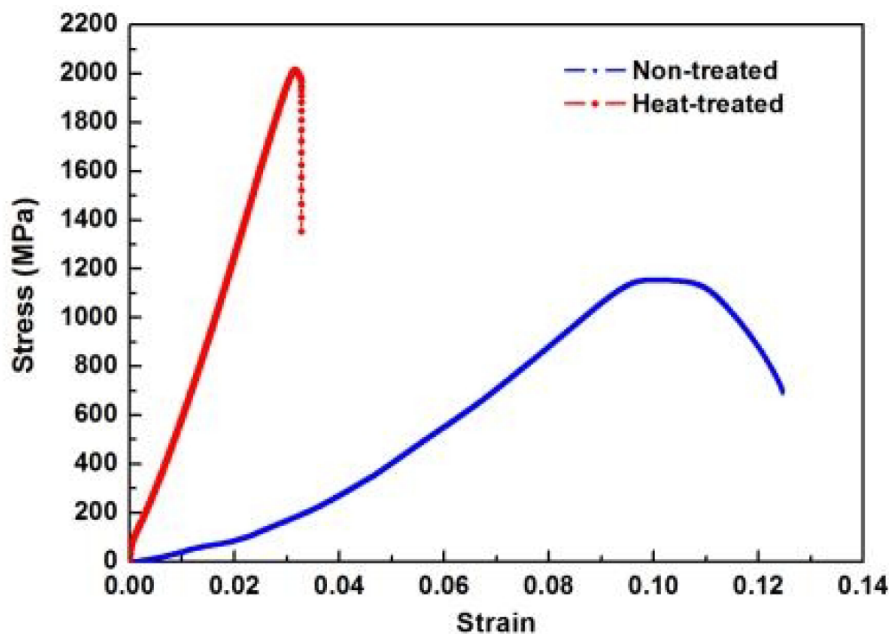


Figure 4-1 Engineering stress-strain graph of heat treated (red) and as-build (blue) MS1 specimens [56]

One aspect that must be considered when studying all these properties is the setup of the machine which is used for printing the samples used for running the tests. In fact, depending on the purpose of the printing, the process parameters can considerably change and hence also the characteristics of the printed parts. For example, the printing settings for pushing to the maximum the production's speed normally lead to higher porosity and defects, which causes a serious reduction in the mechanical properties of the final part. So, it is important to consider which is the setup of the machine, when talking about the final properties of the printed parts.

Consequently, several researches have studied the optimal process parameters that yield to the best mechanical properties [47] [61] [46]. It is important to consider that a balance must be found between the quality of the final parts and the productivity of the whole system, which depends both on the time and energy required for the printing.

The properties that are principally affected by the variation of the process parameters are porosity, hardness and roughness, while the microstructure seems to be not particularly affected [46]. The parameters that influence the final printed parts are mainly the scanning speed, the power and width of the laser and the layer's thickness. Fagali de Souza et al. [46] observed that the increase of the layer thickness has a higher influence on the building speed, in respect of the scanning speed. The printing accuracy is strongly dependent on the layer thickness, so it is clear that it cannot be increased excessively.

The producer of SLM machines, in order to raise the productivity, have consequently tried to increase the laser power and its scan speed. This latter, if risen too much, produces higher shear stress in the melted volume which leads to a bad quality of the surface finishing and more importantly to higher porosity. Also for the laser power there are some limitations, in fact if the energy adsorbed by the molten pool is too high, the penetration of this melted volume may reach lower layers, producing a structure called *keyhole*. This is a molten deep cavity that is a source of spatter formation and can trap some inert gas in its base, which after solidification will create a sub-superficial pore [62].

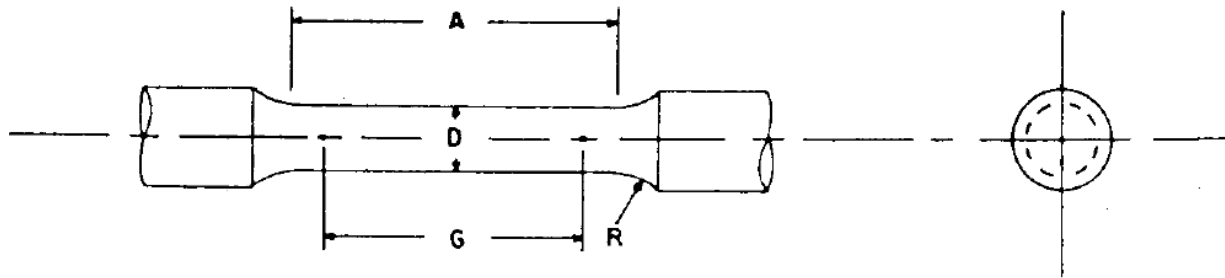
In different studies it has been estimated that the most efficient energy density is around 100 J/mm³ [52] [63]. Apparao et al. [53] observed that the best depositing process settings are, laser power: 260 W, laser scanning speed: 850 mm/sec and Hatching space: 0.12 mm. Other researchers that studied the optimum process conditions, considers as optimal parameters an energy density of 71.43 J/mm³, laser power of 300 W, scan speed of 700 mm/sec, and overlap rate of 40%. With these printing parameters were produced specimens with relative density of 99.8% and low roughness equal to Ra= 35 μm [61].

4.1 Verification of the tensile resistance of Maraging steel

Considering the high variability of the data that can be found in previous researches, it resulted to be convenient to verify the resistance of the material in order to guarantee a certain accuracy of the mechanical properties used to validate the new design of the component. To do so, some cylindrical specimens for the traction test have been printed.

The test has been performed thanks to the McMaster University's facilities, following the American standard ASTM E8M [64]. The E8M specimen are characterized by a gauge length (G) five times longer than the gauge diameter, with the latter equal to $D = 9$ mm.

The principal dimensions of the specimens are shown in the following Figure 4-2:



Dimensions, mm [in.]
For Test Specimens with Gauge Length Five times the Diameter [E8M]

	Standard Specimen Specimen 2
G —Gauge length	45.0 ± 0.1 [1.750 ± 0.005]
D —Diameter	9.0 ± 0.1 [0.350 ± 0.007]
R —Radius of fillet, min	8 [0.25]
A —Length of reduced section, min	54 [2.0]

Figure 4-2 Round tension test specimen dimensions [64]

The total length of the samples is 94 mm and the diameter of the clamping area is 14,4 mm. Since the samples have been manufactured with DMLS, the surface is rough. In order to guarantee a correct clamping of the gripping extremities, 4 extra mm have been considered on the diameter of these parts that are removed by a surface finishing operation.

The test specimens have been printed on a EOS INT M280 machine, based on the DMLS process, available at the McMaster University's laboratories.



Figure 4-3 EOS INT M280 3D printer [65]

In the following Table 4-3, are shown the principal specification of the EOS M280 printer:

Technical Data	
Building volume (including building platform)	250 mm x 250 mm x 325 mm (9.85 x 9.85 x 12.8 in)
Laser type	Yb-fibre laser, 200 W or 400 W (optional)
Precision optics	F-theta-lens, high-speed scanner
Scan speed	up to 7.0 m/s (23 ft./sec)
Variable focus diameter	100 - 500 μm (0.004 - 0.02 in)
Power supply	32 A
Power consumption	maximum 8.5 kW / typical 3.2 kW
Nitrogen generator	integrated
Compressed air supply	7,000 hPa; 20 m ³ /h (102 psi; 706 ft ³ /h)
Argon supply	4,000 hPa; 100 l/min (58 psi; 3.5 ft ³ /min)
Dimensions (B x D x H)	
System	2,200 mm x 1,070 mm x 2,290 mm (86.6 x 42.1 x 90.1 in)
Recommended installation space	min. 4.8 m x 3.6 m x 2.9 m (189 x 142 x 114 in)
Weight	approx. 1,250 kg (2,756 lb)
Data preparation	
Software	EOS RP Tools; EOSTATE Magics RP (Materialise)
CAD interface	STL. Optional: converter for all standard formats
Network	Ethernet

Table 4-3 EOS INT M280 technical data [66]

The 3D CAD model of the specimen has been imported on the software Magic [35] in a STL file format. Seven samples have been positioned in the software's building area, by specifying their position orientation and all the building settings.

Considering the lower resistance along the building direction (Z) that has been found in some of the researches (previously mentioned), the samples have been printed vertically to obtain the most critical result possible, as it can be seen in Figure 4-4. Another important reason to choose this orientation of the parts is related to the construction of the supporting elements. In fact, being the specimens built vertical, it is not required a complex supporting structure, as the base of the specimens has been connected directly with the building base. Moreover, it is important to not have any support connected to the lateral surface of the specimens, because the removal of the support structure would affect the surface. Due to this alteration, the tensile would not be valid. The position of the samples with this orientation allowed also to save some space, so that it has been possible to manufacture other parts with the same print. On the upside, being the specimens vertical, the time necessary to print them is the maximum, because it requires the highest number of layers and consequently the largest amount of powder. It should be considered that the powder can be recycled (as explained in Paragraph 3.3.2), so all the non-molten material has not been wasted.

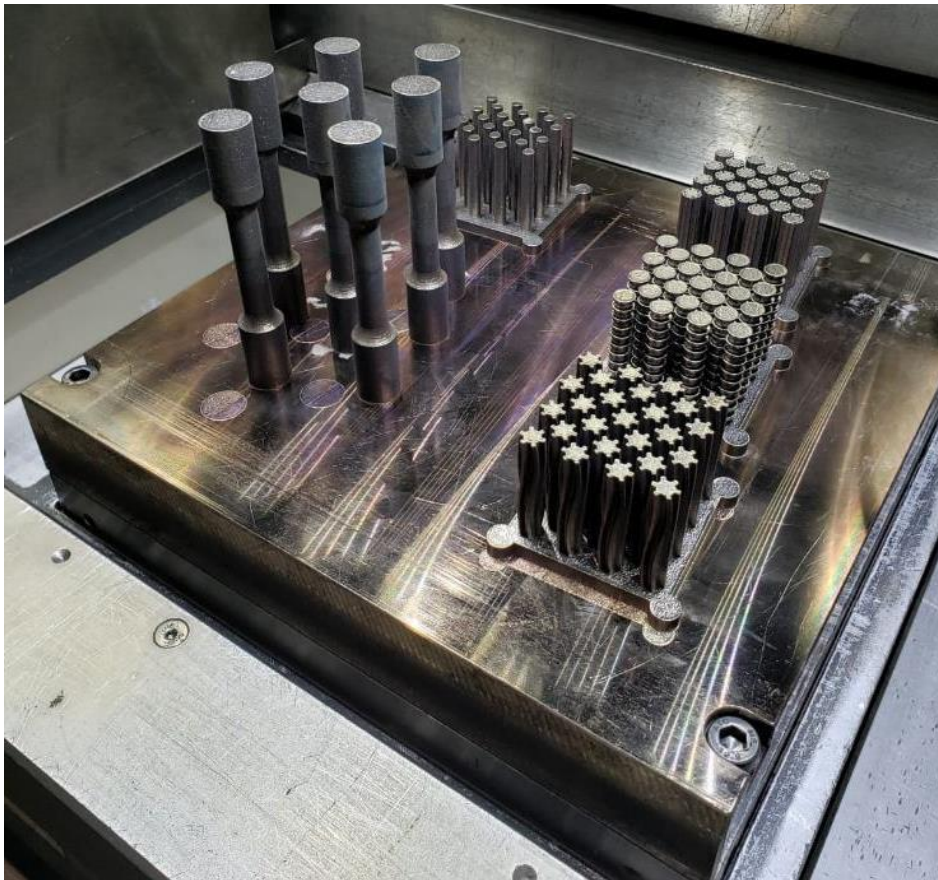


Figure 4-4 Tensile specimens on the building base

In order to detach the parts from the building base, being Maraging steel a hard material, it is not possible to do it manually, but it has been necessary to use a wire Electrical Discharge Machine (EDM).

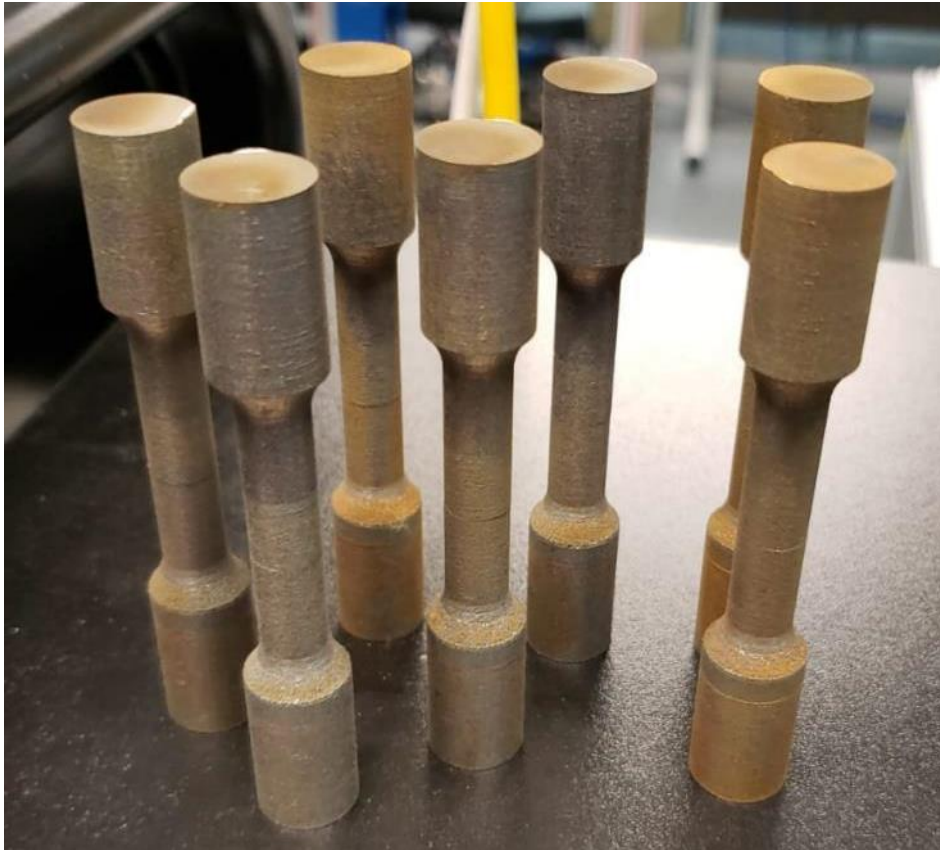


Figure 4-5 Tensile specimens

5 Topology optimization

Topology optimization is a mathematical method whose objective is to find the best distribution of material in a prescribed space, considering a various set of loads and boundary conditions imposed to the case of study. Based on a specific numerical problem, this tool allows to obtain the optimum shape of a structure. It is an iterative method in which each cycle is made by a FEA (Finite Elements Analysis) followed by an update of the design, generally obtained with gradient computation.

With the traditional design method, the shape of a component is commonly defined by intuition or based on older designs whose validity has been already verified. Nevertheless, in these days there is the interest in finding the best possible layout in the shortest time, allowing to save a lot of time and money in the projecting phase. This transformation is being driven even by an always growing ecological awareness for which the reduction of the used resources is a crucial factor.

The computer-aided design of structures was initially started in the 60's, in the field of civil engineering, whose objective function was to find the best cross-sectional area for the beams that were part of truss structures [67]. Nowadays this kind of optimization are only part of a smaller branch, commonly defined as shape optimization. Only after the publication (in 1988) by Bendsoe and Kikuchi of the seminal paper on numerical topology optimization this technology has experienced a terrific evolution [68].

Thanks to the continuous improvements in the computational power of the computers it is nowadays possible to simply solve complex studies, with the use of an iterative process based on the finite element discretization of the object domain and on the transformation of the differential equations system into an algebraic equations system.

In our days, the major field of application of this instrument are aerospace and automotive, in order to achieve generally weight savings. Whichever is the mean of transportation, it is known that the fuel consumption is proportional to the weight. In fact, it has been demonstrated that it can be achieved a reduction in the utilization of fuel around the 5% with a reduction in weight of the 10% [3].

However, even in the fields of the thermo-fluid dynamics, this tool is widely used, in order to achieve generally the smallest drop of pressure and specially the highest heat exchange rate. Some examples of this applications are the phase change material heat storage (PCM) [69] or the proton-exchange membrane fuel cells, also known as polymer electrolyte membrane (PEM) fuel cells (PEMFC) for which the objective is to have the most homogeneous distribution of current density throughout the surface of the fuel cell [70].

Moreover, the optimization tools are nowadays being used also in other researching fields like electro-magnetism, acoustics and MEMS (MicroElectroMechanical Systems) [27].

5.1 Types of optimization

The structural optimization field, can be divided into different branches:

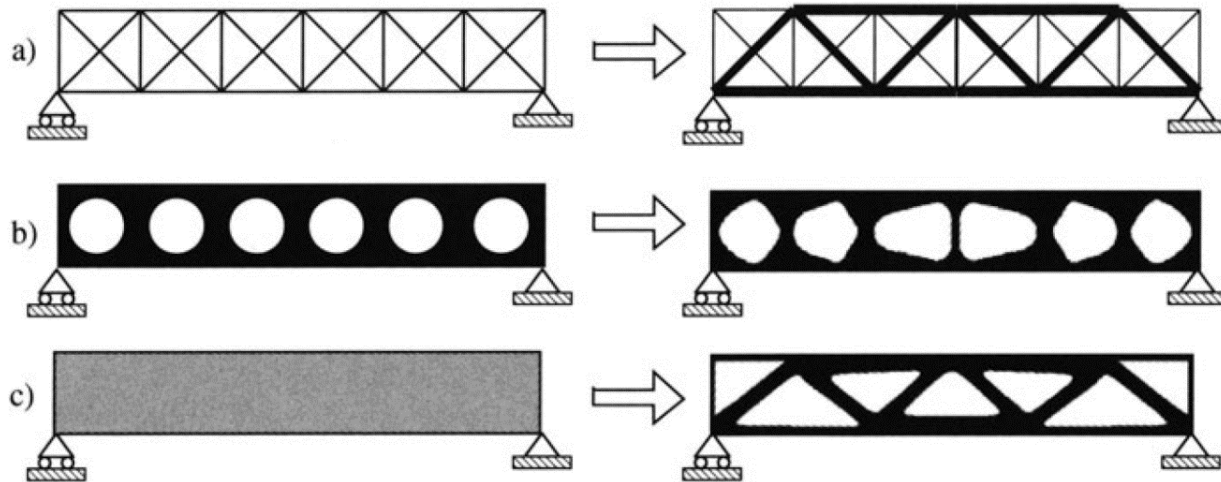


Figure 5-1 Comparing the application of sizing (a), shape (b) and topology (c) optimization on a struss structure [71]

- **Size optimization:** it is principally related to the design of truss structures. Commonly the total domain is predefined and fixed, so for example in the optimization of the structure of a bridge, (as shown in *Figure 5-1*) the objective is to find the best distribution of beams, reducing at the minimum the number of elements used, while guaranteeing a deflection of the bridge under a certain value. Another application of this method is related to the variation of the thickness distribution of a metal plate minimizing for example the compliance of the structure [27]. *Figure 5-1*
- **Shape optimization:** its goal is to optimize the shape of the domain, where the domain in this case is the design variable. As the name suggests, this optimization involves the modification of the shape of the structure, for example changing the geometry of the holes, radius fillets or chamfers, generally in order to reduce the concentration of stress in few narrow areas of the component. It is quite common to apply a shape optimization right after a topology optimization, in order to have a smoother surface, reducing the peaks of the stress.
- **Topology optimization:** this method in the past has been also defined as *layout optimization* or *generalized shape optimization* [72]. While in shape optimization, the holes inside can only be deformed, topology optimization can completely change the geometry of a component, by introducing or removing some holes or even combining the pre-existing holes. It is the most general but even most complex of the optimizations that have been described, so it is the most powerful tool that today is available. In fact, in the available softwares, can be used a wide variety of design variables, objectives and Boundary Conditions (B.C.).

With the aim of getting the best result from an optimization, the “design space” should be the largest possible, so that the optimization algorithm will be able to search for the optimum result. If the domain is reduced, the final result may not be the best one, as a geometrical restriction (like a hole) may produce a completely different shape (which probably is not the ideal one). In this thesis, the attention will focus on this kind of optimization.

5.2 Mathematical definition of the problem

The general optimization problem can be defined as follows:

$$\left\{ \begin{array}{l} \text{minimize } f(x, y(x)) \\ \text{subjected to } \left\{ \begin{array}{l} \text{equilibrium constraints} \\ \text{design constraints on } x \\ \text{behavioural constraints on } y(x) \end{array} \right. \end{array} \right.$$

Where:

f is the *Objective function*, which is the objective that should be minimized or maximized (depending on the application). Typically, this can be the compliance (inverse of the stiffness), the displacement of a specific point, the stress, the frequencies or even the volume (as it has been done in this thesis work, as shown in chapter 6).

It is possible to have more than one objective function, making the problem more complex. Especially in these cases, it results quite useful the concept of the Pareto optimality, which establish that a solution can be defined as Pareto optimal, if there are not any other solutions which may reduce an objective function, without increasing any of the other objective functions.

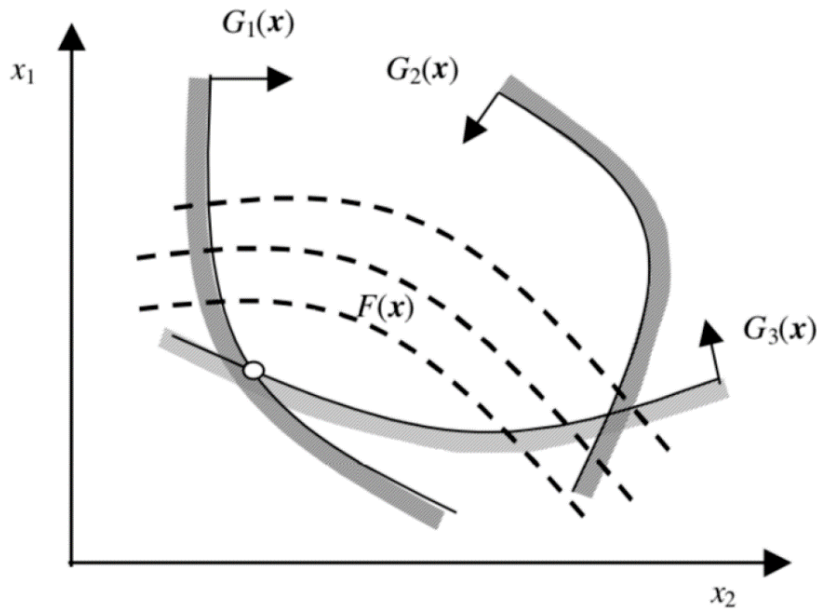


Figure 5-2 Graphical representation of Pareto optimality in a Multi-objective problem

One method used to find the solution for the Pareto theory is the *Scalarization method*, for which the multi-objective functions are transformed in a scalar function for the *Design variables* (\mathbf{x}). One example of the scalarization is to apply a weighted sum of the multiple objectives [73]:

$$\min_{\mathbf{x}} \sum_{i=1}^N w_i f_i(\mathbf{x})$$

Where f_1, \dots, f_N are the objective functions and w_1, \dots, w_N are the weights.

$\mathbf{y}(\mathbf{x})$ is the *State variable* that can be a function or a vector on which the response of the structure depends. Depending on the objective of the problem, it can be a stress, displacement, strain, volume or frequency.

\mathbf{x} is the *Design variable* vector: this parameter controls the layout of the design during the optimization cycles and it can be described both as a discrete or continuous variable. The design variables are collected in the vector \mathbf{x} and are scale factors of the elemental properties, so that there is one design variable for each finite element. The design variable may be linked to the thickness or the porosity. Instead of assigning a physical meaning to this variable, usually it has been preferred to consider it as a mathematical scale factor. The optimization will look for a final design, characterized by a scale factor that will be equal to 0 or 1, so that it will not be necessary a physical interpretation for the values between the two limits. The application of this filtering technique will be described in the following paragraph 5.2.1.

5.2.1 Penalization

The design space volume Ω^{mat} , is discretized in order to perform the topology optimization, based on the FEA (Finite Elements Analysis). The design variable that is commonly chosen for the optimization problems is the density, which is a function varying over the design domain. In the FE discretization the density is commonly approximated to be constant for each element, it results that the problem has one design variable per element.

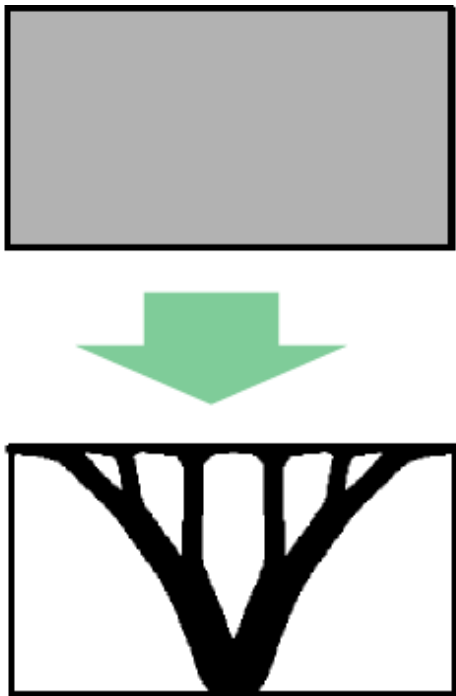


Figure 5-3 Before and after topology optimization [69]

As it is shown in the previous Figure 5-3, comparing the first and the last stages in an optimization, it can be observed that the total domain at cycle 0 is completely grey because the design must still be defined, in this condition, the density is supposed to have a fixed value that usually is 0.5 (that does not have a precise physical meaning). On the other hand, at the end of the process, it can be clearly distinguished the area where there is material (black) and where the space design is empty (white). During the evolution of the optimization, for each element it must be evaluated if it is necessary to have material in that precise point or not, thus the design variable which is used to do this verification is the density ρ , whose value can be between 0 (for the void area) and 1 (for the solid area). The density is a continuous variable and all the intermediate values of density, with $\rho \in (0; 1)$, represent fictitious material, being part of a “grey area”, lacking in a precise physical meaning.

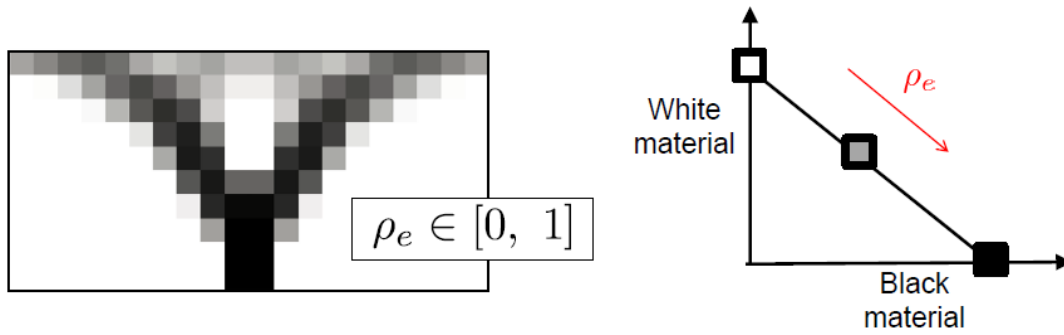


Figure 5-4 Density between the value 0 and 1

In order to have a more defined structure, different techniques (that are presented in the next paragraphs), have been introduced to penalize intermediate densities and to force the final design to be represented, for each element, by densities of 0 or 1.

5.2.2 Homogenization method

One of the first algorithm developed was the *Homogenization Based Optimization*, which considers the use of composite materials as the basis for describing the variation in space of the material properties. With this approach, the domain is seen from a microscopical point of view, as a periodical repetition of the same base cell. This microstructural model provides regularization of the topology optimization problem via relaxation of the design space, for which the mechanical properties of the single element can be representative of the whole structure, assuming a homogeneous material.

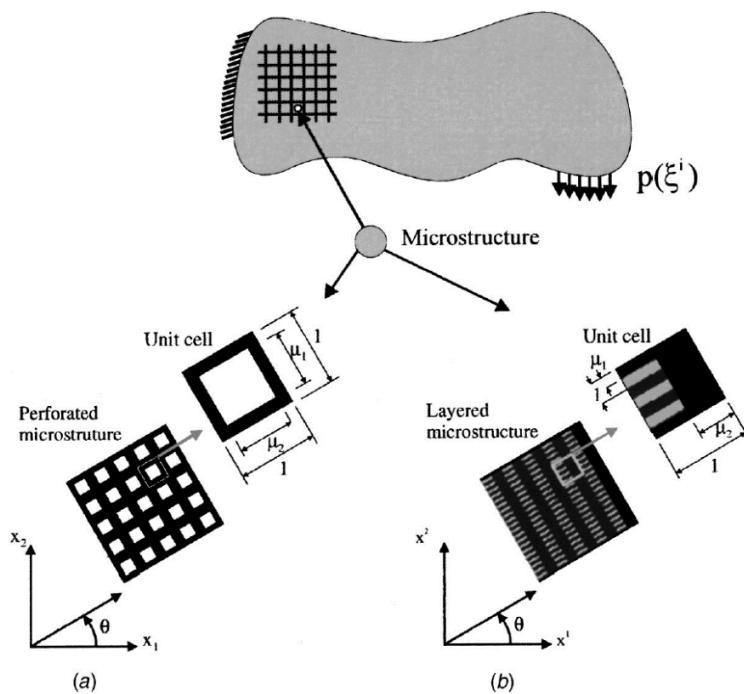


Figure 5-5 Homogenization approach: Microstructures elements as perforated squares (a) or layered rectangles (b)

The penalization of the intermediate densities, is obtained by defining a certain perforated microstructure for the basic cell, characterized by a solid and void part (of density respectively of 1 and 0) [72]. In this way, an extremely large number of infinitesimal voids are created inside the structure and it follows that more design variables per element are required than when using the density method, which will be described in the next paragraph. Moreover, one important limitation of this approach, is that it can be applied only using the compliance as a constraint or cost function [74].

5.2.3 SIMP method

In the last decades several algorithms have been developed, but the most successful has been the *Solid Isotropic Microstructure with Penalization* (SIMP). Its success is principally due to the great result it produces and the simplicity in the implementation in commercial finite elements codes. It was firstly introduced by Bendsoe [68] and the name was later suggested by Rozvany et al [75]. Initially, the SIMP model was developed with the aim of reducing the complexity of the homogenization approach, improving the capability of the algorithm to reach the convergence with a solution made only by 1 and 0 densities.

This model is even called *Power-law approach*, because the material property is given by the following power law:

$$E(\rho_e) = g(\rho_e^p)E_0 = \rho_e^p E_0, \quad g(\rho_e) = \rho_e^p$$

where E is the Young's modulus of the solid (isotropic) material and p is the penalization parameter. If $p > 1$ intermediate densities are penalized and hence 0-1 solutions are favored. Choosing a too small penalization factor, leads to the presence of a large percentage of grey area. On the other hand, for values of $p > 1$, the problem becomes non-convex, so it will have multiple local minima, and taking a p excessively high may cause a too fast convergence to local minima, so that the optimization will reach an end, but on the best result (global minima). It has been demonstrated in several papers, that the ideal number that ensures the most efficient convergence to an almost 0-1 solution is $p = 3$ [76] [77]. As it can be observed in the diagram of the following Figure 5-6, the densities are strictly linked to the value of the penalization power p , and it clearly illustrates that the use of the SIMP material model will force the topology design variable toward the limiting values 0 and 1.

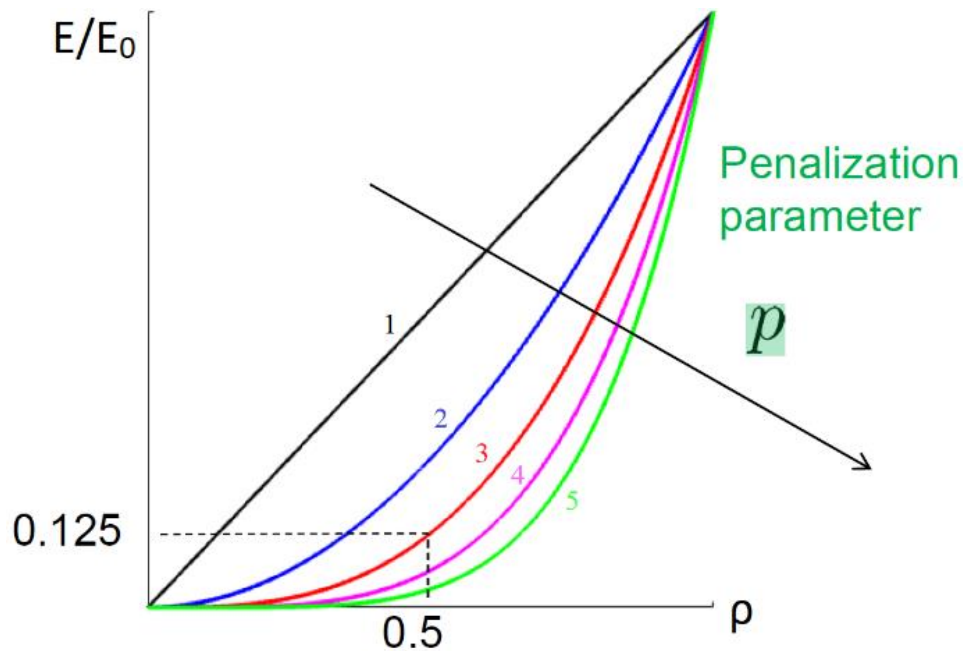


Figure 5-6 SIMP interpolation scheme

A drawback of the SIMP approach is that the topology optimization result is strictly dependent both on the penalization parameter and on the dimension of the finite element mesh applied. Regarding this last aspect, it can be observed in the following Figure 5-7, the high dependence of the final result on the mesh discretization. In this example, it is made a topology optimization of a beam, clamped on the left side and with a concentrated force on the other extremity, on the point on the principal axis of the structure (figure (a)). Three completely different results have been obtained by using the same exactly parameters, while changing only the mesh elements' size. It can be clearly observed that the finer is the mesh, the most precise can be result, characterized by really thin elements that when using a coarse mesh. The optimization (d) has an optimal result for several aspects like the deflection, the maximum stress (on the clamped boundary) and of course the volume. In fact, comparing it with the optimized part (b), the maximum stress is reduced by 7% while the volume by the 24%. This optimization has been obtained using the software Abaqus, which will be described more deeply in the next chapter 6.

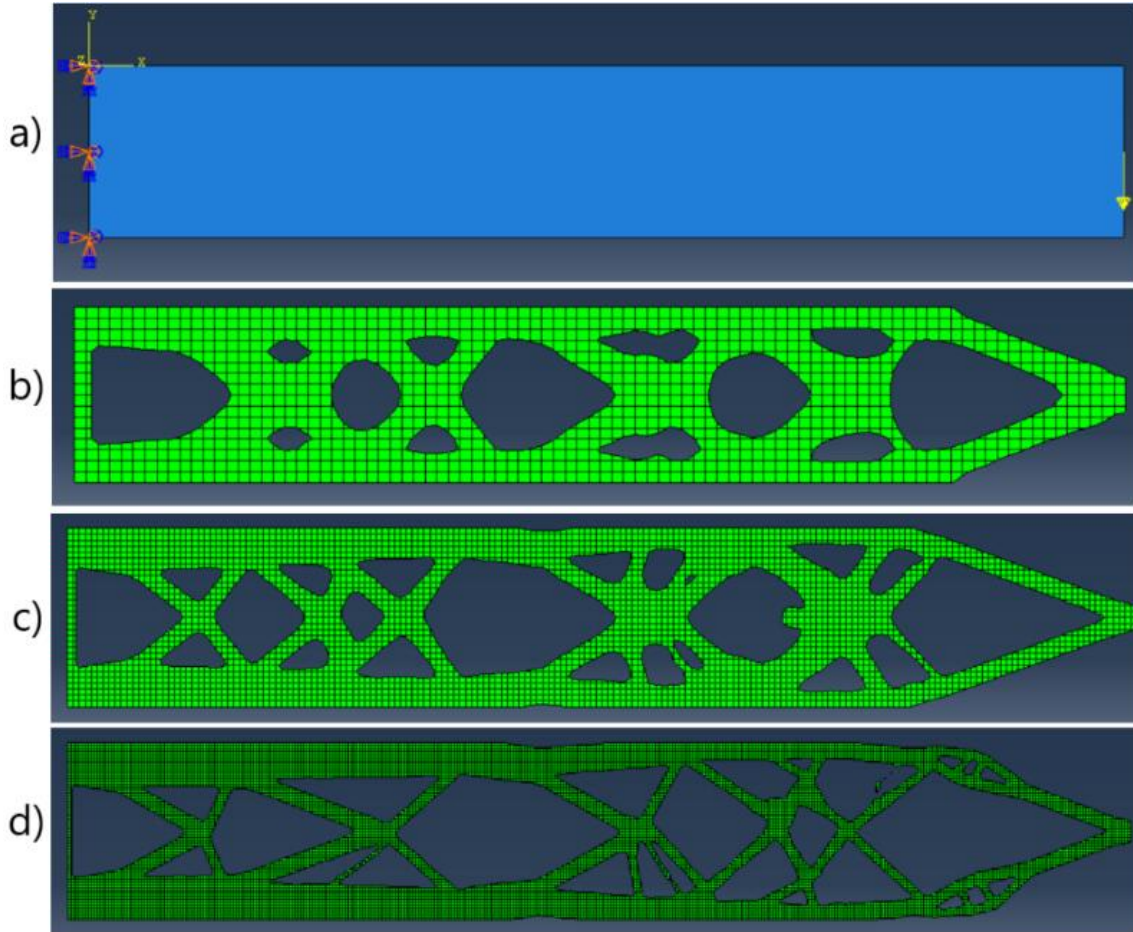


Figure 5-7 Clamped beam topology optimization: a) model; b) Result with mesh size 1; c) Result with mesh size 0,5; d) Result with mesh size 0.25;

In order to guarantee that the model is well-posed, in the definition of the problem it can be included a perimeter or volume constraint. The volume constraint can be defined with the following formulation:

$$\int_{\Omega} \rho \, d\Omega = \Omega_i^{mat} \leq V$$

Where V is the total volume of the initial design domain and Ω_i^{mat} is the volume at the i -th iteration of the optimization.

In the problem analyzed in this thesis, the focus is on the two variables stiffness E and displacement u . Considering the finite element discretization, E is supposed to be constant in each element.

The static equilibrium for a linear elastic material can be defined as:

$$K(\rho) u(\rho) = f$$

where $\rho = (\rho_1, \rho_2, \dots, \rho_N)$ is the vector containing the nodal density variables, N is the number of total nodes, K represents the global stiffness matrix, u and f are the displacement and load vectors. The global matrix K is composed by the elements' stiffness matrices K_e :

$$K = \sum_{e=1}^N K_e(\rho_e)$$

Where the element stiffness matrix can be defined in the following way:

$$K_e = \int_{v_e} B^T E(\rho_e) B dv_e$$

Where B represents the strain-displacement matrix, E is the effective elastic tensor and v_e is the volume of the e^{th} element [78].

In this thesis, the SIMP algorithm has been used in the application of the theory, and in the following two paragraphs are presented the two different approaches to the problem that were available on the software Abaqus, which has been used for the study.

5.2.4 Compliance problem

More than 90% of the researches on topology optimization for mechanical components have focused on the Compliance problem, which has the aim of minimizing the compliance of the structure, allowing to obtain a part characterized by high rigidity. In fact, the compliance is defined as the inverse of the stiffness ($C = \frac{1}{K}$)

The main reason of this attention on this algorithm, derives from its mathematical foundation that are quite solid and facilitated in the past a great improvement of the field [79]. The volume (or the mass) in this problem is not the objective function but instead a constraint. It can be prescribed as a constraint that it must be reached a reduction of the volume of a certain amount (for example a certain percentage of the initial domain's volume), or it can also be imposed a certain value \bar{V} that should be reached. The topology optimization problem for the minimization of the compliance with a constrained volume, can be defined as [71]:

$$\left\{ \begin{array}{l} \min_{\rho} C(\rho) = \frac{1}{2} f^T u \\ \mathbf{K} \mathbf{u} = \mathbf{f} \\ \text{s. t. } \left\{ \begin{array}{l} \sum_{e=1}^{n_e} \rho_e v_e \leq \bar{V}, \quad e = 1, \dots, n_e \\ 0 \leq \rho_{min} \leq \rho_i \leq 1 \quad i = 1, \dots, n_i \end{array} \right. \end{array} \right.$$

Where \bar{V} is the total volume function which cannot be exceeded, v_e indicates the volume of the single finite element and n_e is the total number of elements, ρ_i is referred to the i^{th} design variable, and ρ_{min} is a small positive number that must be defined as a limit to avoid singularity in the stiffness matrix.

5.2.5 Stress-constrained problem

Even if the solidity of the compliance problem cannot be questioned, it is not always the stiffness of a structure the main target of a study. In fact, in most of the practical applications, the fundamental requirement would be to have the lightest possible structure, which is able to sustain the applied load. So that, even though the rigidity of a structure is an absolutely important property, the first requisite is that the component does not exceed the failure limit. This optimization problem, may be written in a simplified way, as follows:

Minimize Mass

Subject to: $F(\sigma(\rho)) \leq 0 \quad \forall x \in \Omega$.

All the functions are defined in the global domain Ω . The function F representing the material failure, is function of stress field $\sigma(x)$ and strain field $\varepsilon(x)$.

It is generally more useful to have a global, instead of a pointwise failure criterion, because the whole component must resist to the loads. Applying a discretization of the domain (using the finite elements analysis) it will be necessary to have a local evaluation of the applied stress, so that with a large number of elements even the constraints on the numerical problem will be incredibly high. This is the principal aspect that makes this procedure much more complex and computationally demanding if compared with the Compliance problem, for which the check is global.

$$\left\{ \begin{array}{l} \min_x V = \sum_{e=1}^{n_e} \rho_e v_e \\ \text{s. t. } \left\{ \begin{array}{l} \mathbf{Ku} = \mathbf{f} \\ \sigma_e^{VM} \leq \bar{\sigma}, \quad e = 1, \dots, n_e \\ 0 \leq \rho_{min} \leq \rho_i \leq 1 \quad i = 1, \dots, n_i \end{array} \right. \end{array} \right.$$

In which σ_e^{VM} represents the equivalent von Mises stress of the e^{th} element, and $\bar{\sigma}$ is the prescribed limit for the stress (fatigue, yield, rupture or others), while the other variables have already been described previously. In order to compute σ_e^{VM} it can be considered a mean value of the stresses in the nodes of the element, or in a simplified way, it may be taken for the whole element the stress of a single node, by choosing the centroid element, which is defined as the super-convergent stress point [80]. Following this method, the element stress vector will be defined as [78]:

$$\sigma_e = \rho_e^s E B^c u_e$$

Where B^c is the strain-displacement matrix for the centroid element, u_e is the displacement of the e^{th} element and s is the exponent, that usually is equal 0,5 [81] [78]. The von Mises stress for the e^{th} element can be computed as:

$$\sigma_e^{VM} = (\sigma_e^T A \sigma_e)^{\frac{1}{2}}$$

In which A is a constant matrix that, for the plane stress has the following formulation:

$$A = \begin{bmatrix} 1 & -\frac{1}{2} & 0 \\ -\frac{1}{2} & 1 & 0 \\ 0 & 0 & 3 \end{bmatrix}$$

5.3 Softwares

In the last two decades, there has been a significant effort, in order to create commercial softwares for topology optimization. These tools determine an optimal topology according to the defined optimization problem independently of the designer, even if it goes without saying that the he/she shall support the interactive work in the design process. Firstly, setting up the optimization and secondly verifying the final result, since an isolated optimization calculation often does not yield an optimal result. Thus, it is important to include the designer's creativity and capabilities in order to find a structure that fulfills all the requirements, also those that cannot be imposed in the program.

The most used topology optimization tool packages have been principally implemented inside other commercial finite elements analysis programmes. This is mainly due to the fact that, having all the tools inside one single software makes it easier for the designer to move through the different stages of the designing process, instead of changing several programs which may lead also to some incompatibility issues. Topological optimization is probably one of the newest features incorporated in these softwares and it is attracting more and more designer, being still a fertile area of research. In most of these softwares, the offer seems to be relatively similar as most of the features and options coincide, for example most of them can solve problems with a wide range of objectives and constraints, both with static and dynamic responses. There can be found even some manufacturing constraints like symmetry, extrusion, draw direction (for casting), minimum and maximum member size, and lattice structure constraints. Unfortunately, until today, it has not been introduced the maximum overhang length constraint, which is fundamental for additive manufacturing technology [82]. Thanks to continuous developments of this technology, it is possible that in the next version these tools will be more connected with the additive manufacturing technology and its pro/cons.

5.3.1 Popular structural optimization programmes

In the next lines, some of the most common industrial softwares, will be briefly described.

Autodesk – Netfabb, has been bought by Autodesk in 2015. This software is particularly useful for additive manufacturing, in fact it is mainly focused on the printing operation (similar to **Magics**) rather than the designing and FE simulations. In fact, the simulation and optimization tool, was introduced only few years ago and it has several limitations. But in the AM field it may be advantageous since it includes some feature like the definition of the best position for the print on the building plate, the construction of the supporting elements and other specifications that in the other programs are absent. From the simulation point of view, the program is slightly limited if compared with other softwares [83].

Altair – Hyperworks Optistruct published in 1994, was one of the first structural optimization tool developed, and today it is still one of the most used in the industrial field. It is quite complete, including some particular features like minimum member size, maximum thickness, draw direction, patterning, extrusion constraints, and pattern grouping. Altair offers even a second

software for topology optimization called **Inspire SolidThinking** mainly designed for designers who want to get a quick result from the optimization, as the software automatically produce a mesh. Of course, even if it provides an user-friendly interface, this software is quite limited as it only allows to deal with static loads (forces, pressures and restraints) [82] [84].

Ansys is a quite famous multiphysics simulation software, in which the topology optimization solver, was introduced only in recent times. Being principally developed for FEA, it offers a complete package, including different kind of structural optimizations and a wide range of constraints. One negative aspect is that the manufacturability restrictions are practically missing, even if in this thesis project, these constraints were not necessary [85].

MSC - Nastran/Siemens Unigraphics - NX: Nastran is a quite famous structural FEA software, initially developed in the '60s for the American aerospace agency NASA. It offers a large number of analysis and the structural optimization tool allow to obtain size, shape and topology optimizations. After purchasing the software, Siemens introduced the Nastran's packages in its well-established CAD software NX [86].

Finally, **Dassault Systemes - Simulia Abaqus TOSCA** is with Hyperworks Optistruct, Ansys and Nastran one of the most complete software. Initially, Dassault Systemes, with the collaboration of **FE Design** that developed the optimization software TOSCA, introduced in 2011 the *Abaqus Topology Optimization Module (ATOM)*, which was already able to deal with both implicit and explicit optimizations. The TOSCA Structure optimizer can be used even with other FEA platforms, and it is considered one of the most reliable in the market. After the acquisition of the FE Design company from Dassault Systemes, the complete potentiality of TOSCA has been introduced in Abaqus CAE.

Initially, this thesis work was started using the Student license for Hyperworks, but having the availability of the complete software of Abaqus (with TOSCA) on a server, it resulted to be more convenient to move to this software, due to the computational power that is required for the optimization process. A deeper description of the Abaqus platform is consequently proposed.

5.3.2 Abaqus

Compared with Hyperworks, Abaqus is more user-friendly, because the definition of the analysis is more linear and simplified. This comes with a drawback as due to this streamlining, Abaqus has less options and not every operation that is available in the other program can be accomplished. Despite this, Abaqus seems to be complete enough to carry out complex analysis.

One of the advantages of Abaqus FEA is that it offers a complete suite of programs and functions which make it easier the passage from modelling, analysis, results visualization and post-processing. The suite is made by several programs [87]:

- **Abaqus/CAE** (Complete Abaqus Environment, same acronym of Computer Aided Engineering) which is a complete environment where the whole analysis can be defined, carried out and verified.
- **Abaqus/Standard** that is a FEA based on an Implicit integration method, useful for solving static and low-speed dynamic problems.

- **Abaqus/Explicit** that is another FEA based on an Explicit integration scheme; it is recommended for non-linear problems that involve complex contact with high deformations, so with transient dynamic analysis. The two solvers Implicit and Explicit can be combined, using the solution of one of them as the starting point for the other.
- **Abaqus Multiphysics**: like other similar FEA software, Abaqus can deal with Multiphysics problems, with the possibility of combining mechanical, fluid dynamic, thermal and electromagnetic fields.

The Abaqus/CAE main window workspace is quite intuitive, and it is composed by these subsections:

- Viewport: in this area different windows can be open, where the software shows the model, so it is an output area;
- Context bar: allows to choose on which Module of the model the user wants to work;
- Toolbox area: depending on the module in use, several options of the screen may change and in particular the toolbox area allows a quick access to the most used functions linked to the current module;
- Model/Results Tree: it provides an overview of all the aspects that have been defined for the model in the form of tree nodes, allowing also to quickly navigate through the module;
- Prompt region: when using some functions, in this area there may appear some messages to interact with the user, showing instructions to follow and suggesting further commands;
- Message area: in this zone Abaqus shows some messages which can be both status information and warnings. It presents also a command line interface where Python commands can be entered being the whole program based on Python scripting language.

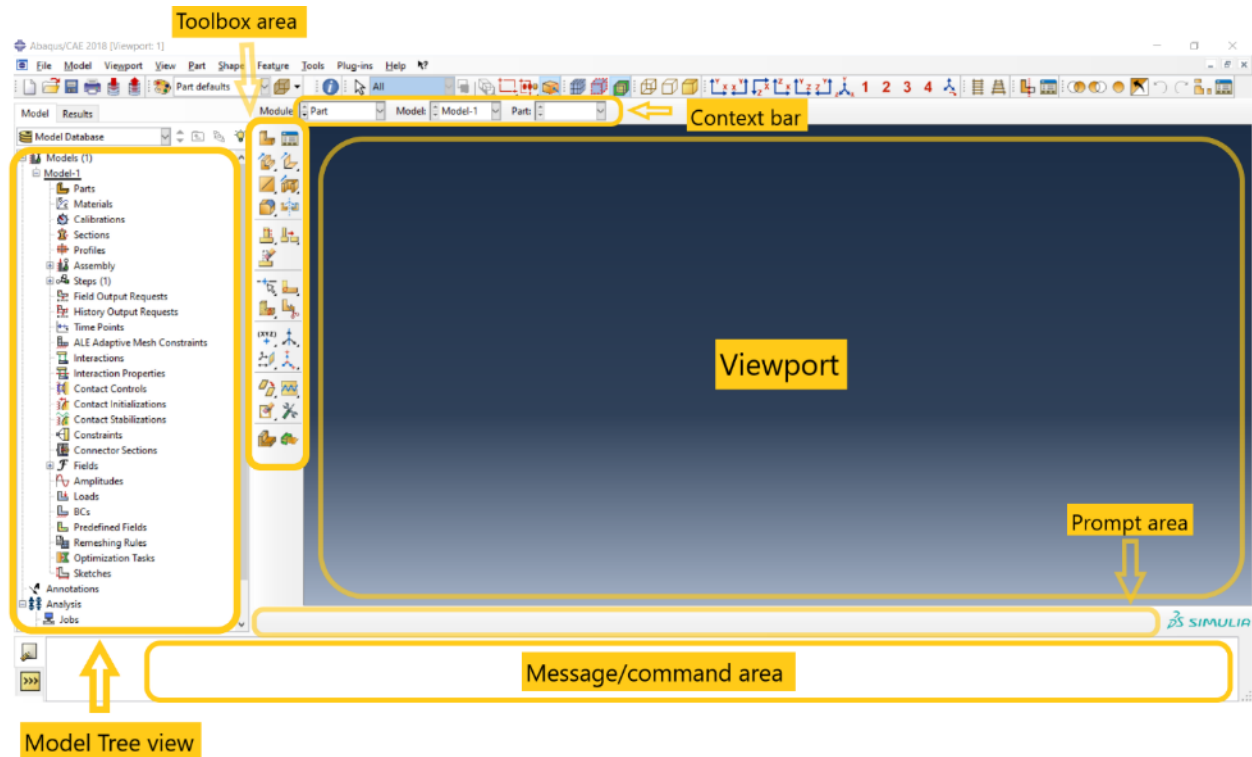


Figure 5-8 Abaqus/CAE workspace components

The definition of the model, as previously said, is based on different modules that shown in the next Figure 5-9, each one referring to a different aspect for the complete setup of the analysis. As it can be seen, there is a complete module dedicated only to the optimizations that can be of four different types: topology, shape, sizing or bead. In this thesis it has been used only the topology optimization.

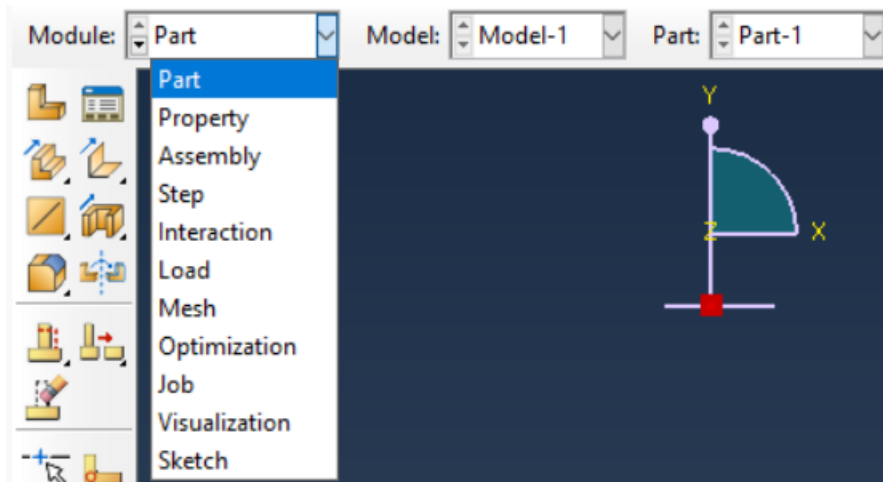


Figure 5-9 Abaqus modules

Further details regarding each module is provided in the next Chapter 6, where, following the modules order, it is explained, the process for the definition of the optimization.

6 Re-design of the suspension mounting

In the following chapter, all the different stages for the re-design of the component will be shown, like the definition of the design space, the fundamental data for the setup of the optimization and the validation of the final design.

The objective of the study is to redesign an existing steering knuckle, reducing to the minimum the weight, but maintaining the level of the stress under the prescribed limits. The original part made of an aluminum alloy, is fabricated by casting and some subsequent processes. Cast process is known to have several limitations, on the other hand, the part will be redesigned to be made in Maraging steel (whose properties has been described in Chapter 4) and will be printed with the Direct Metal Laser Sintering technology (with a EOS M400 machine) exploiting the reduced constraints that an additive manufactured product has.

Moreover, it takes advantage of the potentiality of topology optimization, which allows to obtain a lighter structure able to resist to the numerous load cases that are considered. The starting point for a topology optimization, is the creation of the design space, as it is described in the following Paragraph 6.1.

6.1 Definition of the design space

The **design space** is defined as the closed volume (if working in 3-dimensions), which forms the boundary for the topology optimization. Generally, if the objective is to redesign an existing component, the design space is a simplified and enlarged volume with respect to the volume occupied by the original part, with all the existing holes filled with material.

In order to guarantee the maximal freedom to the optimizing software, the design space must be defined as the largest possible. In fact, if the designer defines a volume smaller than the maximum available volume, because of a possible shape he may have already thought about before the optimization, this reduces the number of possible solutions that the software can look for and eventually even preclude the optimal result. On the other hand, a minimum concern must be applied on the definition of the design space, as obviously if there are not boundaries, an infinite area cannot be prescribed.

Moreover, the larger is the volume the higher will be the number of finite elements, and of course the computational cost. Furthermore, even the time necessary for the process will rise dramatically. Consequently, the designer must be able to find a compromise between the completeness of the analysis and the computational cost of the optimization, with the aim of not excluding the path that may lead to the optimal configuration.

During the definition of this volume, there may be some surfaces or part of the volume which should be excluded from possible modification introduced during the optimization, so that in these areas no material is removed; these are defined as the **non-design spaces**.

The following Figure 6-1 shows the design space, which has been defined for this project.

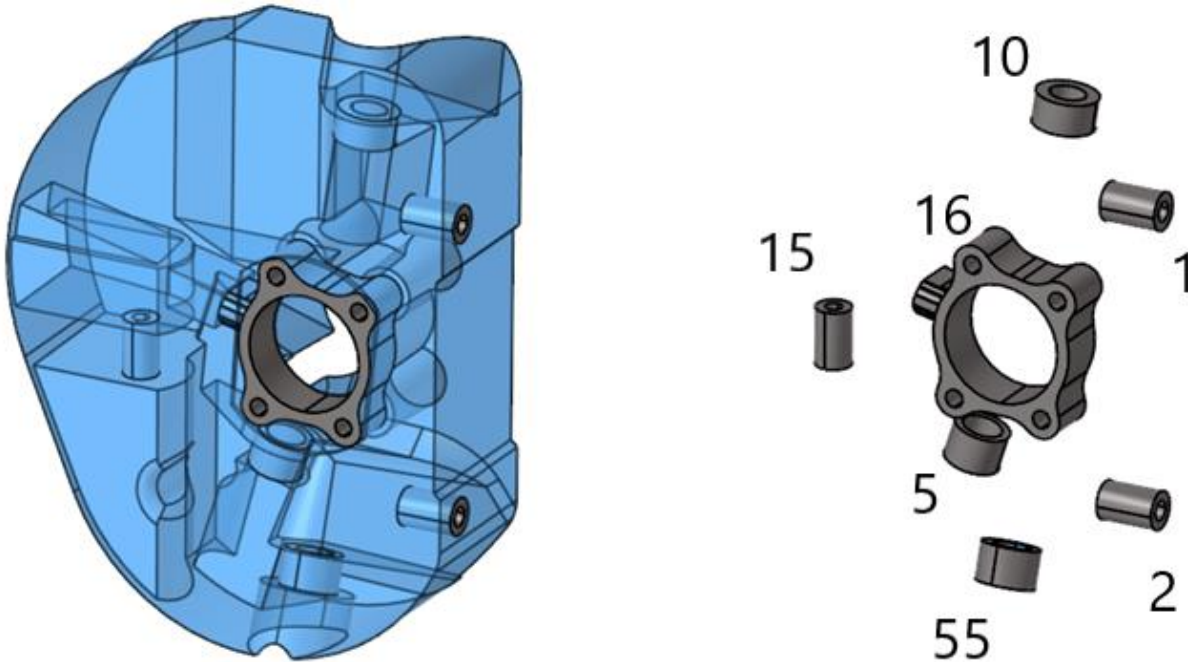


Figure 6-1 Design space and non-design space

As it can be observed, in this case there are 7 elements of the volume that are excluded from the space design. These elements even if they are not interested by the topology optimization, are obviously necessary and are part of the finite element analysis (which is done at each cycle of the optimization to verify the stress on the part, after some finite elements have been removed in the design space).

All these non-design volumes are the contact areas of the component with the other components of the suspension system. For each non-design element, it is taken a precise point outside the volume that is coupled with the internal surface of the hollow cylinders, on which the forces or the boundary conditions are applied (this will be explained more accurately later). The numbers that are shown in Figure 6-1, identify these points but, to simplify the discussion, it has been used the same numeration to refer to the non-design elements.

Comparing the original component and the constructed design space, the non-design areas are the onliest that the two parts have in common and these areas will remain unchanged during the optimization. This is necessary to guarantee a seamlessly assembly of the re-designed steering knuckle with the rest of the suspension systems. In the following list, the role of each connecting part is described:

- 1, 2: are the connecting elements of the brake caliper

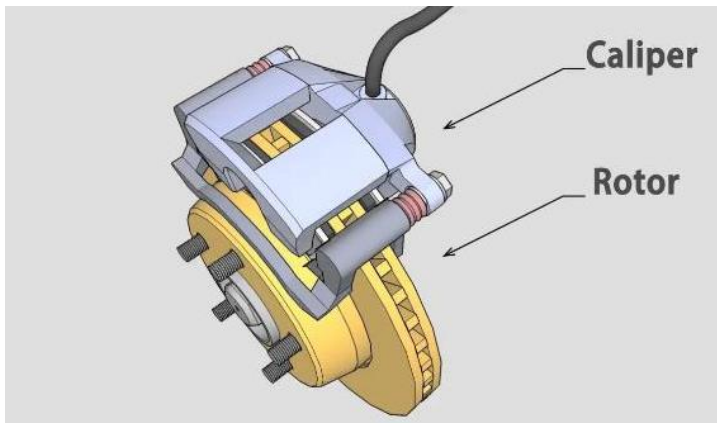


Figure 6-2 Brake caliper

- 5, 55: these points are connected to the lower arms of the suspension
- 15: it is the connecting element with the steering arm
- 16: the internal surface of the largest hole is the wheel's bearing housing; this non-design part is more complex than the other, because it includes also the 4 holes for the bolts, necessary to assembly the bearing. Moreover, this component includes on the side also the housing for the ABS control sensor, as shown in the Figure 6-3:

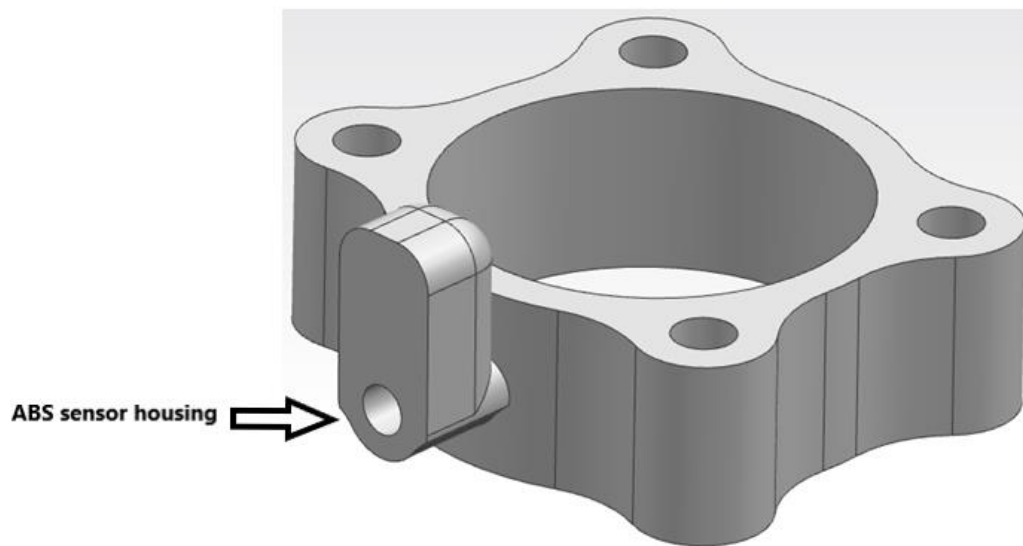


Figure 6-3 Non-design part (16): bearing housing and ABS sensor housing

The space design has been defined, working on the CAD software NX Siemens Unigraphics. As it can be observed in the previous and next pictures, the geometry is quite complex. Theoretically for a topology optimization it is better if the starting design space is a massive full solid, but for this study there are a large number of constraints, so considering all these limitations the largest possible volume has been taken.

The constraints that it is necessary to consider, are mainly related to the assembly and to the correct functionality of the whole system. For example, it has been left the space for mounting all the bushing, this can be easily seen for the non-design parts number 10 (the one at the top) and 15, but it is valid for all the others.

In the upper part of the element number 15, the hole reaches the housing for the ABS sensor, as it can be seen on the (d) view of Figure 6-4.

Moreover, for the assembly of the wheel bearing, on the internal part of the steering knuckle (that is shown in the views (b) and (c) of Figure 6-4), it has been left the space for positioning the bearing itself as well as the space for the screwdriver for the tightening of the four bolts of the bearing. Finally, it is important to consider the maximal angle of movement of the arms in respect of the steering knuckle. As is evident for the elements 10, 5, 55 and 15, it was left the space for the free movement of the arms, avoiding any collision with the component. The space design was limited on the upper and lower part, even from the dimension of the car's rim (17"), and on the external part by the presence of the brake disk.

After building the design space, the part has been imported into the Abaqus code, for defining all the parameters, necessary for the FE analysis.

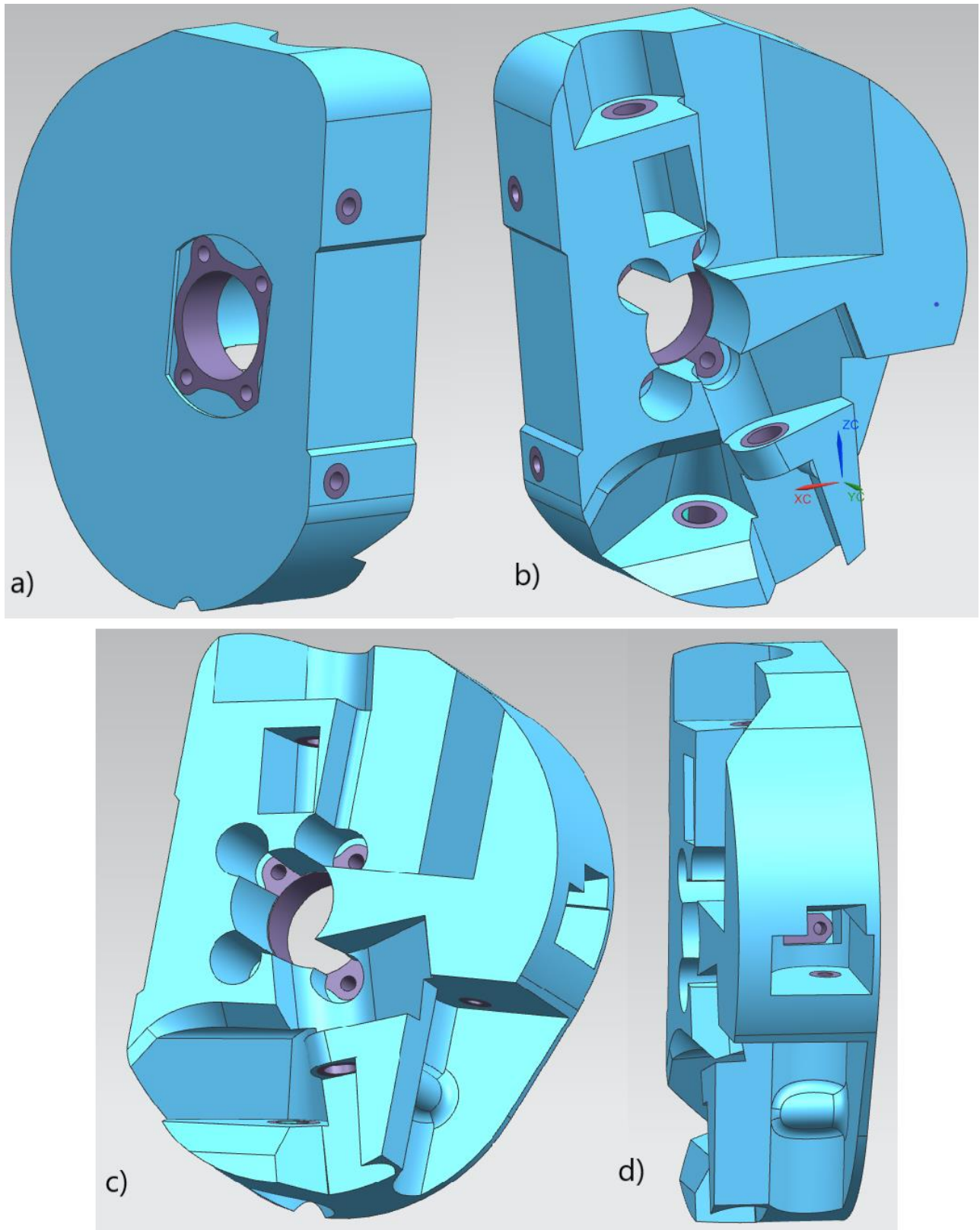


Figure 6-4 Different views of the space design

6.2 Adjusting the part

After having imported the part on Abaqus, it resulted to be convenient to reduce the complexity of the analysis, by combining all the non-design elements with the design space, having only a single part left. In fact, by keeping as different parts all the non-design elements it would have been necessary to define a contact behaviour with the design space (a *tie* constraint between the shared surfaces of design and non-design) that used to increase the computational cost of the analysis. Instead, all the non-design parts were eliminated and reconstructed as partitioned volumes of the design space, having finally one single component. This was done, by exploiting the *partition cell* function, which allows to divide one single cell into two, so defining an internal boundary, while maintaining them as part of the same component.

This partition function when designing with Abaqus is quite important, as it allows to obtain the best quality and uniformity for the mesh if a component is correctly partitioned in several almost basic geometries. Being the component quite complex, it has not been possible to partition the whole component in a set of sub-cells of basic geometric solids. Nevertheless, the partition function turned out to be quite useful as only one part was left, even if the non-design, being different cells, could be excluded from the optimization process.

After several attempts, necessary to get the best result from the optimizations, it resulted that some areas of the design-space were not interested by any load and were always removed from the optimized parts, no matter what the defined parameters were. So, considering the large size of the part, and the limited computational power, these areas were eliminated from the initial design space. In this way, the total number of finite elements was reduced, and consequently it has been possible to reduce even more the mesh size, which was not small enough to get a smooth and precise result. In fact, as previously explained in the paragraph 5.2.3, the SIMP method for the topology optimization is highly dependent on the mesh size [88]. In the following Figure 6-5, it can be seen the modified design space, whose volume is around the 85% of the initial design space volume, shown in the previous Figure 6-4.

The CAD available on Abaqus does not have all the functions that a complete CAD program like NX or Solidworks have, but it has proved to be enough for the task.

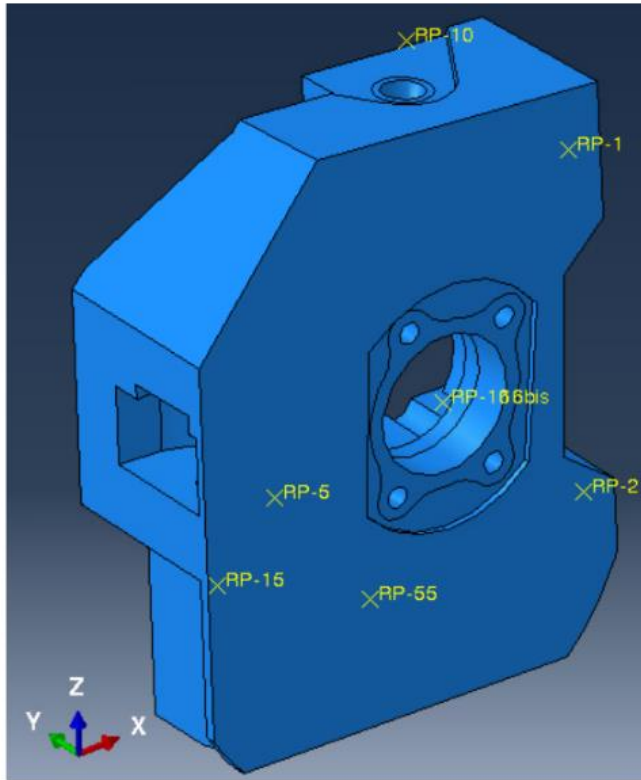
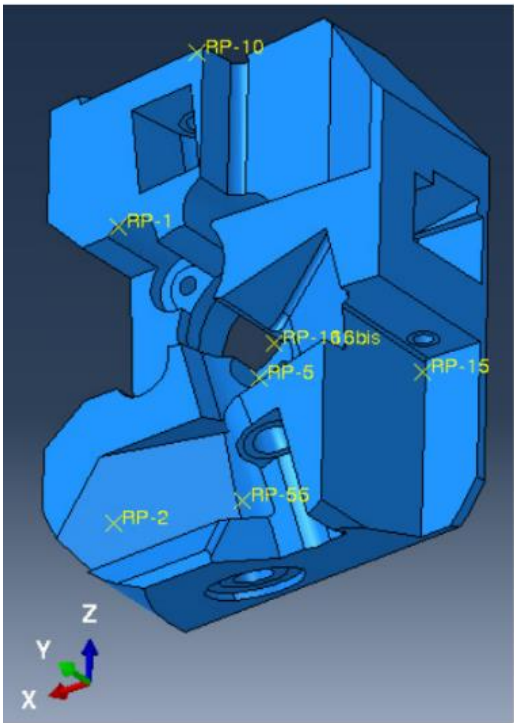
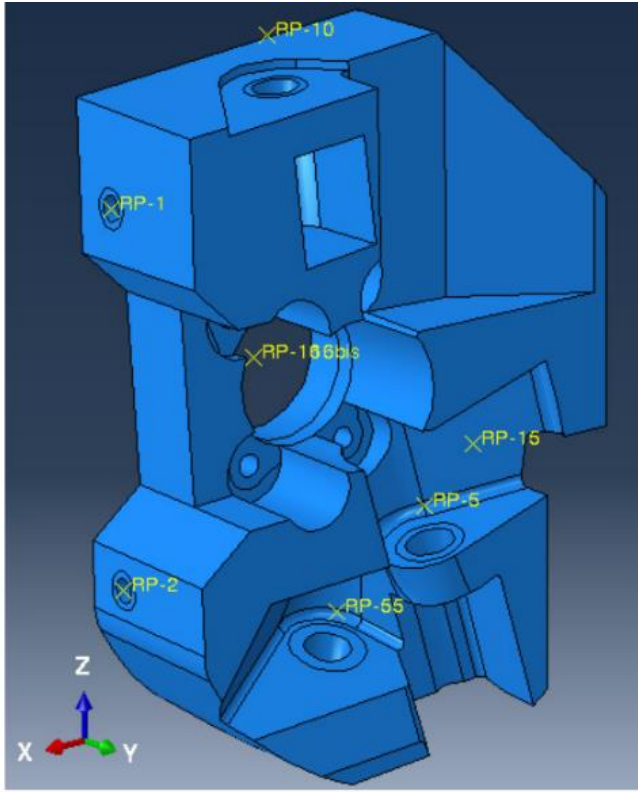


Figure 6-5 Modified space-design

6.3 Material properties

As it has been thoroughly explained in the chapter 4, the material that is chosen for the analysis is a Maraging steel. Abaqus can deal with a truly large number of material properties, and of course it has not problem with the non-linearity of the material. However, the plasticity cannot be considered in the precise type of analysis that was used (*Static, Linear perturbation*). Luckily, for this study the required limits for each step of the analysis were the fatigue and yield limits, so it has not been essential the use of the plastic behaviour. The software works without unit of measurement, but all the properties must be coherent. In the following Figure 5-1 are shown the different possible combination of unit of measurement for the basic quantities:

Quantity	SI	SI (mm)	US Unit (ft)	US Unit (inch)
Length	m	mm	ft	in
Force	N	N	lbf	lbf
Mass	kg	tonne (10 ³ kg)	slug	lbf s ² /in
Time	s	s	s	s
Stress	Pa (N/m ²)	MPa (N/mm ²)	lbf/ft ²	psi (lbf/in ²)
Energy	J	mJ (10 ⁻³ J)	ft lbf	in lbf
Density	kg/m ³	tonne/mm ³	slug/ft ³	lbf s ² /in ⁴

Table 6-1 Abaqus consistent unit of measurement [89]

In this model being the part dimensions in mm, the consistent units are the one of the second column of Table 6-1. The onliest material properties that are necessary for this analysis are:

- Young's modulus $E = 160000 \left[\frac{N}{mm^2} \right]$
- Poisson's Ratio = 0,31
- Mass density $\rho = 8 \cdot 10^{-9} \left[\frac{tonne}{mm^3} \right]$

These properties have been assigned not only to the design space cell, but also to the non-design cells (thanks to the function *Assign section*).

6.4 Assembly

Having combined the non-design elements with the central volume, only one part was left, and it has not been necessary to assemble any part. The onliest procedure has been the one defined *Create instance* that is necessary to import the part, for continuing the analysis definition process.

6.5 Interactions

In the interaction module, it is possible to define the type of contact between the surfaces of two different parts. Initially, when the non-design elements were considered as separate parts it was used the *Tie* constraint function, connecting the external surface of the non-design parts, with the respective internal surfaces of the design part.

In this project the onliest required interactions were those between the points of application of the forces, and the respective surfaces on which the forces are in reality applied. The exact position of the points and the respective forces were provided by Maserati.

These points have been inserted as *Reference points* in the program, by defining their coordinates.

The type of interaction that has been used is the *continuum distributing coupling*, which constrains the motion of the coupling surfaces (or nodes) to the translation and rotation of the control node [90]. The constraint distributes the loads so that the resultants of the forces (and moments) at the coupled nodes are equivalent to the forces and moments at the reference point. For each coupling, all the degrees of freedom were constrained, so that the nodes cannot translate or rotate in respect of the surfaces.

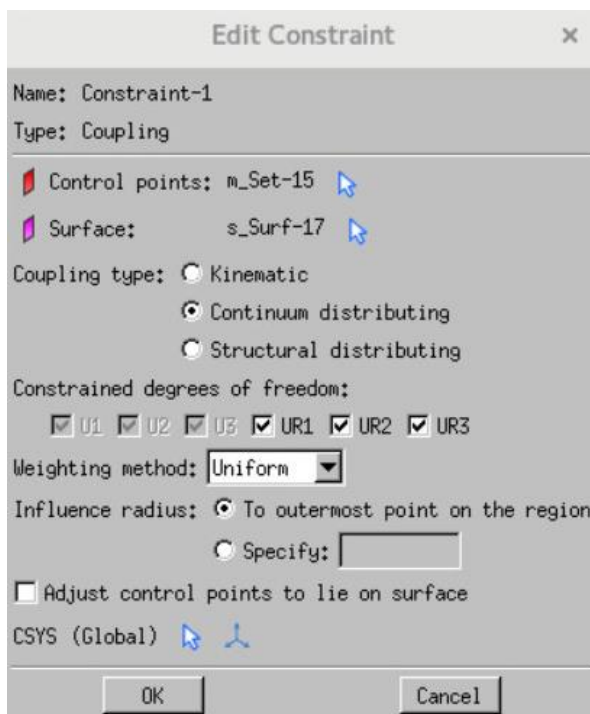


Figure 6-6 "Edit constraint" window

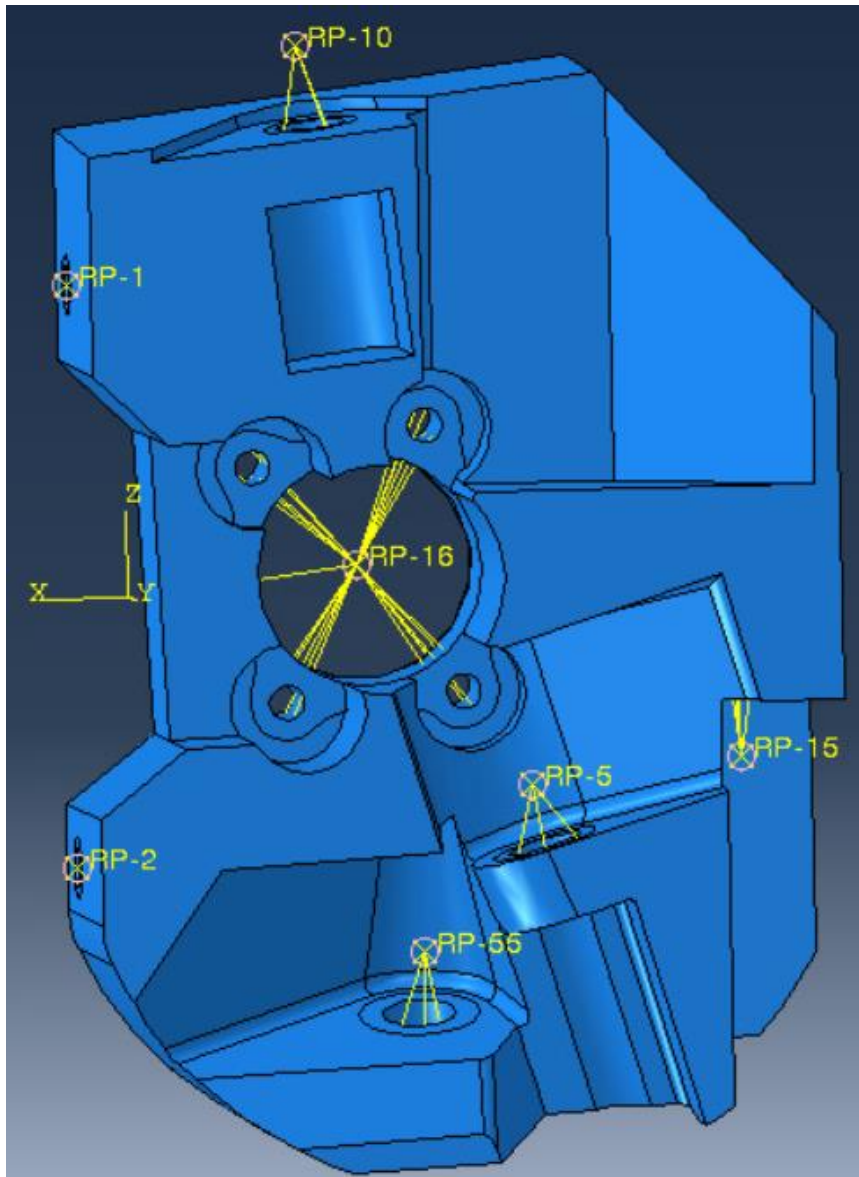


Figure 6-7 Interactions between reference nodes and non-design surfaces

Due to a limited graphical power of the computer, each constraint in Figure 6-7 is represented just by few lines that connect the reference points with the respective surface. This is only a visualization issue, as the reference points are connected uniformly to the whole area of the surface.

It is interesting to highlight the particular constraint that is applied at node 16. It is connected (as shown in Figure 6-8) to a small surface with height of 4 mm, where there will be the housing on the bearing. Due to the kind of assembly obtained by a flange connection, a large amount of the load will be adsorbed by the 4 bolts necessary for the mounting of the bearing, so even these 4 surfaces have been included in the coupling.

Moreover, it was created a second node coincident with node 16, 16bis, which is not constrained with the bearing surface and its flange bolts, but it is linked with a continuum distributed coupling with the nodes 1 and 2 that are the connecting elements of the brake caliper (Figure 6-9). In this

way, applying a torque in the point 16bis, it is possible to simulate the stress caused by an emergency braking on the component. In the following figures it can be noticed that some elements are highlighted in red and purple colour. During the definition of the constraints, the software highlights the master surface/point in red, while the slave in purple, in order to distinguish them more easily.

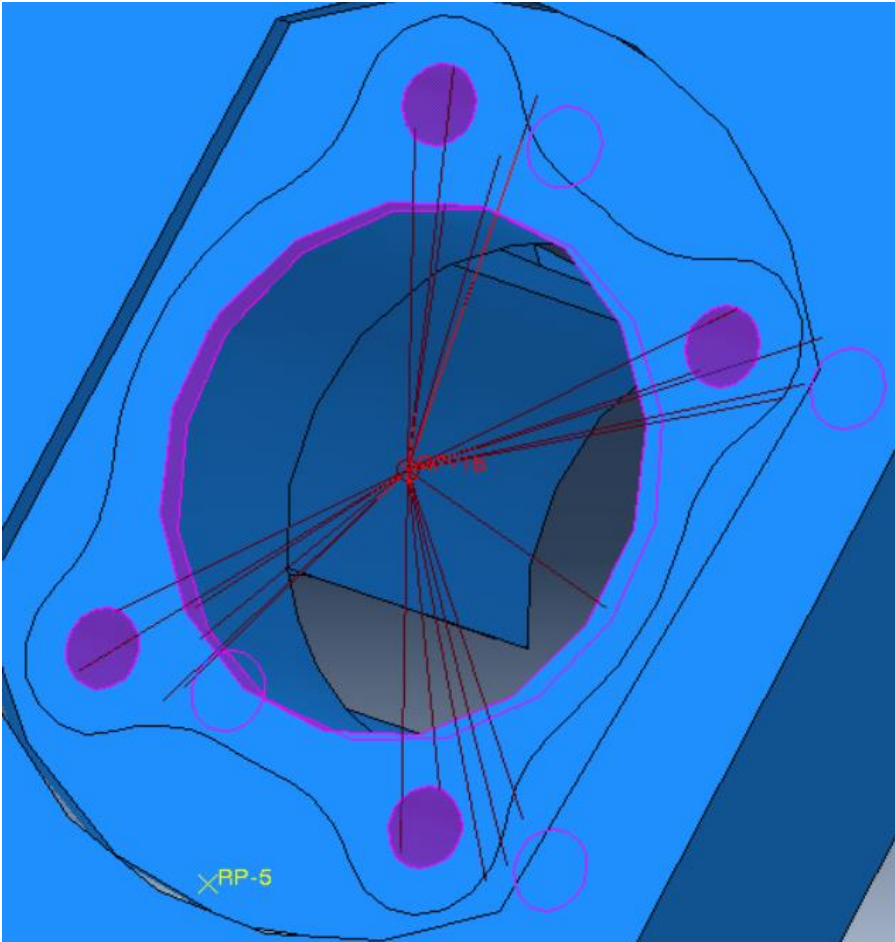


Figure 6-8 Interaction node 16

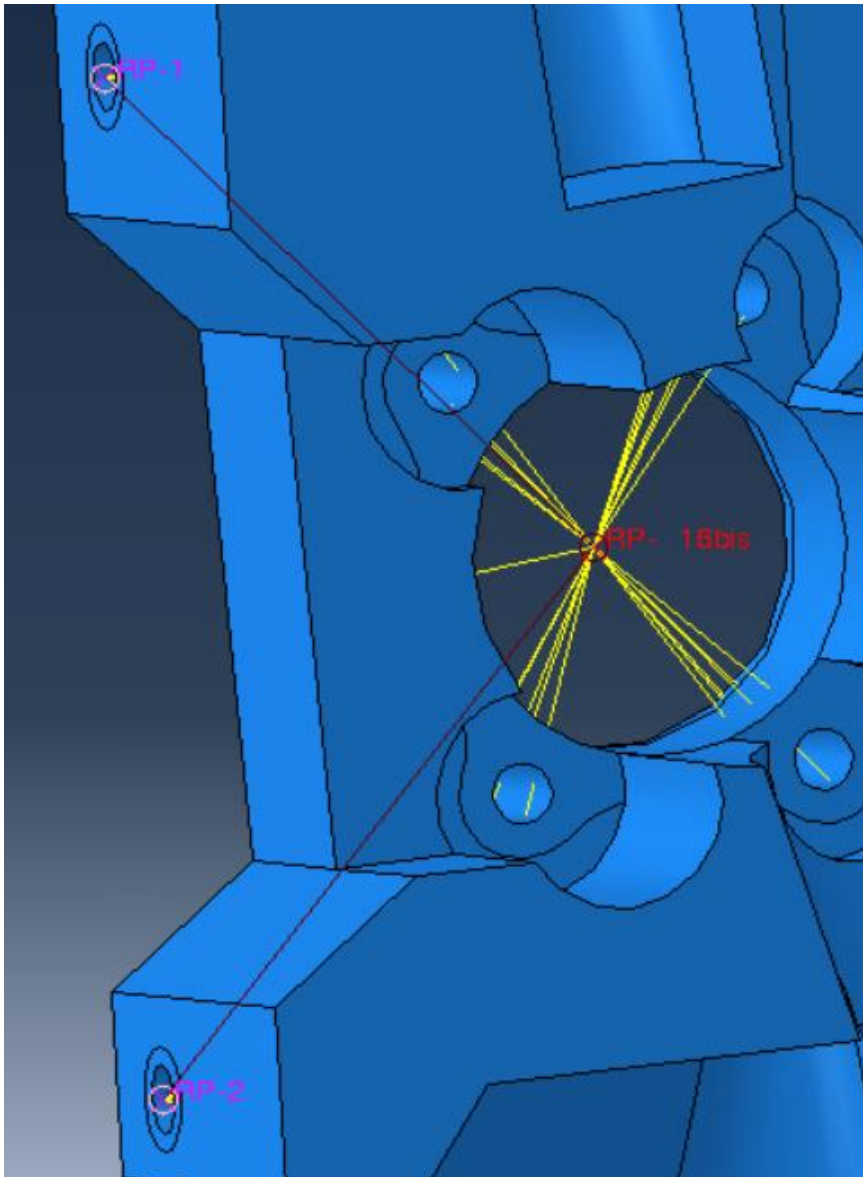


Figure 6-9 Interaction node 16bis with node 1 and 2 (Bracking couple)

6.6 Steps

Considering that a large number of loading conditions have to be verified, the *General, Static* step couldn't be used, because of a superposition of the stresses of different steps. Instead, it was considered the *Static, Linear perturbation*. This step, as already explained in Paragraph 6.3, cannot deal with the plastic deformation of the material, but the limits that are imposed for the optimization, restrict the analysis to the elastic behaviour. The *General, Static* step was initially tested, and not only it had the problem of the overlapping stresses, but it requires even much more time (100 or more iterations vs 1 of the Linear perturbation).

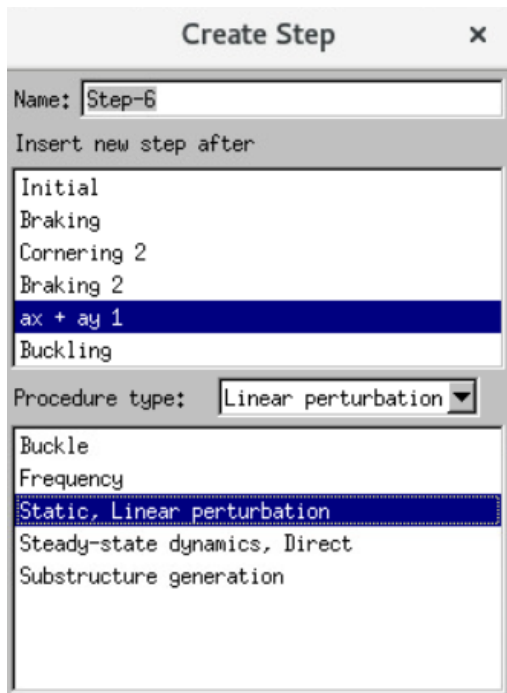


Figure 6-10 "Create a new step" window

Using the *Linear perturbation* analysis, Abaqus/Explicit cannot be used, and only Abaqus/Standard is available. The response of this analysis is the linear perturbation response about the base state [90]. In this project, the initial step, is the unloaded component, so at the start of each step, the part is not influenced by the previous loading conditions. The time step of linear perturbation step, which can be treated as a very small number, is never accumulated into the total time.

If in the analysis a geometric non-linearity is included, the stress stiffening or softening effects are included in the linear perturbation analysis. The *Static, Linear perturbation* step can deal with multiple load cases, which are required for studying this component.

For the validation of this steering knuckle have been considered many load cases. It is considered the **Steering buckling**, which verifies that the component resist to a high load applied on the bushing (15) connected to the steering rod.

Then it must be verified that the connecting elements of the braking caliper (1) and (2) resists to an emergency **braking couple**.

Finally, a set of cyclic fatiguing loading conditions has been considered, listed in the following Table 6-2:

Steering Knuckle fatigue loading cycles			
Stabilization #2	Cornering 3	Braking 1	ax + ay 4
Vertical 1	Cornering 4	Braking 2	ax + ay 5
Vertical 2	Bump	ax + ay 1	ax + ay 6
Cornering 1	Rebump	ax + ay 2	ax + ay 7
Cornering 2	Acceleration	ax + ay 3	ax + ay 8

Table 6-2 Fatigue loading conditions applied on the component

For the fatigue analysis, it has not been provided a spectrum of real working conditions, with a history of different amplitudes for each mission, but only the maximum peak value of the loads. It results that the fatigue loads are overestimated, as the loading condition considered is the one with the highest amplitude. These limit values are hardly reached in a normal utilization of the car, so it is quite far from an effective working condition.

The effects of variable amplitude loads on the suspension component is consequently neglected due to the availability of only these data. This can be considered positive for safety reasons, and for the substantial reduction in terms of computational cost. On the other hand, if a non-overestimated load value was used, a lighter component would have been obtained.

Therefore, instead of using a fatigue step, which moreover is not available with the linear perturbation analysis, the fatigue loads have been considered as static peak loads, so it has been used the *Static, Linear perturbation* step also for these load cases.

In order to define an effective value of working load, it is necessary a spectrum of real working conditions, characterized by a fluctuation of the stress excitations, with various amplitudes. A more precise evaluation for the fatigue stresses could have been obtained by considering *Miner's Rule*, based on the idea of cumulative damage [91].

Due to the large number of loading conditions, only the cycles with the highest loads have been utilized in the topology optimization (as well as the steering buckling and the braking torque). In order to choose the most suitable steps, it was performed a preliminary FE analysis on the design space (Paragraph 6.9), in this way the most critical conditions were highlighted. Moreover, it has been considered also the different loads of each step; in fact, some missions have higher loads in one area in respect of another. Anyway, most of the neglected loading conditions produced in the preliminary FEA low stresses. While those that were more demanding, had similar forces with the other conditions, considered for the optimization.

Afterwards, when the new optimized component was obtained, a FEA has been done, verifying that the component is able resist to all the loading conditions. The loading conditions that are considered for the topology optimization, in addition to the *steering buckling* and the *braking couple* are:

- Cornering 2
- Braking 2
- ax + ay 1

It goes without saying that a more precise result may have been obtained by using all the loading conditions, but the time necessary for the optimization would have been of almost a week. Having a better performing computer, it could have been done, but a satisfactory compromise had to be reached.

6.7 Load

In this paragraph it is briefly explained how each loading condition has been defined:

- Maximum braking torque: applied on the node 16bis, along the Y axis (horizontal axis, parallel to the rotation axis of the wheel). The component is clamped at the nodes 5, 10, 15 and 55 and as already said in the interactions paragraph, the node 16bis is connected to the two mounting elements of the braking caliper. It results that the area of the bearing assembly will be completely unloaded and all the load is correctly concentrated only on the elements connected to node 1 and 2. The torque is computed by multiplying the load of the braking caliper with the effective radius: $T = F \cdot r_{eff}$
- Buckling steering tie rod's connection: applied on point 15, this force simulates the effect of the maximal load that can be applied by the steering rod. The force is applied along the -y direction of the vehicle (from the inside to the outside) and it is clamped on the centre wheel, point 16.
- For each fatigue loading condition, it is provided a set of loads (and moments) applied in all the nodes (5, 55, 10, 15, 16) except for the points 1 and 2 that are already tested with the braking torque step.

These loads maintain in equilibrium the component and consequently no constraint should be specified. In this situation, the inertial relief option should be used, so that the simulation would be more stable. Unfortunately, while this technique can be applied on Hyperworks – Optistruct (software used in FCA, so that the forces were provided the considering their common utilization), in Abaqus the inertial relief cannot be used with topology optimization and a different method was used.

The node 16 (on which both forces and moments are applied) has been clamped while on all the other nodes, the loads were applied normally. At the end of the simulation it has been verified that the constraints on node 16, had adsorbed the same loads that were provided as input forces.

It is not possible to report in this text the forces acting on the nodes, being these data sealed by Maserati.

The procedure for the definition of the forces acting on one point, for a single step is shown in Figure 6-11:

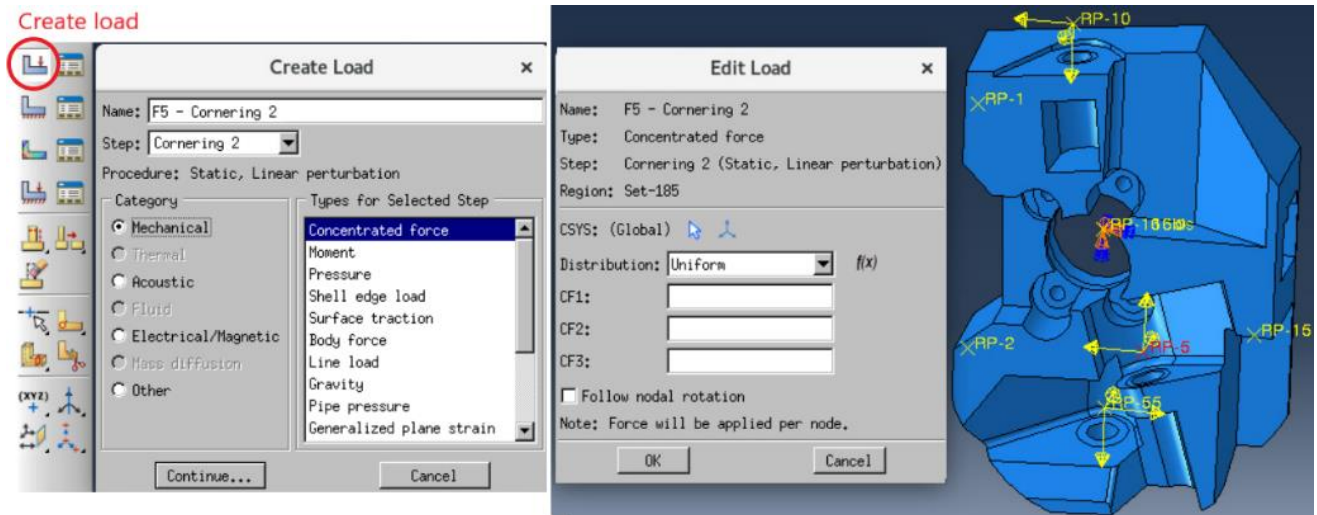


Figure 6-11 How to create a load on Abaqus

- 1) After defining the name of the force and specifying the step, it must define also which kind of force it is. As it can be seen, there is a wide range of forces available, not only mechanical, but also acoustic, electro-magnetic (and for a different analysis also thermo-fluid dynamical);
- 2) The point, the edge or the surface on which the load is applied, must be chosen;
- 3) Finally, it is possible to insert the components of the load in the 3 directions.

The boundary conditions can be defined with a similar procedure; in this case the used type of constrain was the *Encastre*, which sets both all the displacements and the rotations to zero.

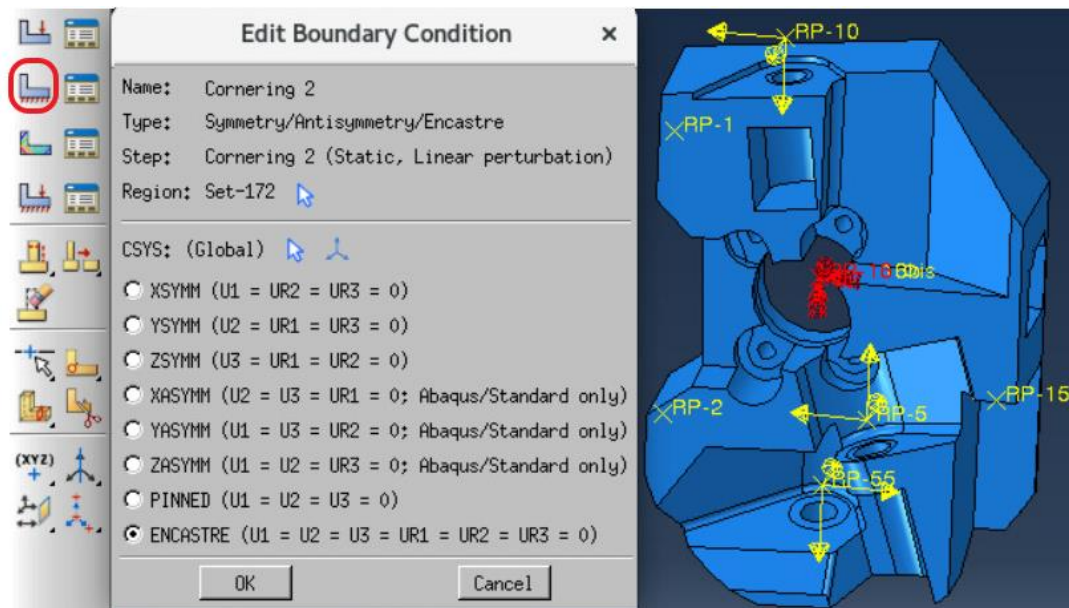


Figure 6-12 Boundary condition definition

Finally, when working with Linear perturbation steps, Abaqus requires that a *Load Case* is defined for each step. For each Load Case, it is necessary to specify its loads and B.C. [87].

6.8 Mesh

The component has been discretized with a tetrahedral mesh, with 3D10 elements. In fact, with a complex geometry like the one of the design space, it is not reasonable to use hexahedral elements because to fit the geometry results in high element distortion, so that the program itself does not allow to use a hexahedral mesh.

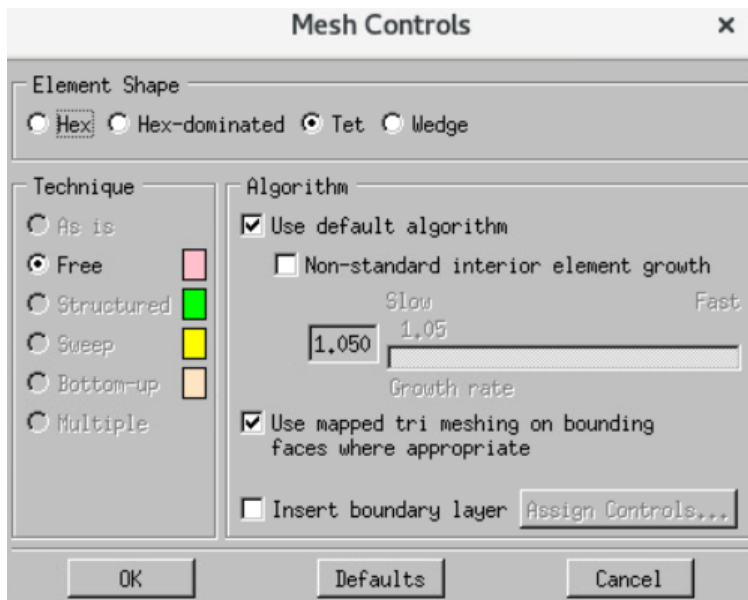


Figure 6-13 "Mesh Controls" window

The brick elements can be used only for simple and linear geometries. Usually for a simpler geometrical model, it would be crucial the use of partitioning to divide the whole body into fundamental geometrical shapes. In this way the program would be able to construct a structured hexahedral mesh. Due to the complexity of the part, it is impossible to reach only basic geometries also considering the limited options in the definition of the partition faces.

The typical mean dimension of the element has been chosen equal 4,5 mm. This dimension should have been even lower, 3 or even 2 mm, but the available system has a limitation and could not work with smaller size elements i.e. a larger number of elements. In fact, already with the adopted mesh size, the total number of elements is around 470.000, and at this condition the computational capability was almost at its maximum.

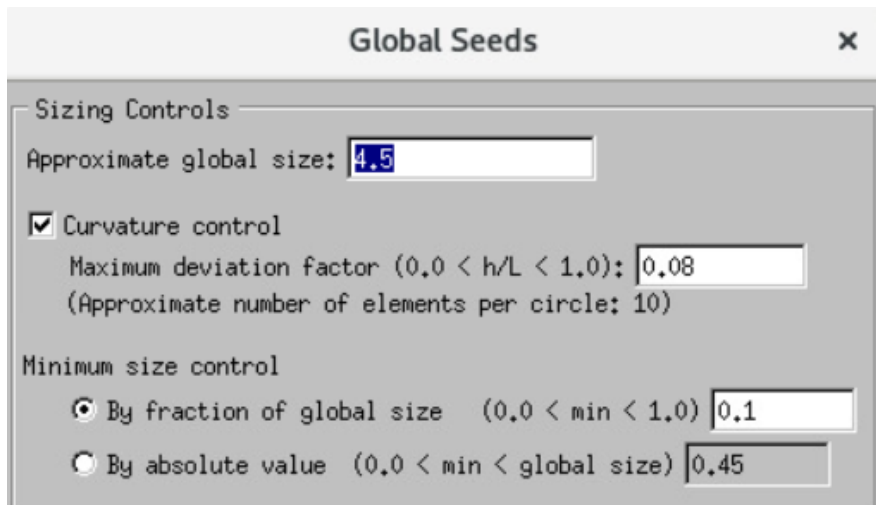


Figure 6-14 Part seeds options

After these options are specified, the program automatically creates a discretization of the volume. However, when the part shape is characterized by a relevant complexity, the mesh quality may result to be not optimal, having a certain number of distorted elements. The information regarding the quality of the mesh can be checked by using the *Verify Mesh* function. Having found some distorted elements, the geometry has been slightly modified and the element dimension reduced in some edges where the distorted elements were located. In this manner, after remeshing the part, there were no more highly distorted tetrahedral elements. Another modification of the element dimension has been brought on the edges of the bushing elements, where, due to the direct application of the force on these areas, a high concentration of the stress is induced; thereby the acquired result is more precise.

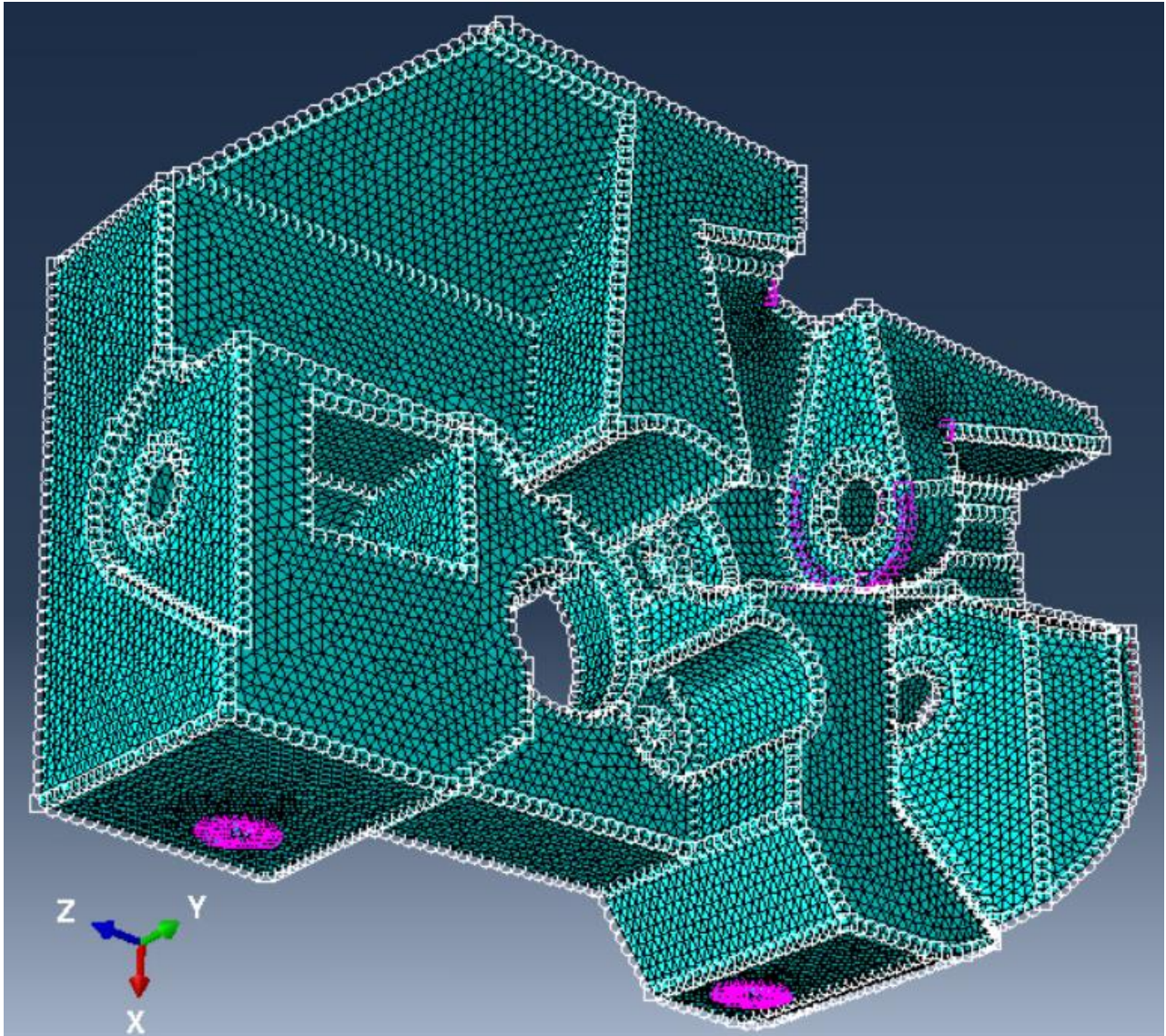


Figure 6-15 Meshed component with some edges' refinement

6.9 Preliminary FEA

Before starting the topology optimization, a finite elements analysis has been performed for different reasons. First, it was used as a verification of the settings of the analysis but, and more importantly, to check where the peaks of the stress field are located and, at the same time, to determine which areas are not loaded. This, along with the results of the first optimizations, allowed to reduce the space design volume. Moreover, this FE analysis allowed to determine which are the most critical loading conditions. It resulted that several load cases are characterized by really low stresses and consequently these steps have been excluded from the topology optimization. This selection of the most loaded cases resulted to be necessary in order to reduce

the time of the optimization, which using all the load cases may have required almost a week to finish. In the following images are reported the results of the performed FE analysis only for the most loaded cases.

Likewise the forces in Paragraph 6.7 and the final stress results in Paragraph 6.13, even in this case it is not possible to show the real values of stress to which the component is subjected, so the legend has been removed. A percentage scale is shown in the first image, which is valid for all the following results. A rainbow spectrum has been adopted for the scale, so the blue areas are subjected to nearly null stress, while the most loaded areas are highlighted in red.

It can be clearly seen that there is a high concentration of the stress on the non-design elements, because of the transmission of the loads (from the reference nodes to the connected surfaces) by rigid beam elements of the coupling. For each step the stress is under the prescribed limits, even if the maximum value of the stress is not really small, so in the optimization it is not expected an enormous reduction in the mass. However, having several zones of the space design that are affected by really low stress (in all the steps), it can be supposed that all these volumes will be removed during the optimization. It must be considered that no material will be removed, if an area is highly loaded in just one step.

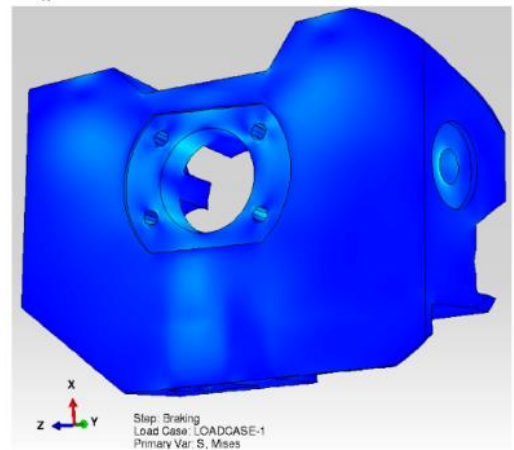
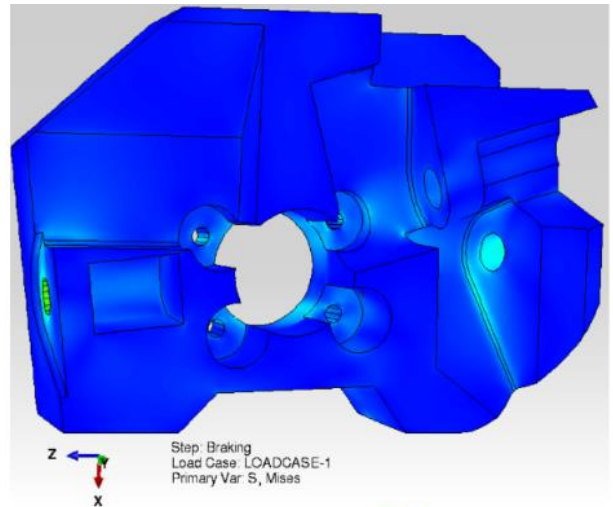
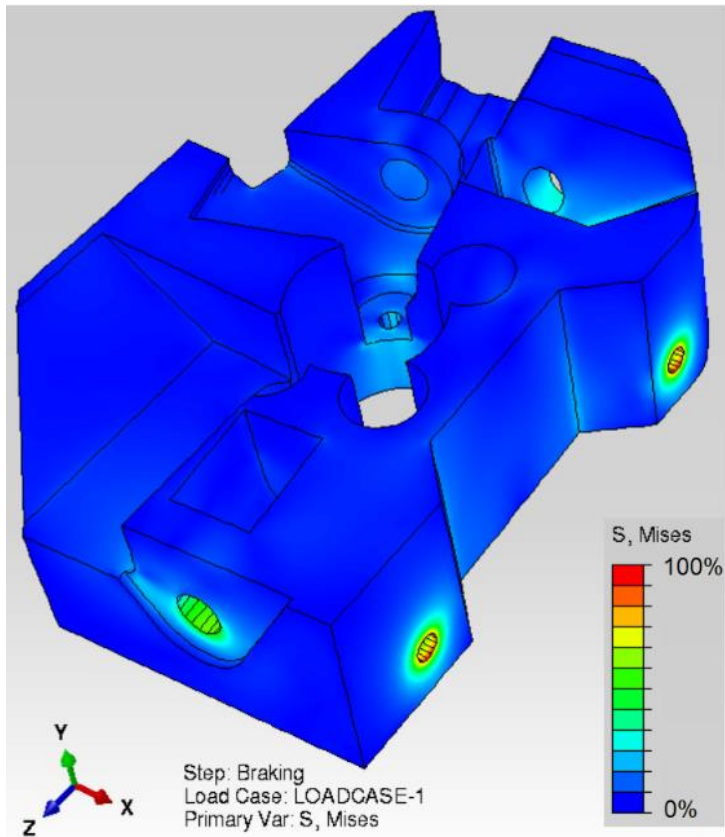


Figure 6-16 Stress on design space: Braking couple

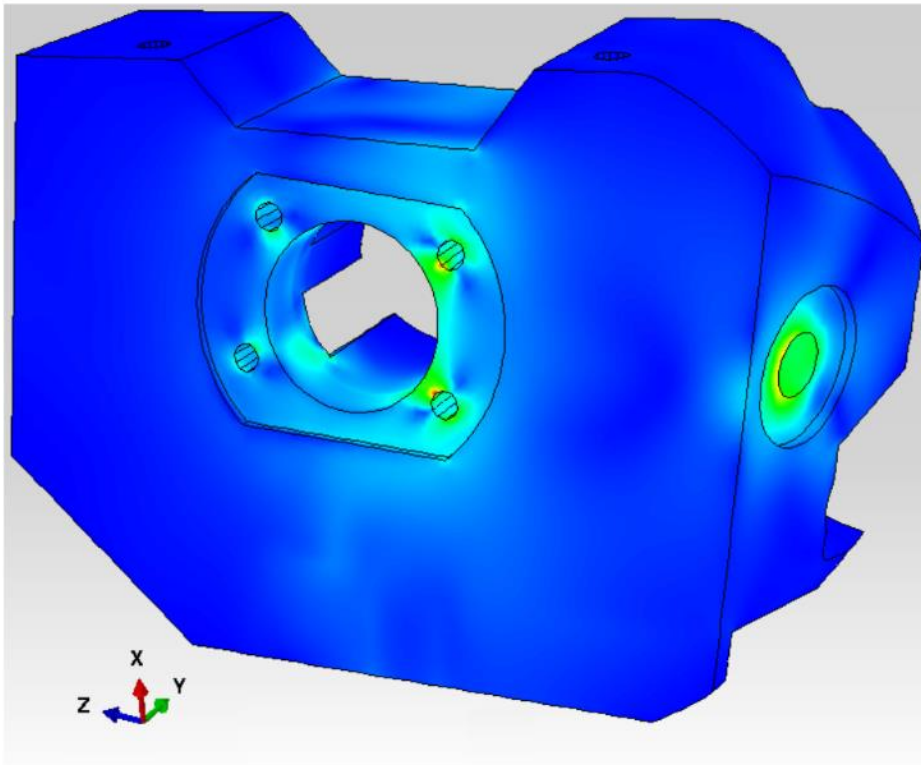
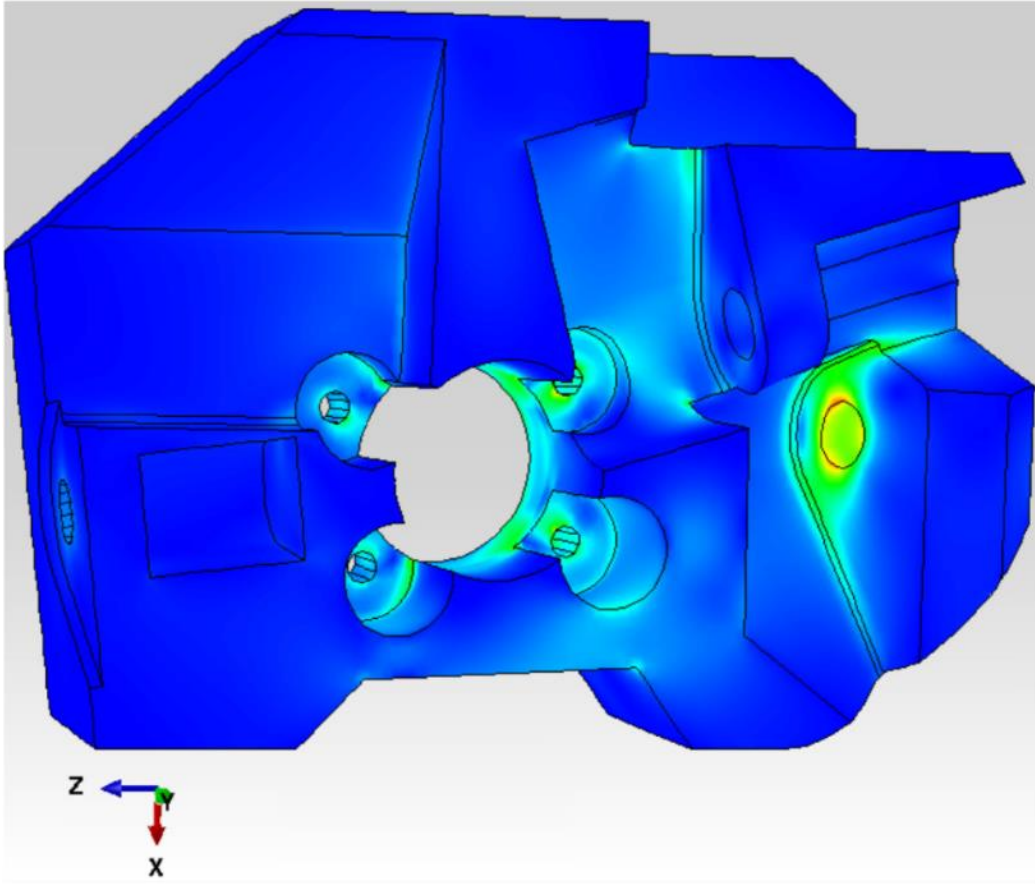


Figure 6-17 Stress on design space: Cornering 1

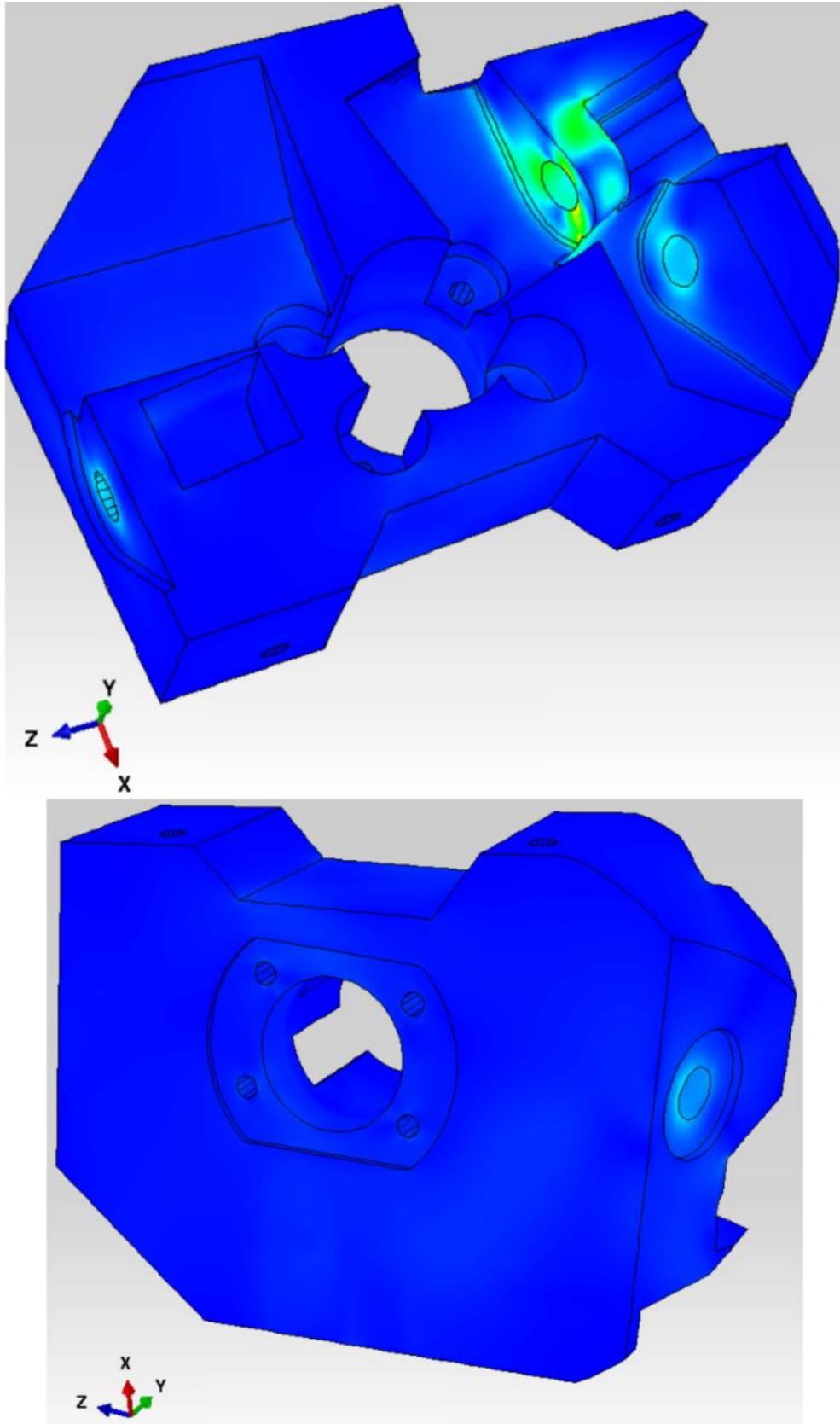


Figure 6-18 Stress on design space: Braking 2

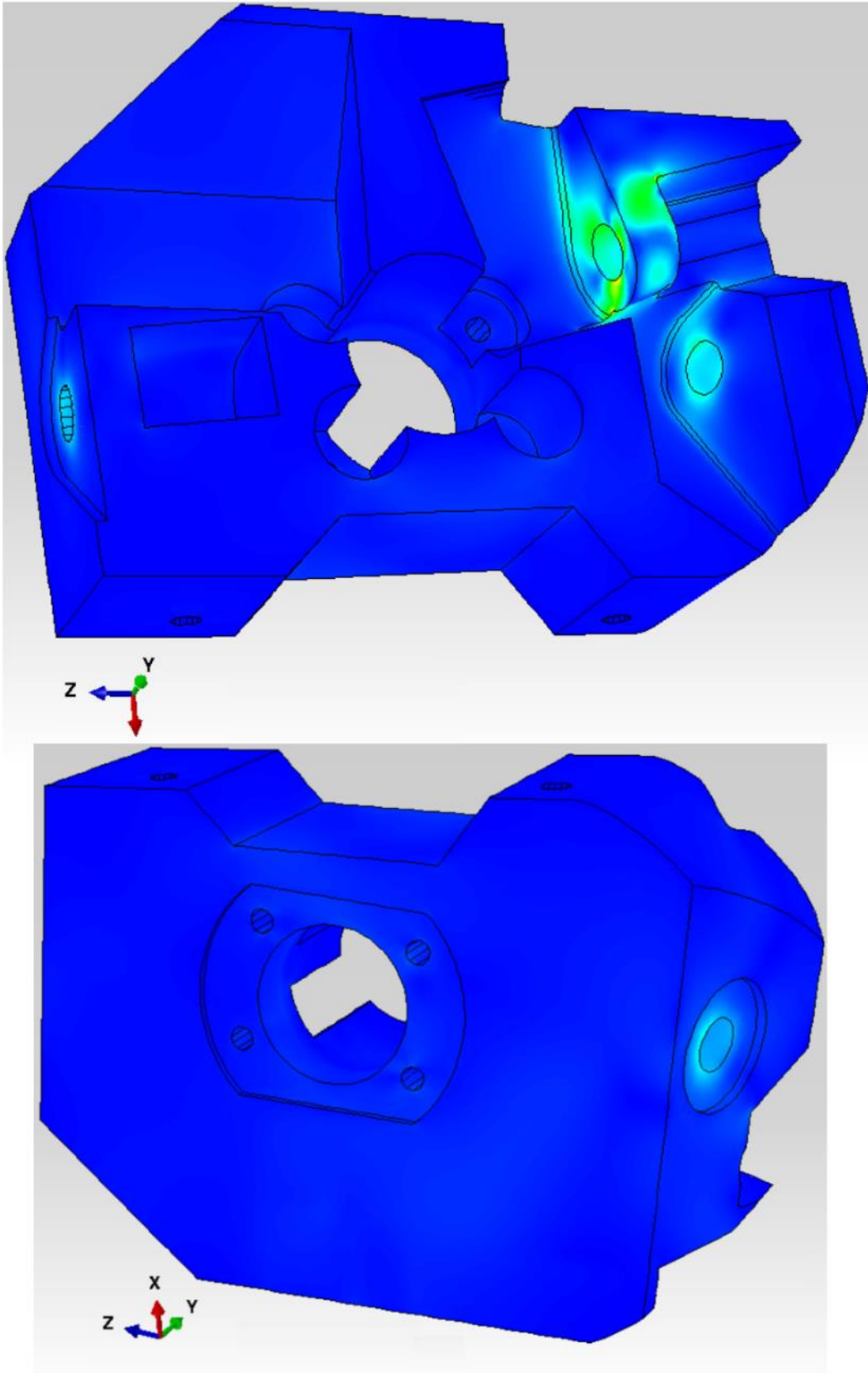


Figure 6-19 Stress on design space: $ax + ay 1$

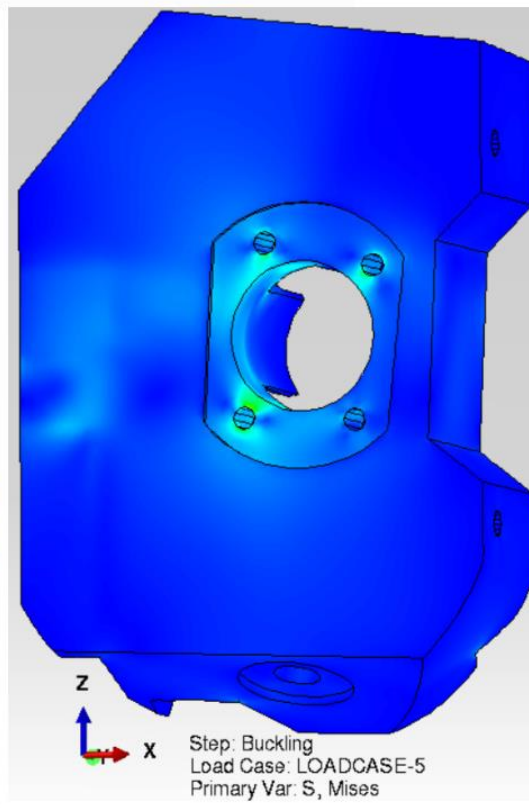
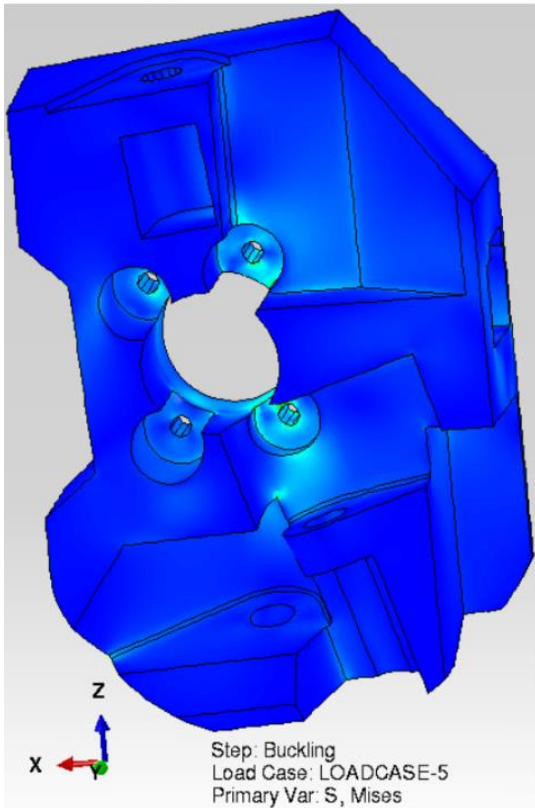
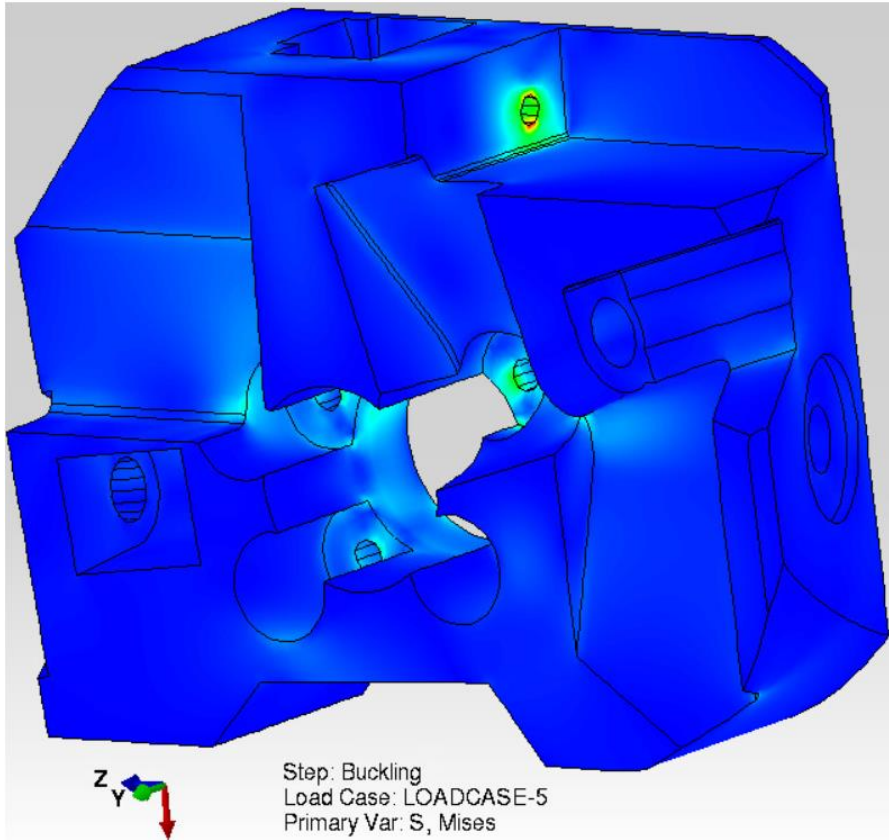


Figure 6-20 Stress on design space: Steering buckling

6.10 Topology optimization

As it has been previously said, the objective of this project is to obtain the lightest possible component, while keeping the stresses under the prescribed limits. The topology optimization tool of Abaqus, if compared with other programs like Optistruct is less diffuse, so in the literature there are not many articles about it. Thus, it had been necessary to do a considerable number of optimizations varying the options, and in the end to take the best result.

When starting to set up the options for the topology optimization, the program asks which volume must be considered for the optimization. In this case, all the cells of the non-design elements have been excluded, so it has been chosen only the design space cell as it is shown in the Figure 6-21 below.

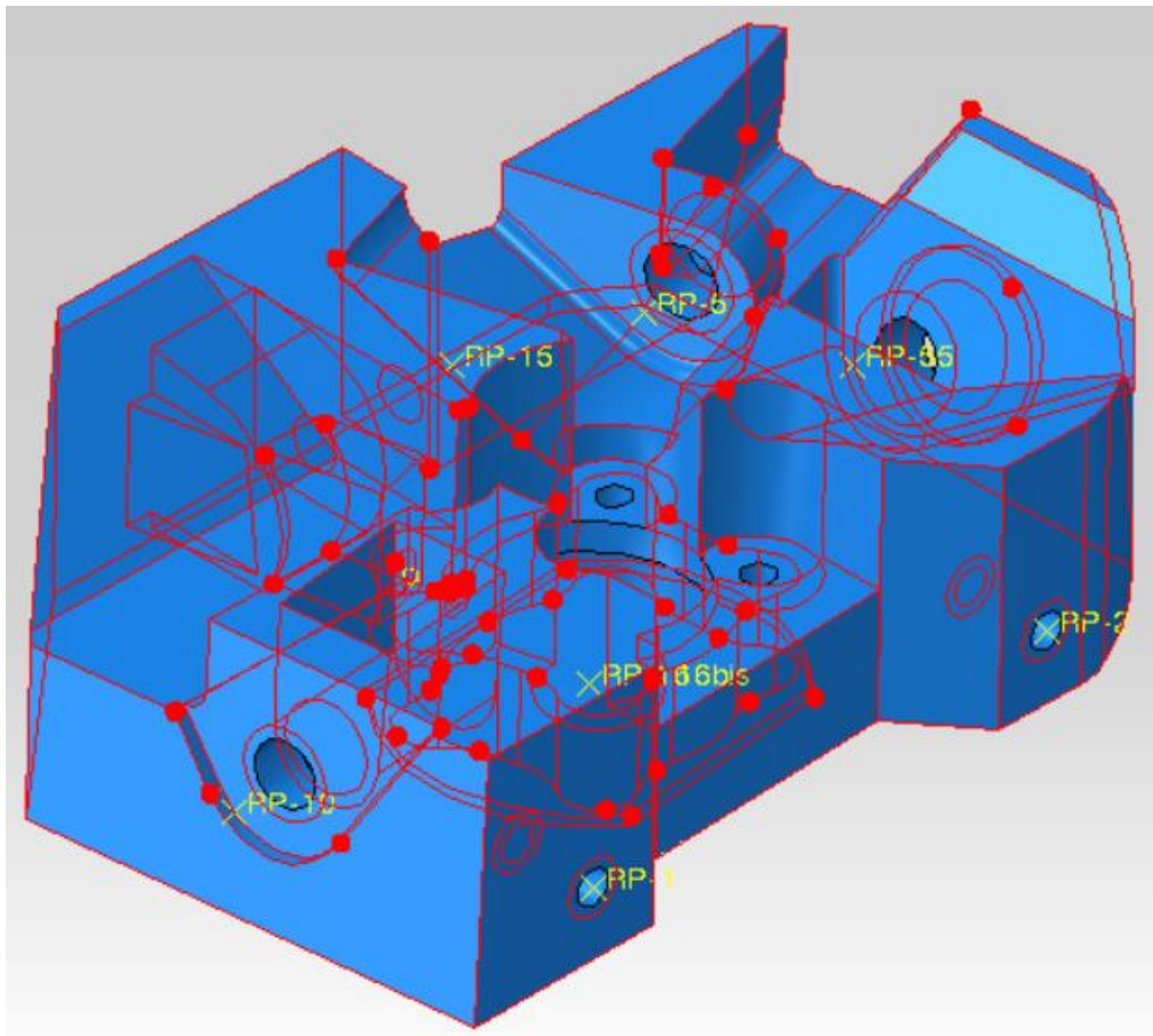


Figure 6-21 Non-design cells excluded from the topology optimization

The minimization of the compliance is the most used method in the literature and even the method suggested by the Abaqus' support. For the compliance problem, it must be used the **Condition-based** optimization, which does not allow the use of the stresses as design variables. This method has been tested, by prescribing the minimization of the compliance of the structure, setting the desired final mass equal to a certain value. This method did not give good results, as imposing a final mass equal to 4 kg, even larger than the ideal objective of 3 kg, the result was a disconnected structure, with the non-design element unconnected with each other.

On the other hand, the **General optimization** (the *sensitivity based approach*), based on the SIMP algorithm (described in the paragraph 5.2.3), is the method that gave the best results. The General optimization is the most complex of the two available algorithms as it allows the use of many design variables, listed in the next Figure 6-22, which can be used alternatively as objectives or constraints. It allows the use of multiple objectives and constraints.

- Strain energy
- Stress
- Energy stiffness measure
- Volume
- Weight
- Displacement
- Rotation
- Eigenfrequency calculated with Kreisselmaier-Steinhauser formula
- Eigenfrequency from modal analysis
- Reaction force
- Reaction moment
- Internal force
- Internal moment
- Center of gravity
- Moment of inertia

Figure 6-22 List of Design variables available for the General optimization approach

Some of the options were slightly changed in respect of the standard setup of the optimization. In particular, as it can be seen from Figure 6-23, it was forced the elimination of soft elements in the region of the design space, applying the *Favor continuity method*. This adjustment has been necessary, because a large part of the volume was not deleted while having a really low value of density ρ and at the same being subjected to almost null stress in all the steps considered. The *Favor continuity method*, as the name suggests, is an option to delete the soft elements but checking before for the continuity of the structure. For example, if there is a small area of "hard" material, namely an area subjected to high loads, completely surrounded by soft elements, in this case in order to prevent a fragmentation of the part, the soft elements are not removed [87].

It has been verified by doing several tests, that a relative material density threshold of 0,2÷0,25 is a balanced value. It has been found a confirmation of this setting even on other similar studies [92]. The penalty factor for the SIMP method has been kept $p=3$ as default.

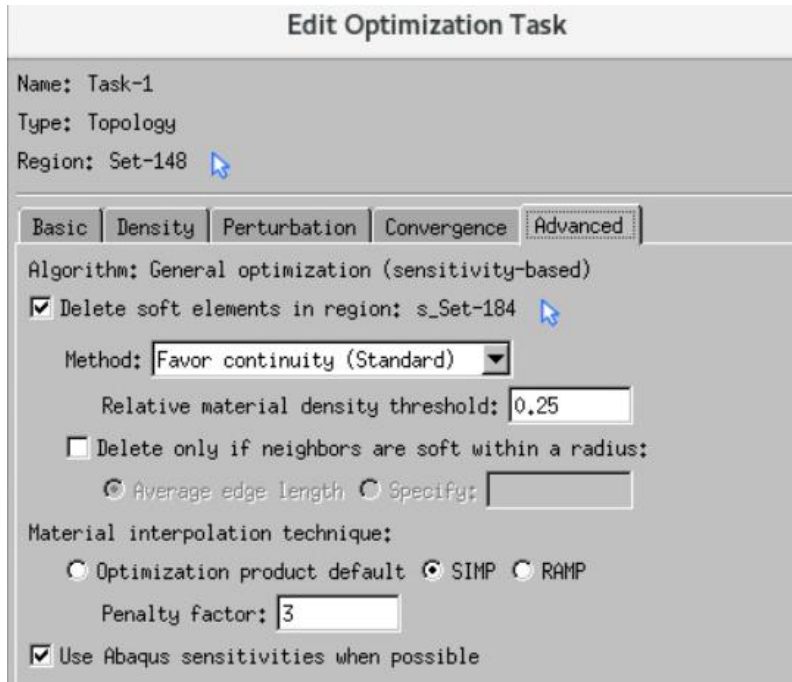


Figure 6-23 Advanced options for topology optimization

Moreover, as suggested even in the TOSCA Manual [93], in the case of an optimization on complex structures, the *Maximum change per design cycle* of the density is kept at a value equal 0,1 (or lower), instead of the default 0,25. In fact, with a higher variation of density between two consecutive cycles, it may result that some elements will be deleted even if they may be necessary for keeping the stresses under the prescribed limits. Thus, reducing the variation per cycle, the removal of elements will be smoother. This variation is suggested in particular for complex components and for complicated setup of the optimization [93].

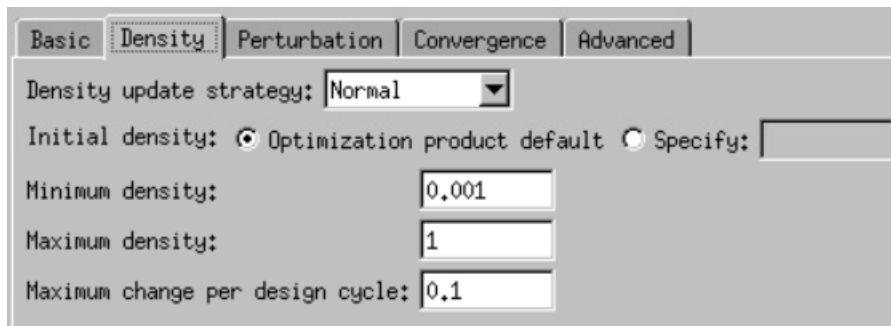


Figure 6-24 Density options for topology optimization

All the different *Density update strategies* have been tried, (*Normal*, *Conservative* and *Aggressive*) but the *Normal*, which is the standard one, guaranteed the best result. The *Initial density* is set as default equal to 0,5 when the volume is set as objective function. In the case of really high limits (with low loads applied on the structure), this initial density may be slightly reduced in order to decrease the total number of cycles and consequently the time for finishing the process.

In the *Design Response Manager*, the variable *Volume*, and two design response variables, computed as *Scaled centroidal Mises*, which are the *Fatigue* and *Yield stresses*, have been defined. The *Volume* (it would be the same by choosing the mass) was defined only for the design space, because as already said, the volume of the non-design space is left out. Meanwhile, for the two limits of stress, it was considered the whole body, because the operative stresses must be under the limits in the whole volume and not only in the design space.

The objective for the optimization is the minimization of the volume, with the previously defined fatigue and yield limits, used as constraint. Hence, the optimizer tries to find the smallest possible volume while keeping the stress under the prescribed limit values in all the elements.

For the *steering buckling* and the *braking torque* steps was specified the yield limit, while for the others the fatigue limit.

The yield limit, found experimentally as shown in chapter 4, is equal $\sigma_y = 1000 \text{ MPa}$.

For the fatigue limit, it was not possible to make the specific characterization tests, and in the catalogue of the producer EOS this data is not provided, differently from other materials (like AlSi10Mg [94]). However, in the literature it is possible to find several researches about this argument [59] [57] [55] and by comparing these different studies, analysing even the printing parameters that were used, the fatigue limit was taken as $\sigma_f = 650 \text{ MPa}$.

In the first optimization runs, that were used as tests, it was noticed that by prescribing in the software the real values of the limits ($\sigma_y = 1000 \text{ MPa}$ and $\sigma_f = 650 \text{ MPa}$), the resulting final part was still really heavy, because only a small amount of material was removed. This was due to the concentration of the stresses in some specific points, due to some inaccuracies of the finite element model. In order to overcome this problem and push the optimization to the limit, the material strength limits were set to higher values. In particular, for the optimization that gave the best result, the limits are equal to:

$$\sigma_f = 1650 \text{ MPa}$$

$$\sigma_y = 1900 \text{ MPa}$$

These two values are extremely high, but the structure, that was finally obtained, has, for all the steps, all the stresses under the prescribed limits. This will be explained later.

The geometrical constraints available for the topology optimization are:

- Frozen area
- Member size
- Demold control
- Rotational symmetry
- Cyclic symmetry

- Point symmetry

No geometrical restrictions have been applied, as for the additive manufacturing technology are not required specific manufacturing constraints, differently to what is required with the casting process. No symmetry constraints could be applied in a complex part like this. The onliest option that may have been useful is the “Frozen area” that excludes a surface or a volume from the optimization. This was done differently, cutting out the partitioned non-design elements.

6.11 Job definition

In the *Job* module it is possible to create, modify the analysis jobs, to monitor their progress and finally to combine and extract the results.

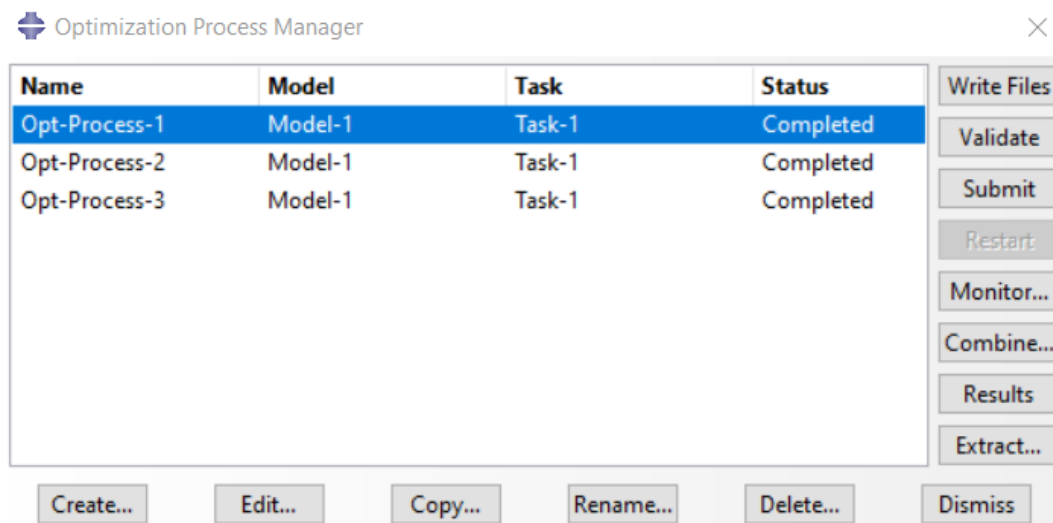


Figure 6-25 "Optimization Process Manager" window

For the topology optimization process, 40 cores of the server available at the McMaster University have been used, and the whole process took around 15 hours. It was prescribed a maximum number of 150 cycles for the optimization, but the software reached convergence at the 117th cycle, so it stopped cycling before reaching the maximum. The number of cycles that the program takes to reach convergence can considerably variate from a job to another, just slightly changing a parameter. Defining a small number of cycles may be a problem, because the optimization could require more cycles before ending.

During the analysis is it possible to visualize live some of the output files that are being created by the program, in order to verify how the process is developing. It is important also to check the warning and the errors that may appear in the *process monitor* window. It is also possible to have a graphical representation of the evolution of the optimization, like the one in the following Figure 6-26. In this graph, it is possible to observe the evolution of the optimization's objective and parameters in function of the cycles. The objective function (volume) starts at the first cycle from a predefined value of 45%, related to the default initial density of the finite elements. In the

first few cycles the volume is rapidly reduced, but the removal of some elements leads to a tremendous growth of the stress on the components. In the graph is reported the peak of the stress for each step of the optimization. Consequently, the vertical axis related to the stress has been removed, being the stresses sealed information. However, it can be seen the trend of the stresses, that after reaching the peak are immediately reduced thanks to a slight growth of the volume. After the first 15 cycles, the volume continues to be reduced, while the stresses are kept under the prescribed limiting stress values.

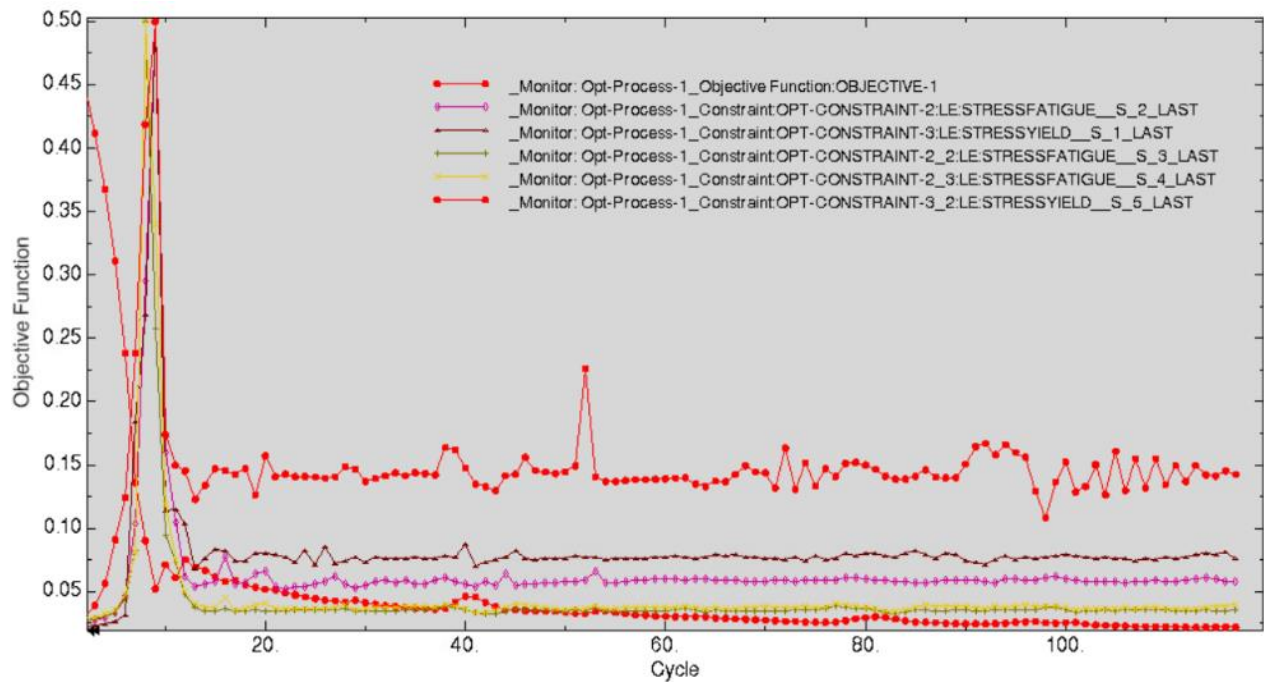


Figure 6-26 Evolution of the optimization (chart)

6.12 Result of the optimization

Before obtaining a good result, several optimizations have been made, in order to tune all the different parameters. In fact, a negative aspect of the software is the high aleatory of the result. Not only the shape of the structure may change significantly just marginally varying a parameter, but even the stresses may variate significantly. Just changing of few MPa the fatigue and yield limits, in some optimizations the stress peaks resulted to be much higher than the prescribed limits, while in other cases the maximum values were (correctly) lower. Because of this uncertainty several optimizations were performed, in order to find the lightest component, with the most convenient shape and with the stresses under the limits.

Some optimizations (like the one in Figure 6-27) were discarded due to the presence of some cantilever structures that should be avoided in order to guarantee a higher stiffness of the whole component. This issue occurred for the connection of the bushing elements of the braking caliper, in fact the stresses in this area (produced principally in the braking torque step) are lower than the limiting values and consequently the program in some optimization tried to remove that portion of volume. This problem, unfortunately, could not be controlled and the optimizations that gave shapes similar to the one shown in Figure 7-27, were simply discarded.

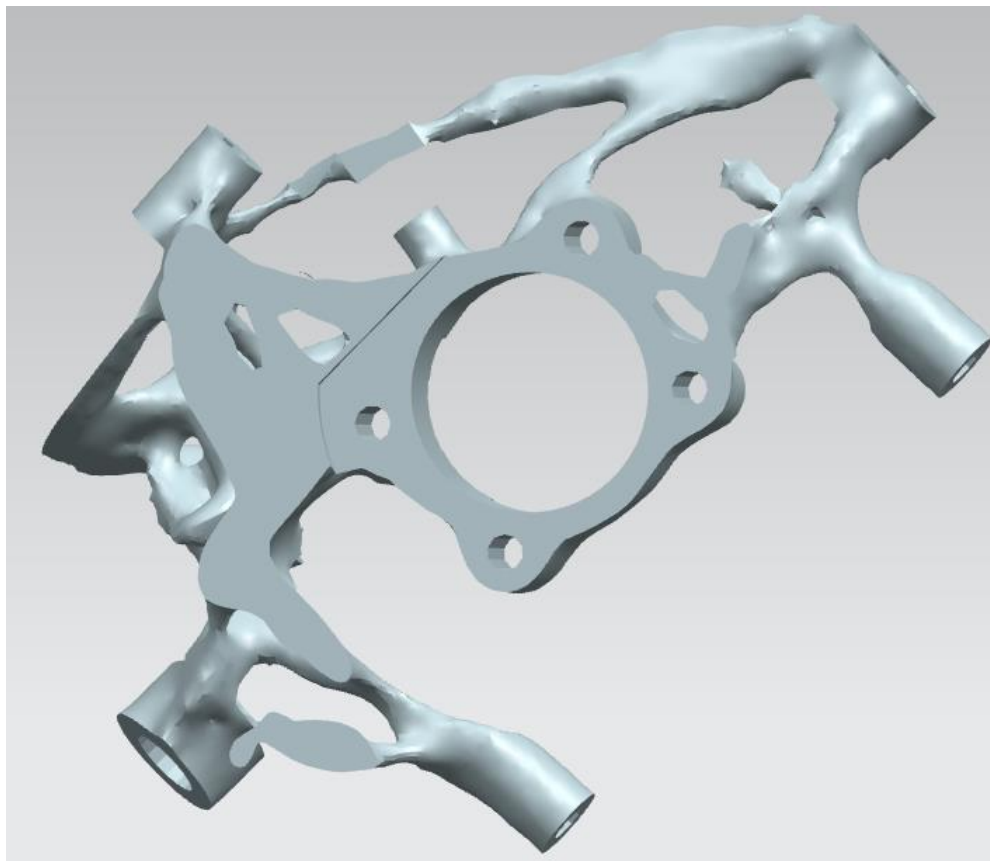


Figure 6-27 Cantilever structures of a discard optimization

The best result that was obtained is shown in the Figure 6-28 below:

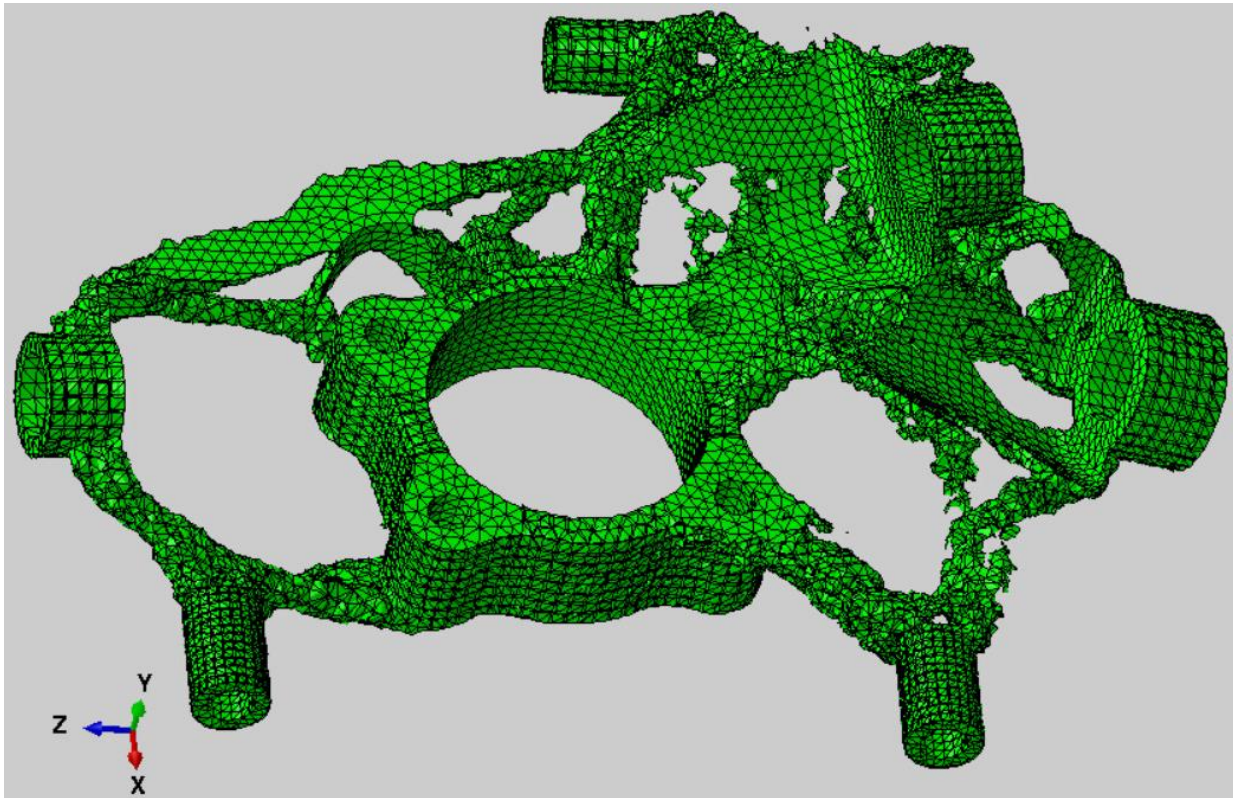


Figure 6-28 Optimization result ISO 0,3

The picture represents not the final part, but the first result that the optimizer gives right after the combination of all the cycles. As it can be seen, in some areas the quality is very low, this is because the default density threshold that the *Visualization* module of Abaqus uses is $\rho=0,3$ which is too high. Instead taking a lower value of density, a smoother surface can be obtained. Gradually reducing the density limit, the holes are filled, and a more convenient structure is produced by setting the ISO value at 0,1.

The direct output of TOSCA had stresses over 2000 MPa (so far beyond the limitations imposed). These really high values were due to a concentration of stresses in few narrow areas. If a finer mesh could have been used, the stresses would have been lower and more precise. However, due to computational power limits of the computer, it has not been possible to reduce the elements size. Moreover, using a finer mesh even the limits could have been reduced, as having lower stresses in the finite elements analysis, more material would have been removed.

It must be even considered that this is only the output of the optimization, and before exporting the part, it has been subjected to a smoothing process, in which the surface roughness is considerably improved. Thanks to this, even the peaks of stress on the FEA verification are reduced.

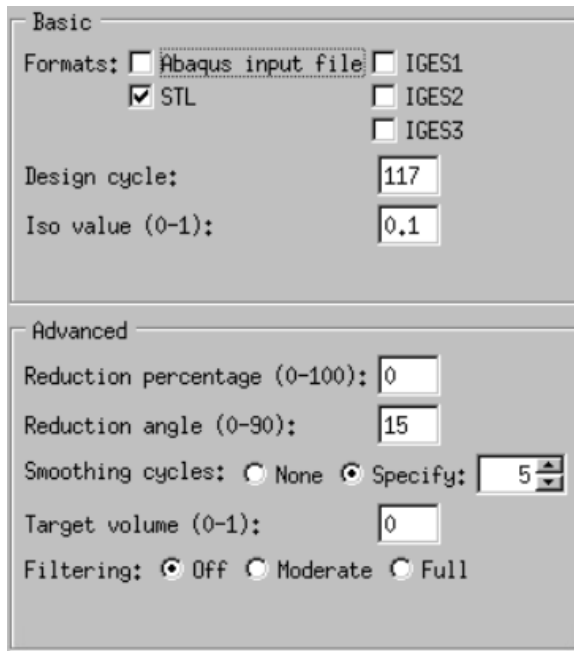


Figure 6-29 Extraction option on Abaqus

The optimized part can be exported as an Abaqus input, STL or IGES file. It was exported as an STL file, with the smoothing settings shown in the previous Figure 6-29.

The STL file was imported in NX Unigraphics Siemens, where all the triangular faces were eliminated, obtaining a *Facet body*. This part is not a solid model, so it cannot be modified using the common CAD methods. Several images of the imported part in NX are reported in Figure 6-30.

Regarding the objective of the optimization, which is the minimization of the mass of the component, it was reached the weight of 4,2 kg. The reduction of volume\mass, comparing it with the initial space design that weighted 66 kg, is of the 93,5%. But this value is not really representative because it was taken the largest possible space design.

The original part, produced by Maserati, is made in aluminum and weights 4,1 kg. So, using Maraging steel, which has a density that is over the triple of the density of aluminum, it was obtained a part that weights almost the same.

In the comparison between the weights, it must be underlined that the non-design elements, which could not be modified, have a relevant influence on the total weight, as their volume is the 35% of the final part. For example, only the central non-design part, which is the housing of the bearing, weights 1 kg if made in Maraging steel.

In an optimization of a different with a smaller percentage of frozen areas, it would be more convenient to use Maraging steel. While in this case, a large amount of non-design areas is a consistent disadvantage for the choice of a heavy material like steel.

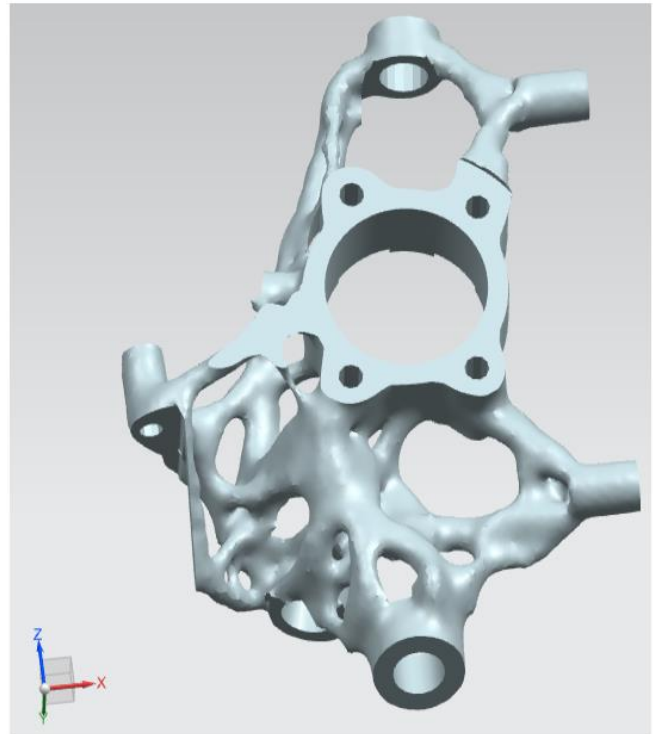
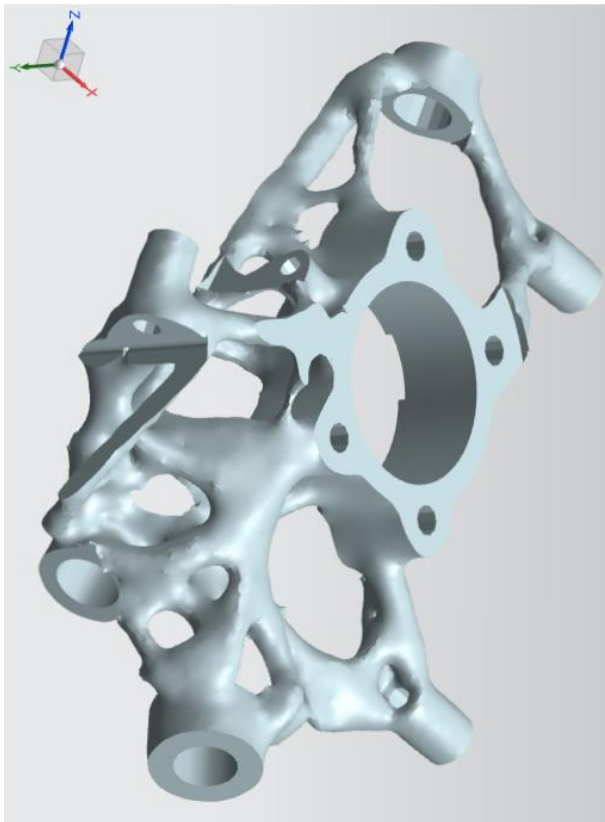
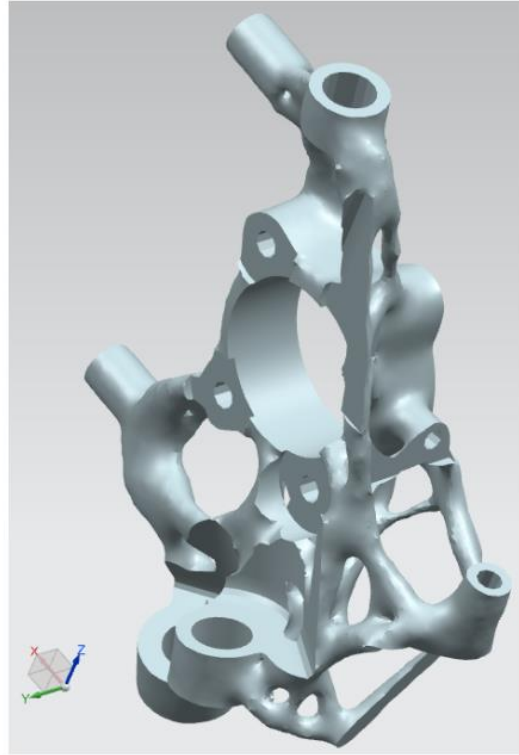
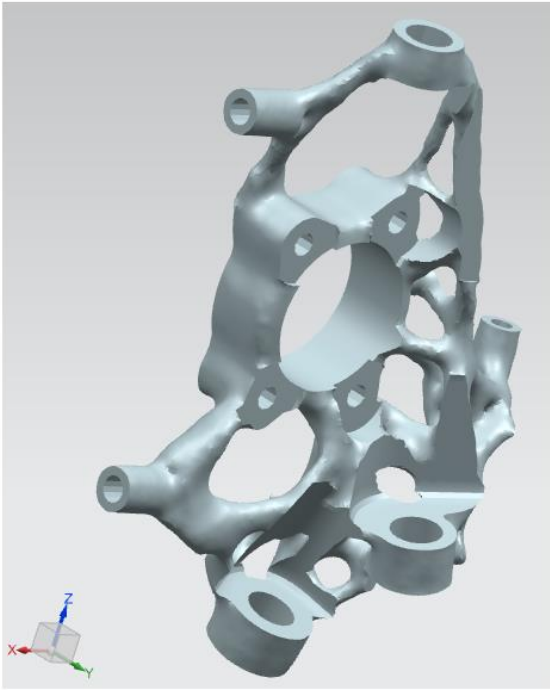


Figure 6-30 Optimized component

6.13 Verification of the optimized part

A particular plug-in tool that is available for the Abaqus/CAE software that is called *Mesh to Geometry*, allows to transform an STL in a solid part. So, the extracted optimized part as an STL file was reimported in Abaqus creating a geometry, and a new analysis was made.

The passages for the definition of the stress-analysis are the same of the topology optimization, so all the passages will not be explained. The only difference is that for the verification, all the load cases are considered, in order to verify that the structure can resist to every possible combination of loads.

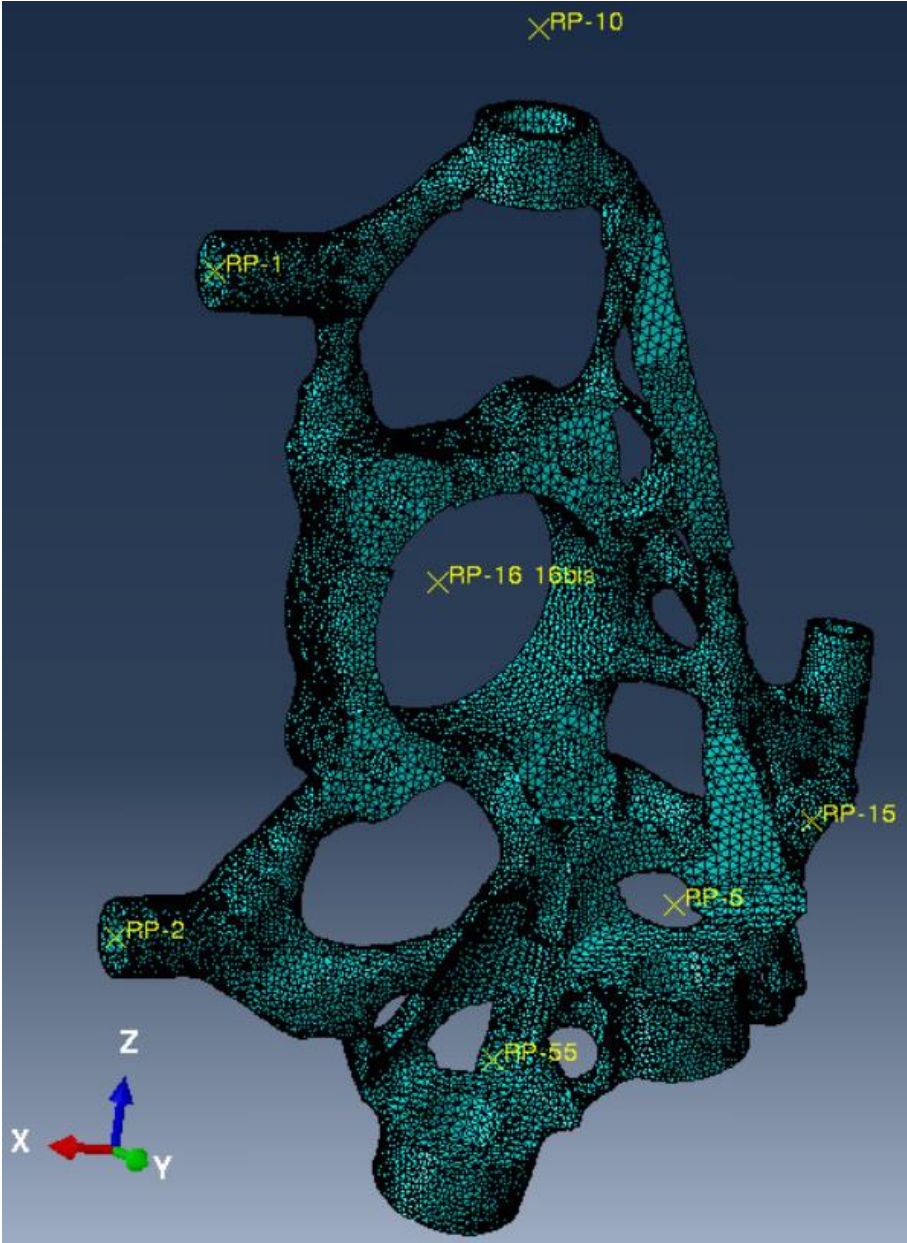


Figure 6-31 Mesh of the optimized component

Thanks to the lower volume, it has been possible to reduce the element mesh size to 3mm (from 4,5 mm of the topology optimization), having a total number of finite elements around 450'000 elements.

In the following images are shown the results of the finite element analysis on the optimized part. Also in this case, the exact value of the stress applied on the component cannot be shown. In the first Figure 6-32, it is shown the legend that is valid for all the results and as it can be seen the results are in percentage, so that on the blue areas the stress is zero or almost null, while the most loaded zones are highlighted in red. However, it is important to underline that, for each loading case, the stress is kept under the prescribed limits (fatigue or yield) that has been provided in Paragraph 6.10.

The verification confirmed the initial hypothesis that was done, when choosing only few loading cases for the optimization. In fact, the steps excluded from the topology optimization, do not produce high stresses on the optimized part. In some these steps (like in Figure 6-32, Figure 6-33, Figure 6-34, Figure 6-35, Figure 6-37, Figure 6-38) it can be observed a high concentration of the load in the small (and thin beam) connecting the element 10 (the upper part of the steering knuckle). In that point there is the highest load, but its value is significantly lower than the fatigue limit, and in general those steps have really low stress.

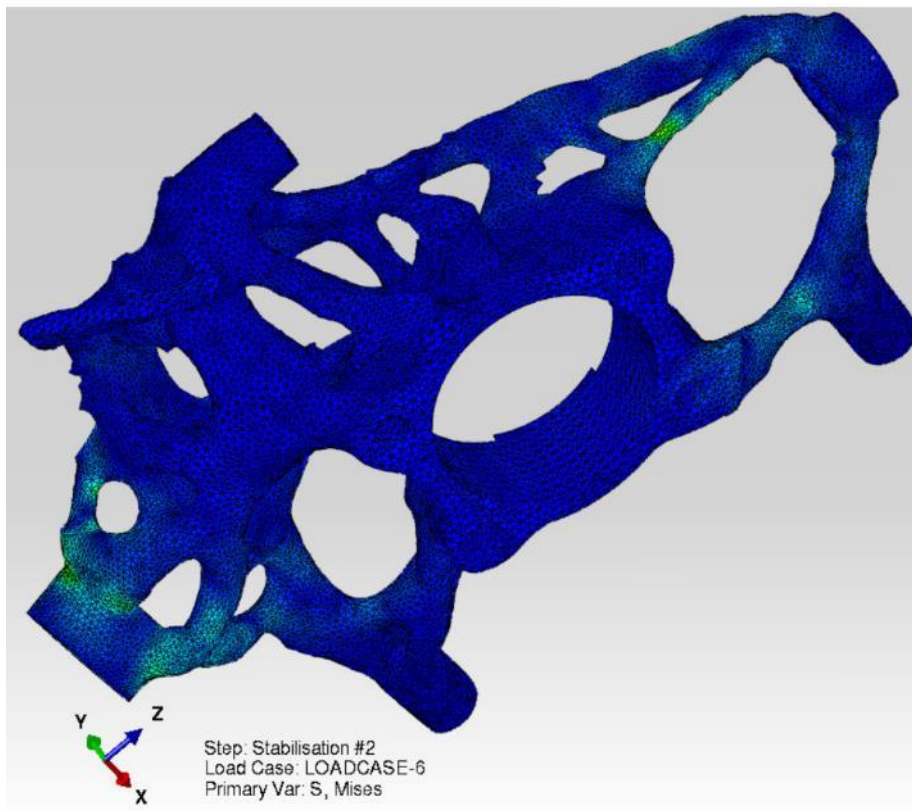
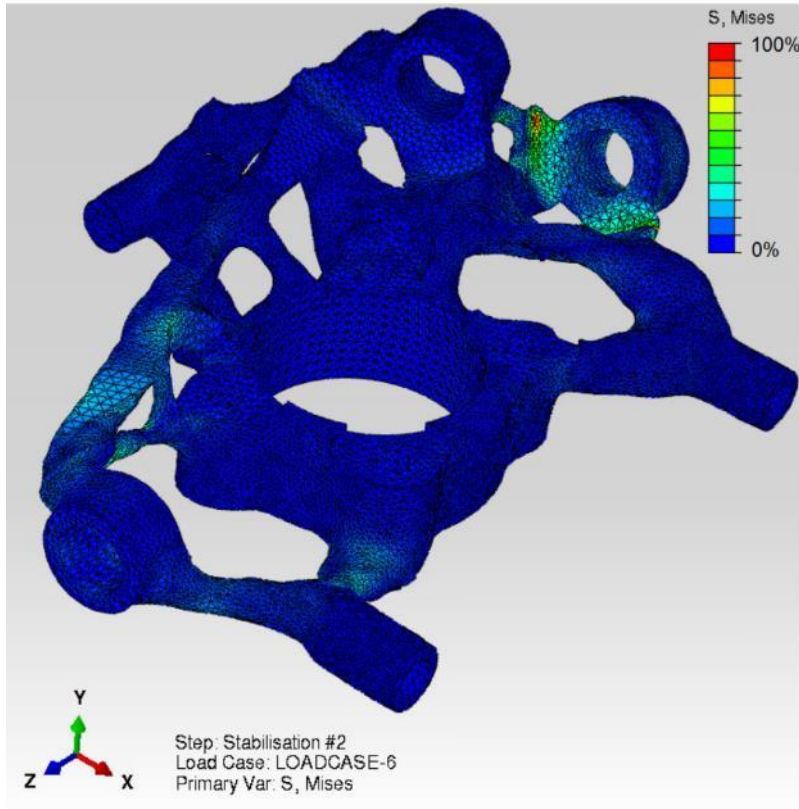


Figure 6-32 Stress results: Stabilisation #2

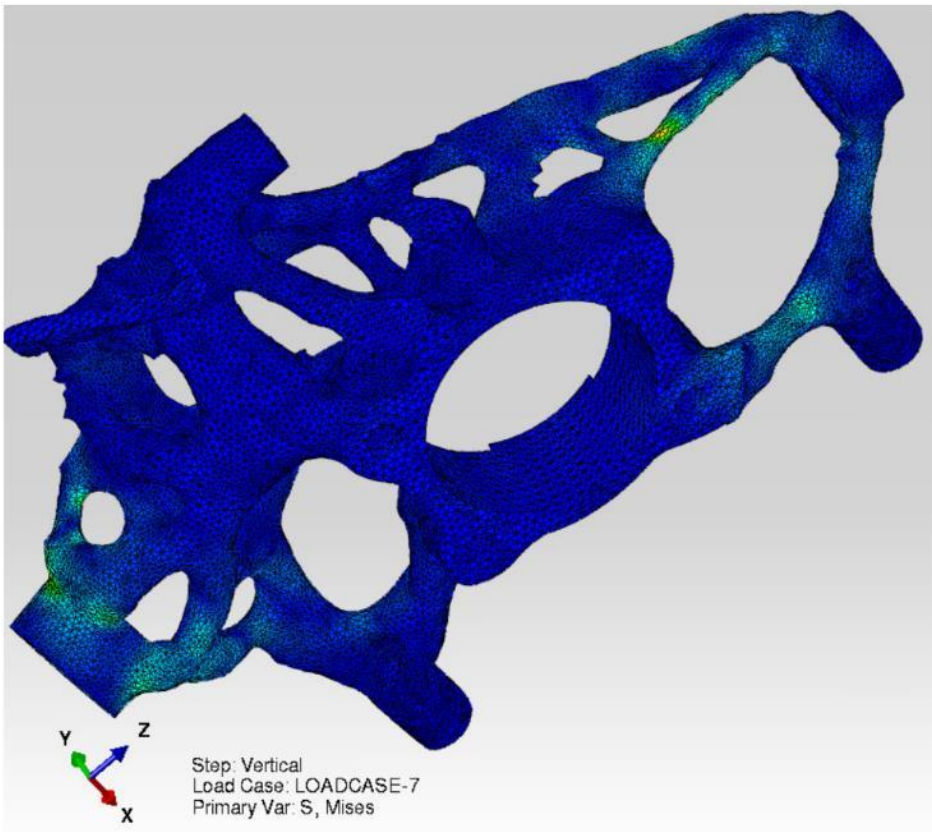
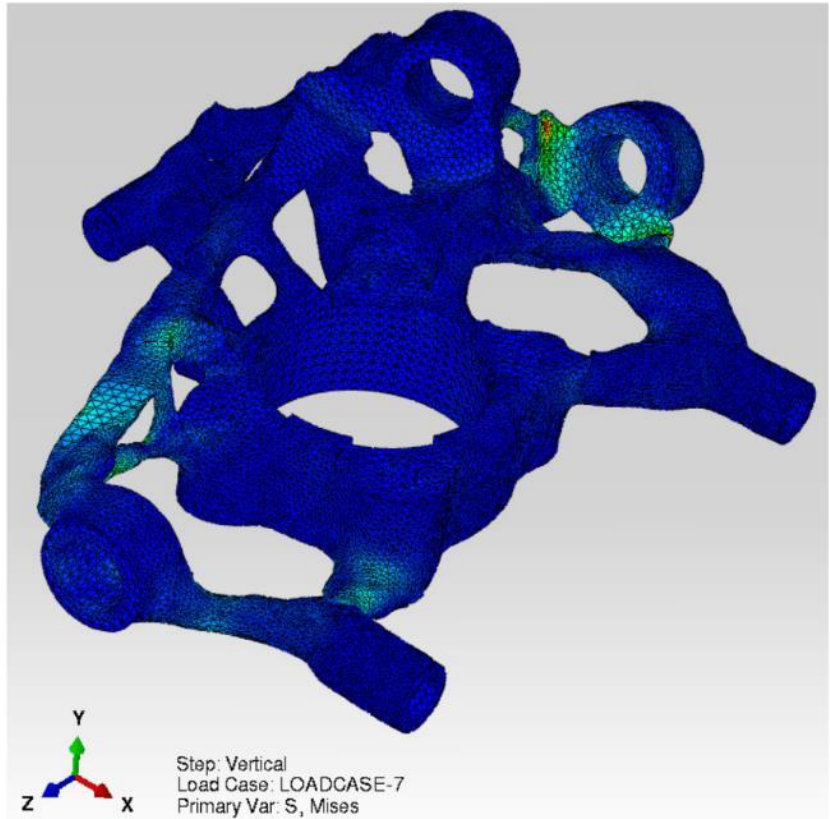


Figure 6-33 Stress results: Vertical 1

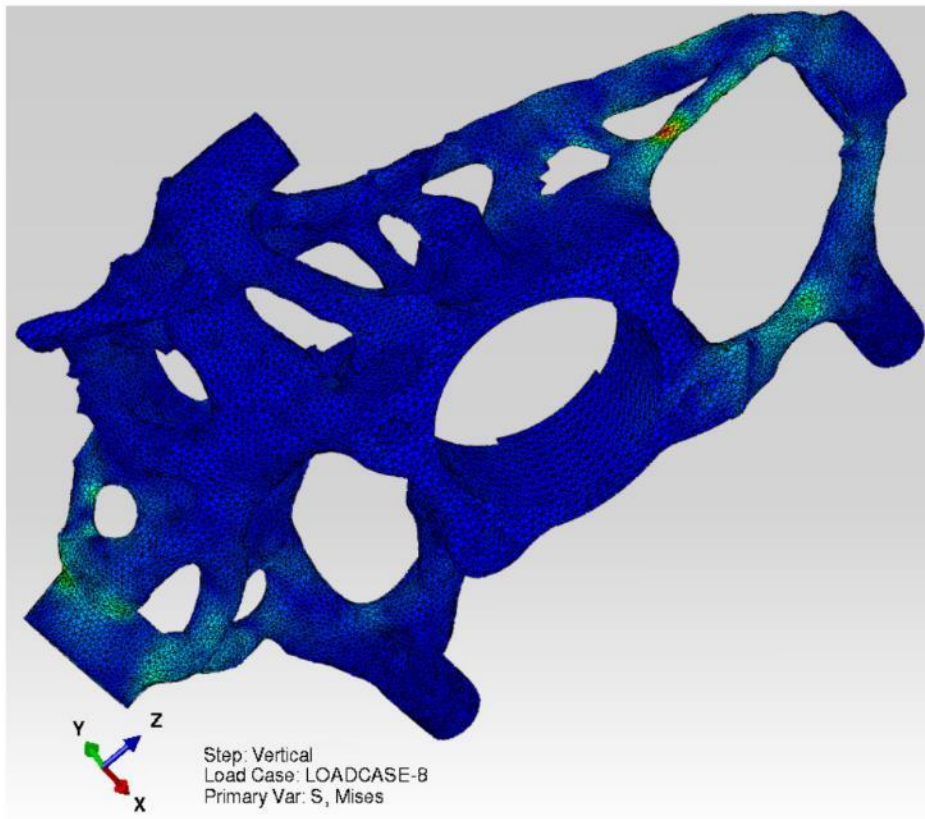
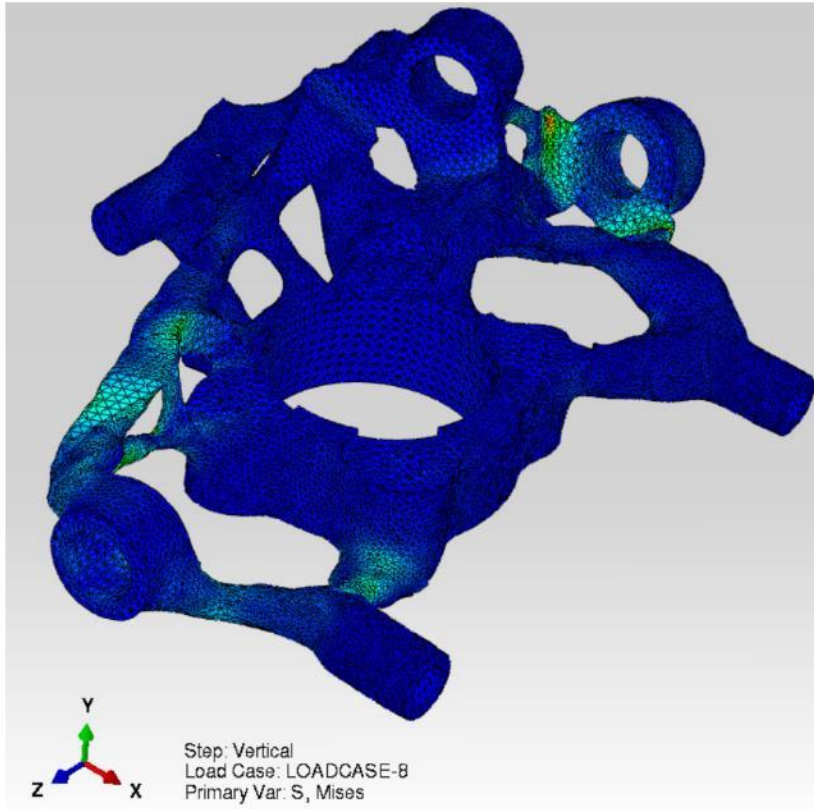


Figure 6-34 Stress results: Vertical 2

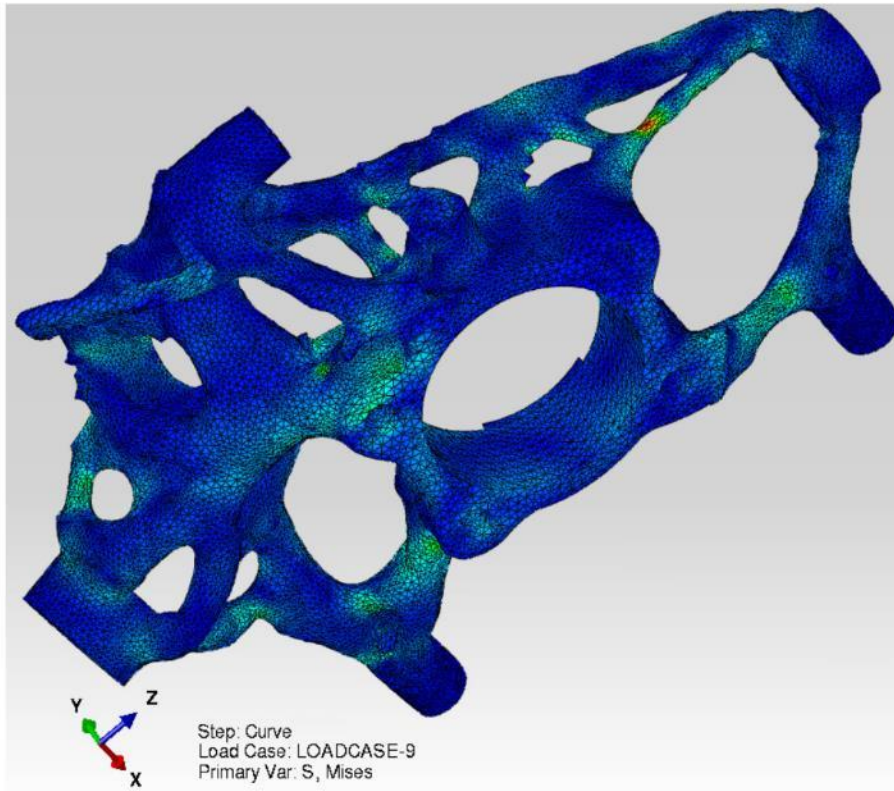
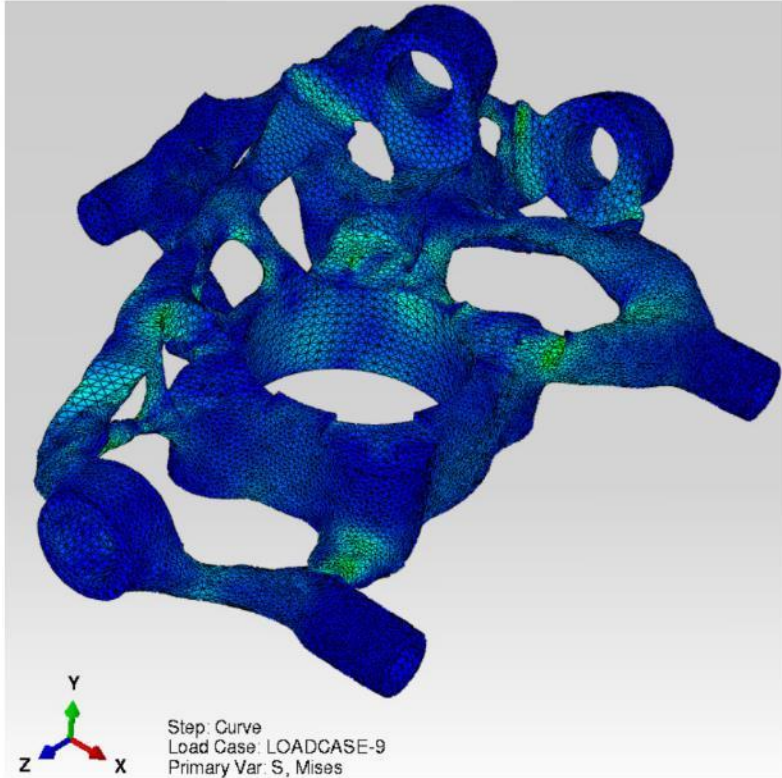


Figure 6-35 Stress results: Cornering 1

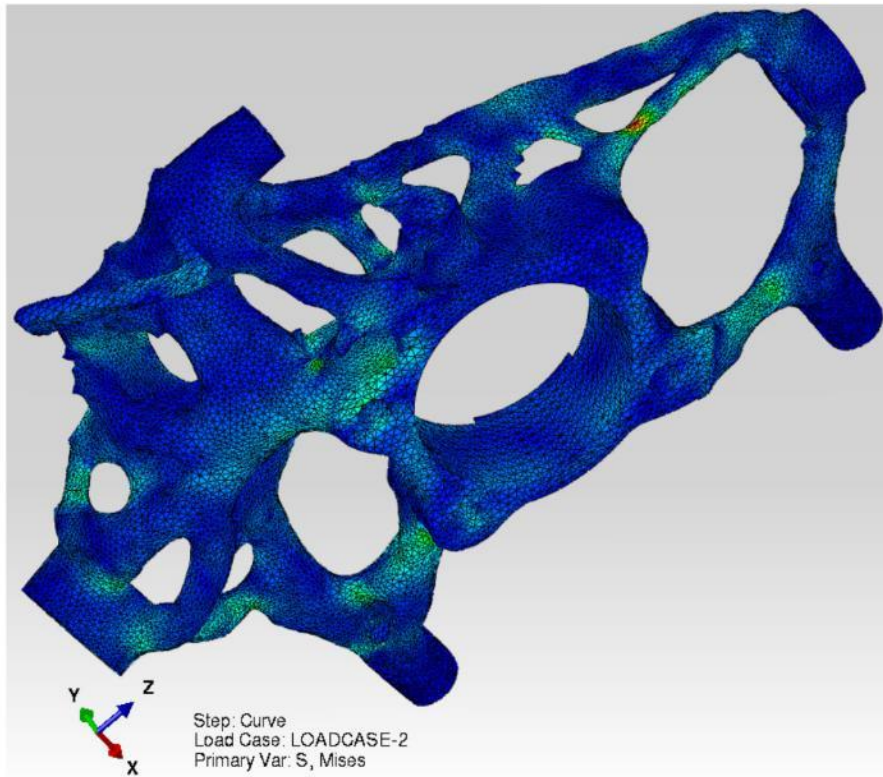
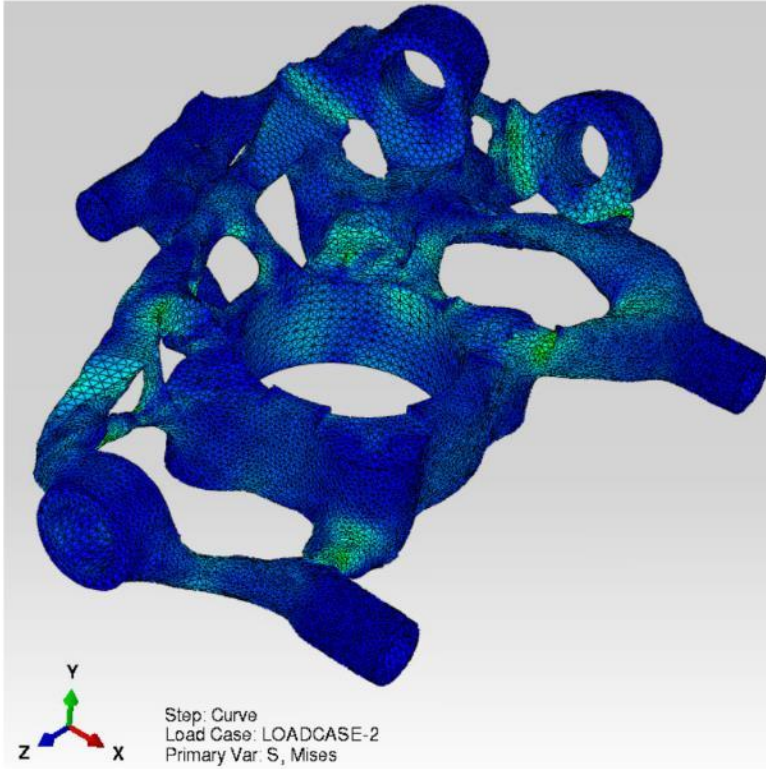


Figure 6-36 Stress results: Cornering 2

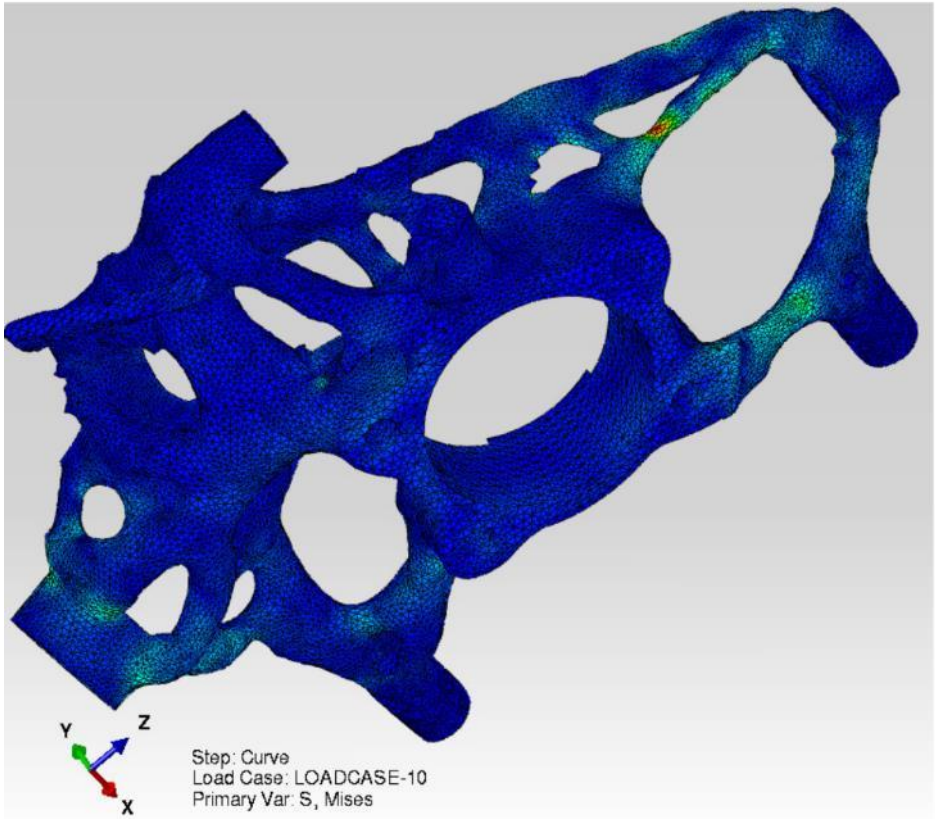
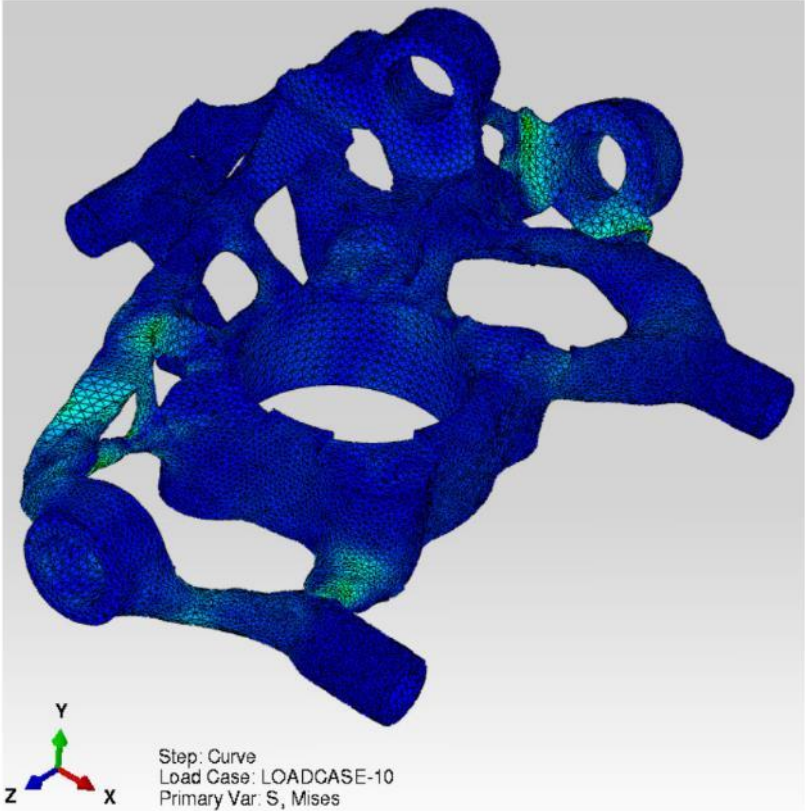


Figure 6-37 Stress results: Cornering 3

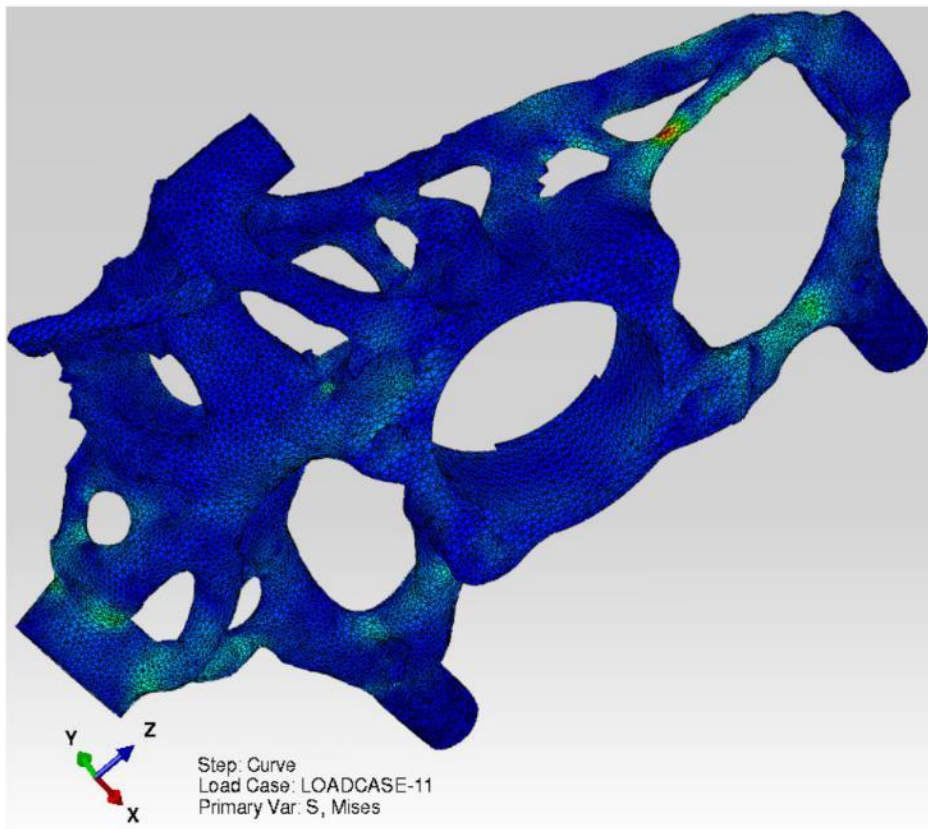
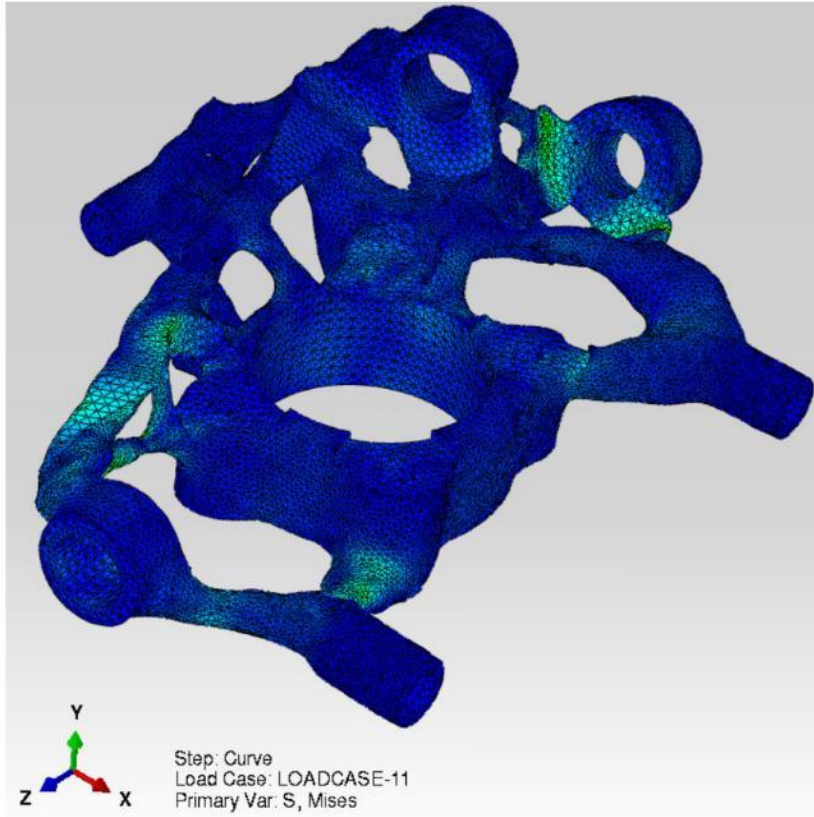


Figure 6-38 Stress results: Cornering 4

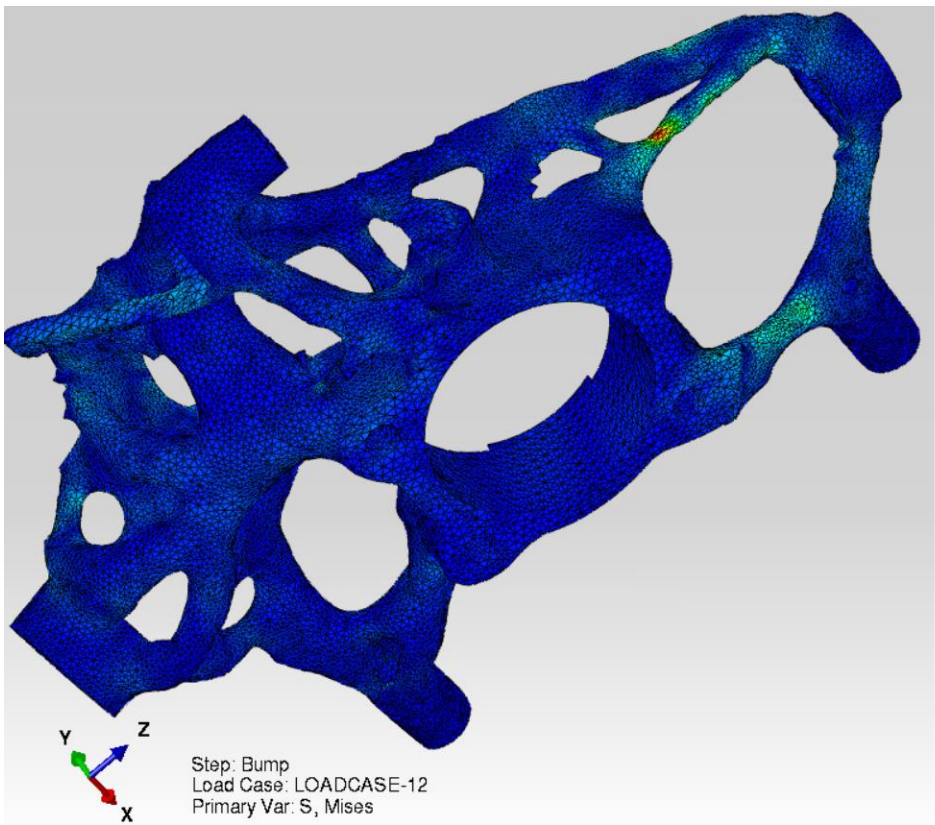
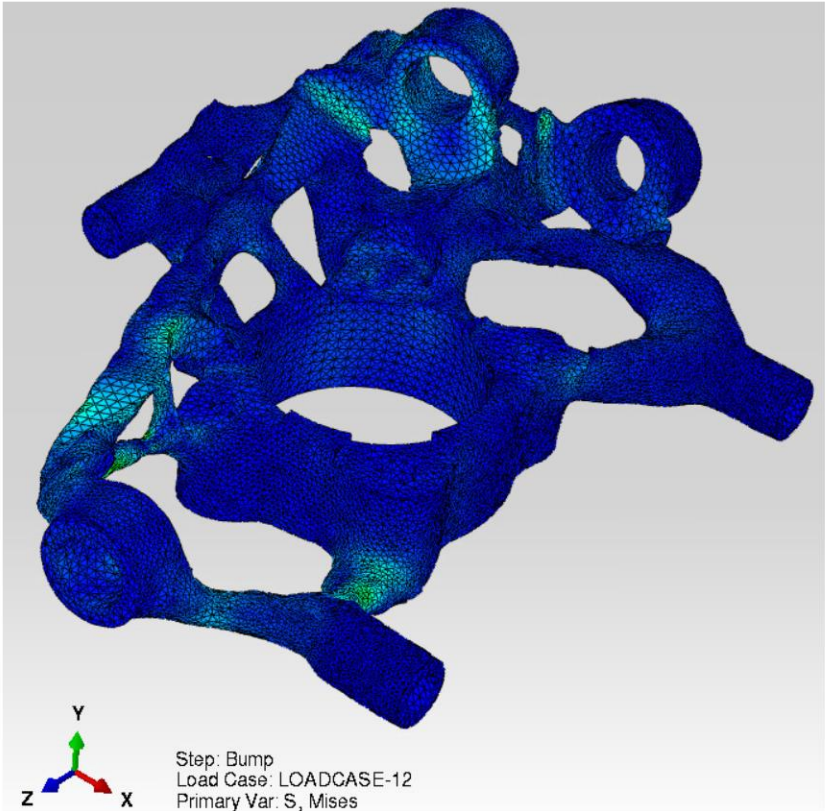


Figure 6-39 Stress results: Bump

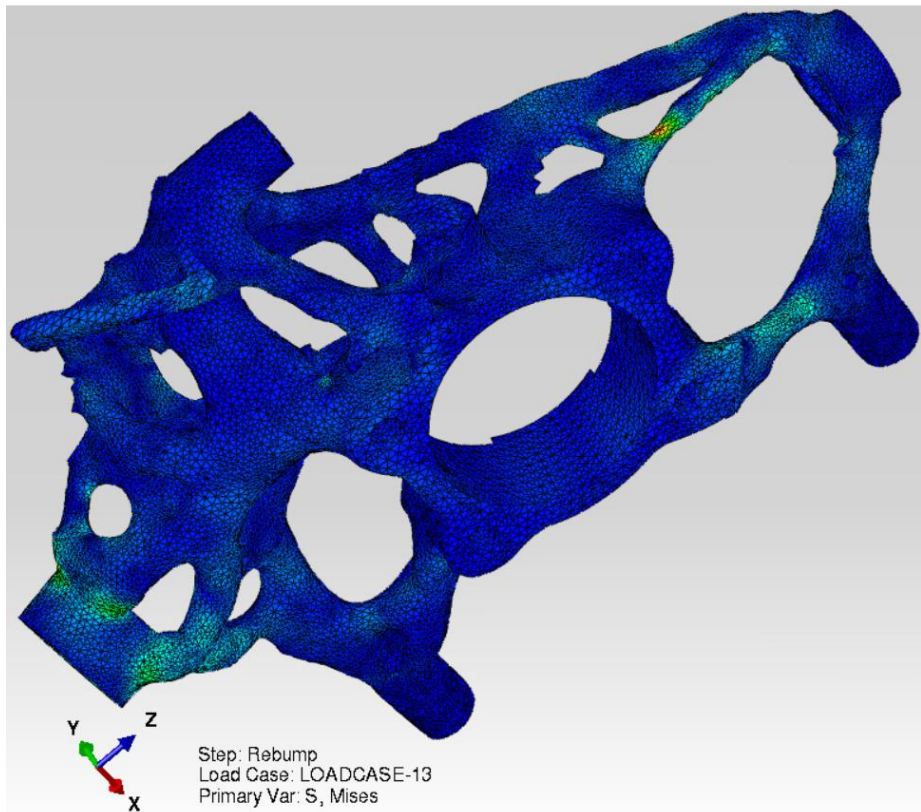
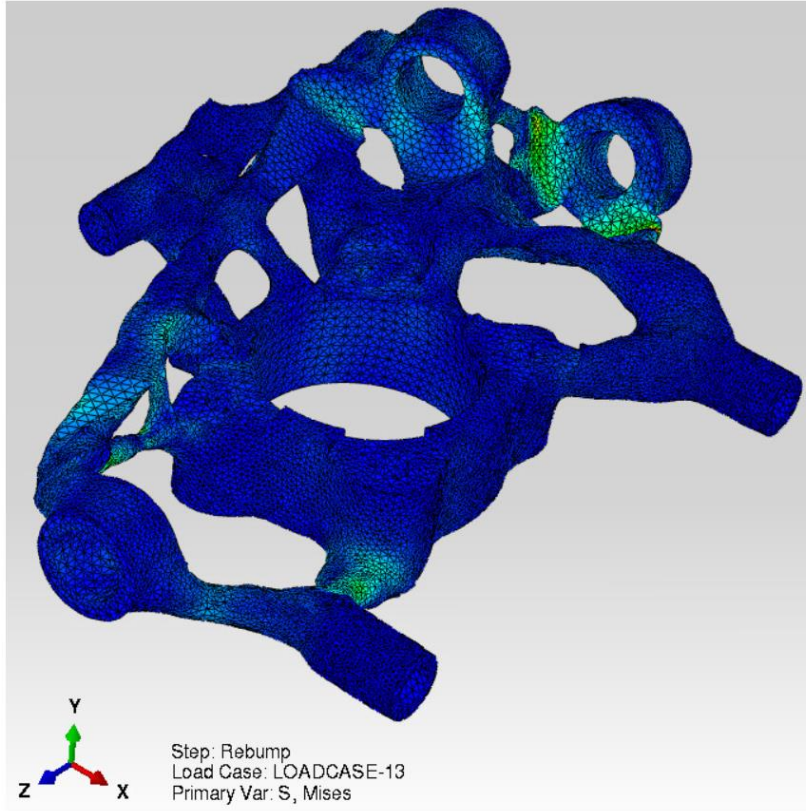


Figure 6-40 Stress results: Rebump

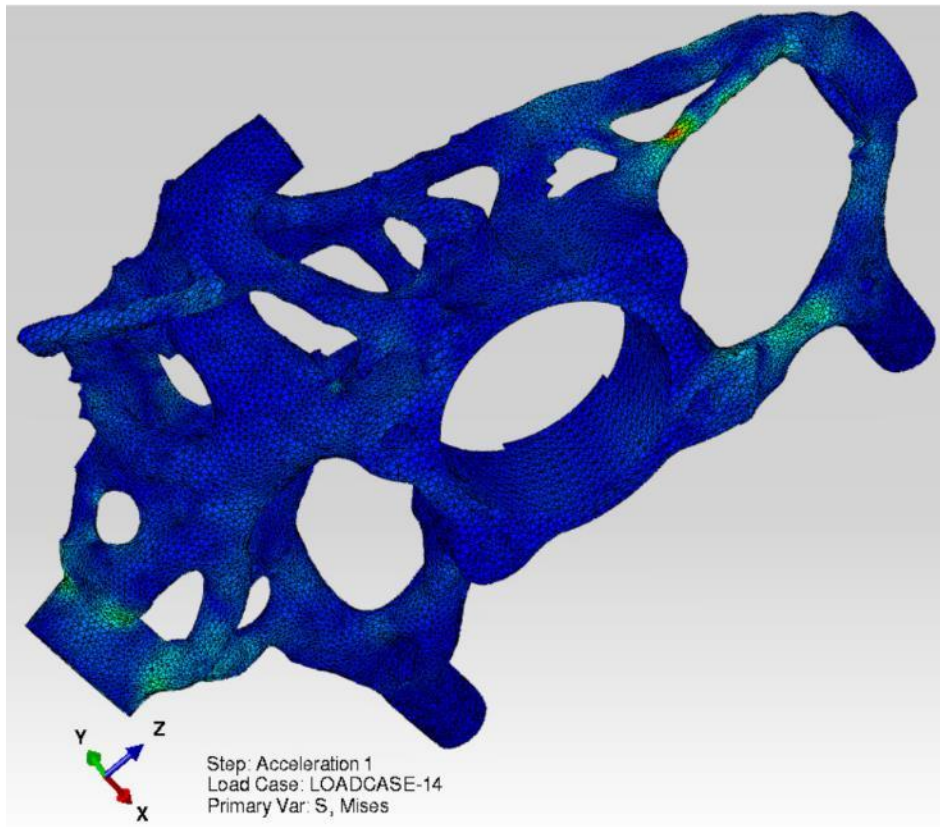
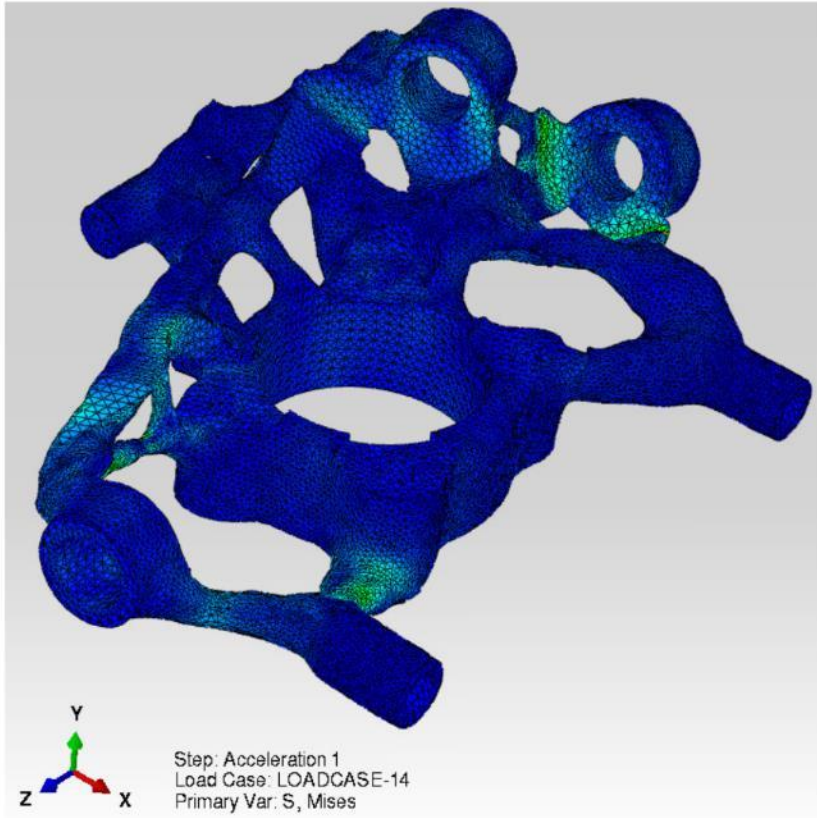


Figure 6-41 Stress results: Acceleration

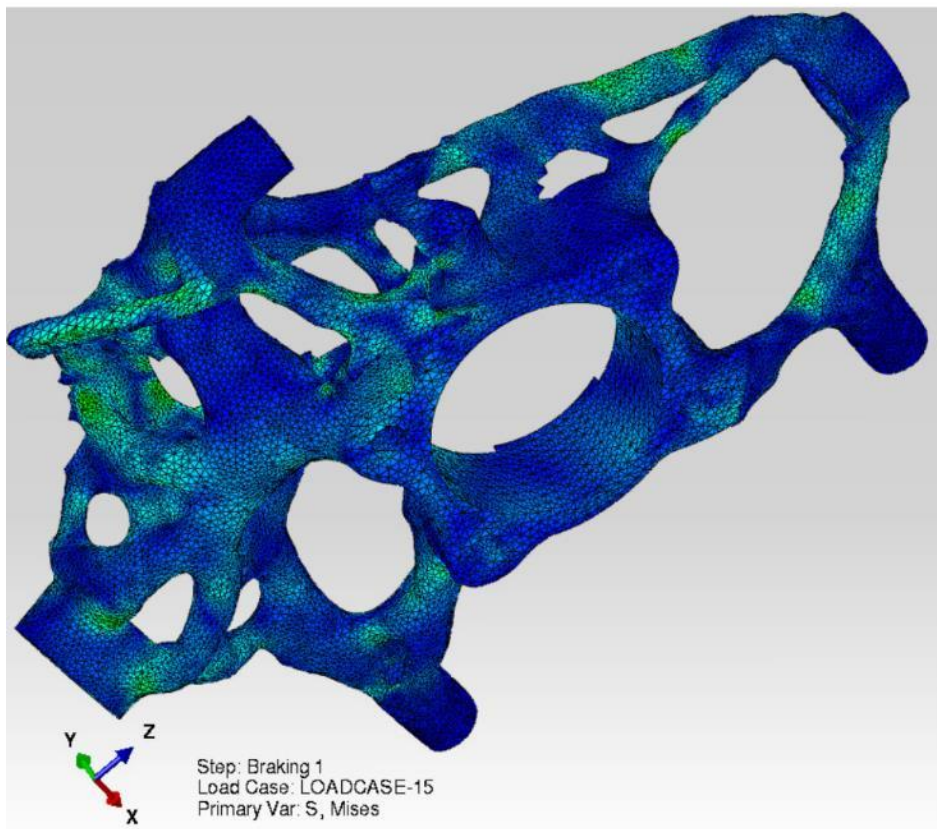
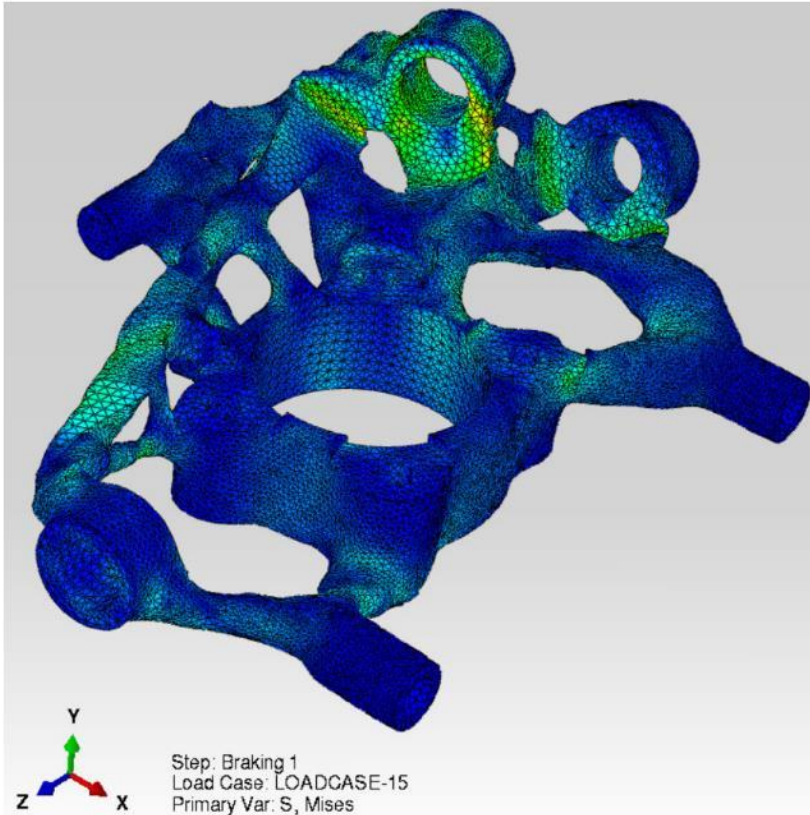


Figure 6-42 Stress results: Braking 1

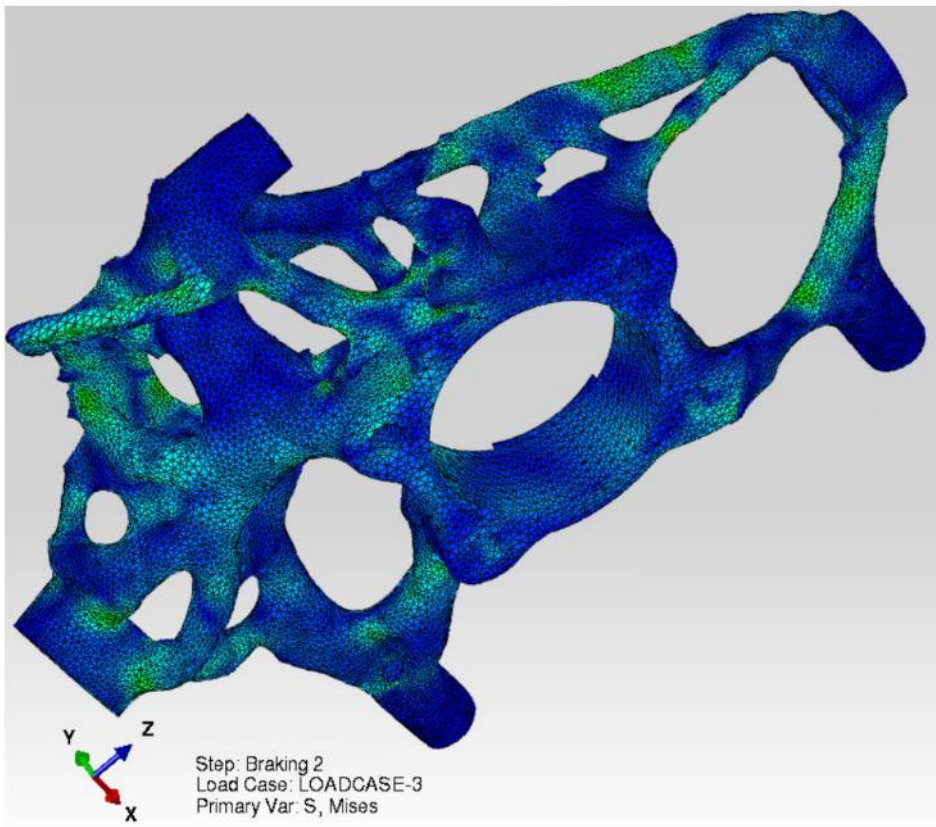
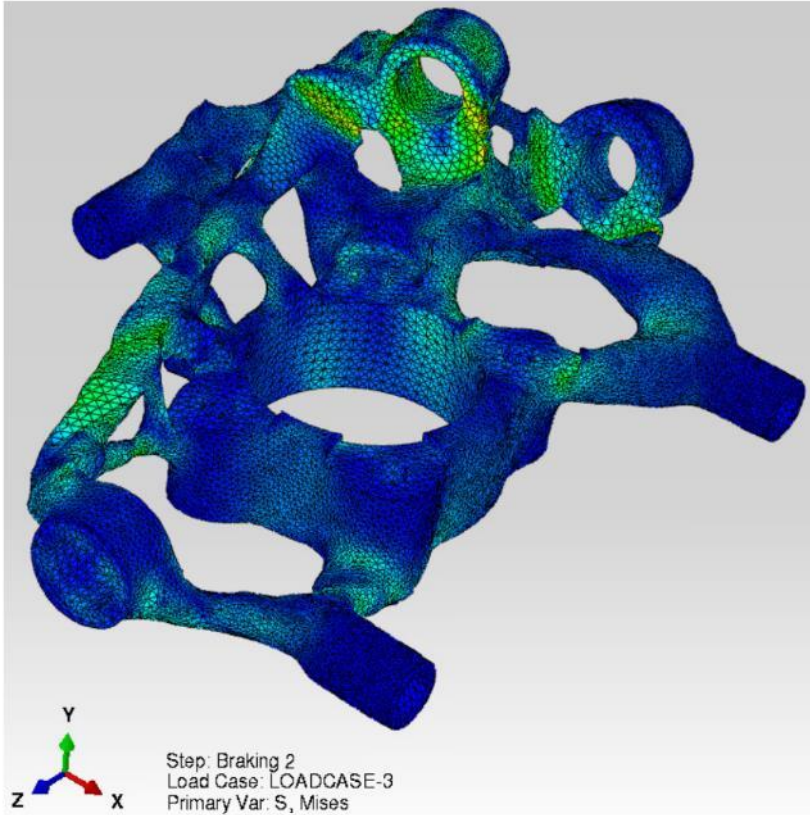


Figure 6-43 Stress results: Braking 2

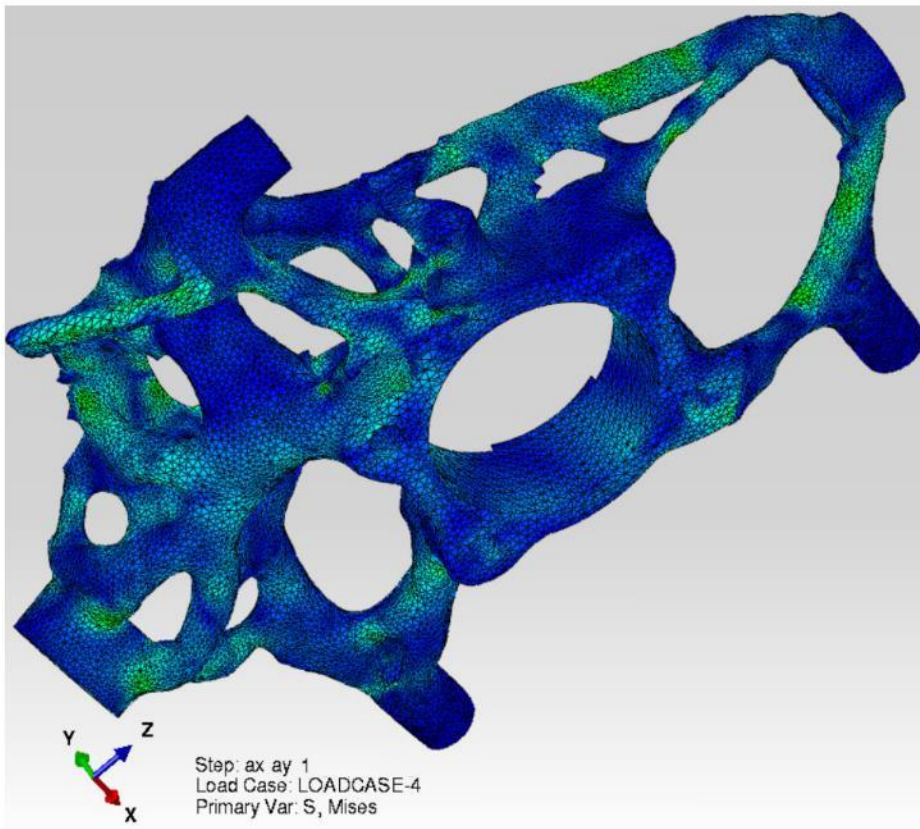
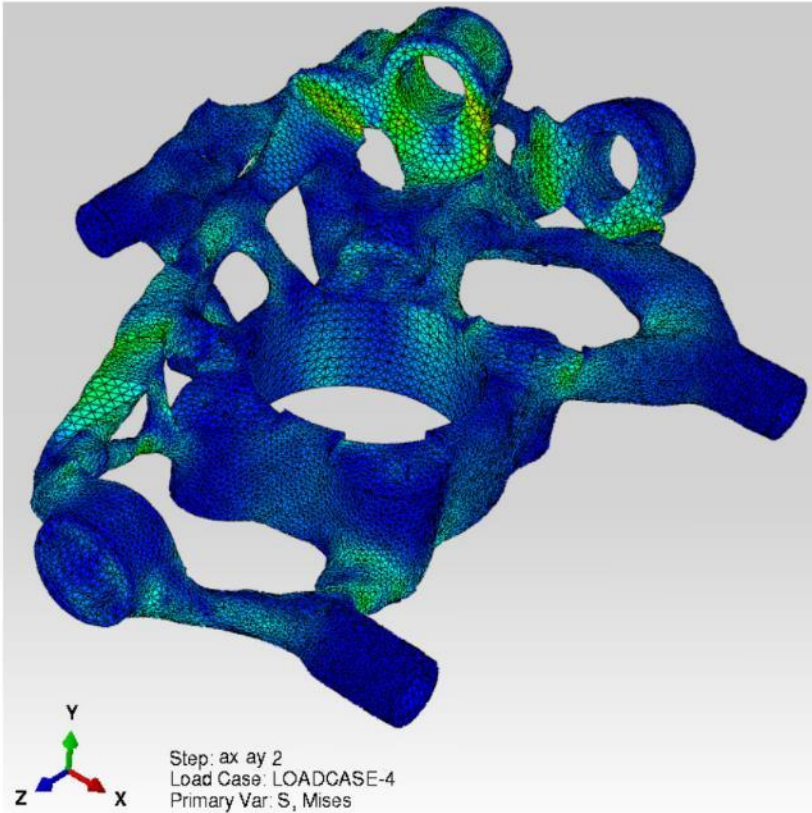


Figure 6-44 Stress results: ax+ay 1

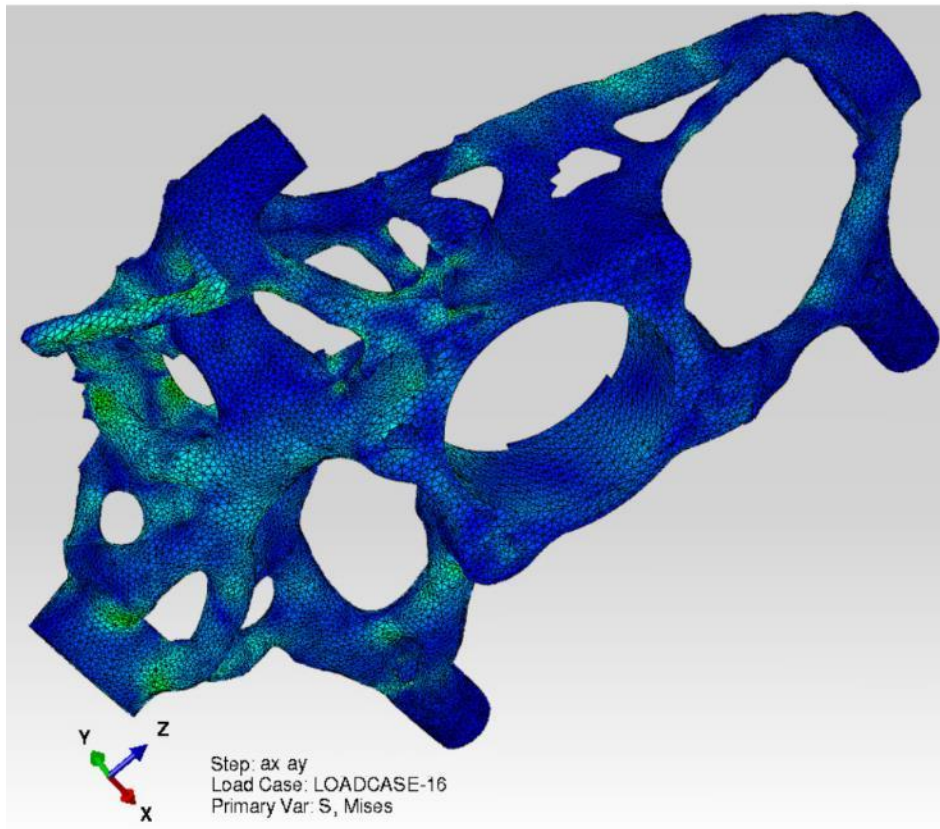
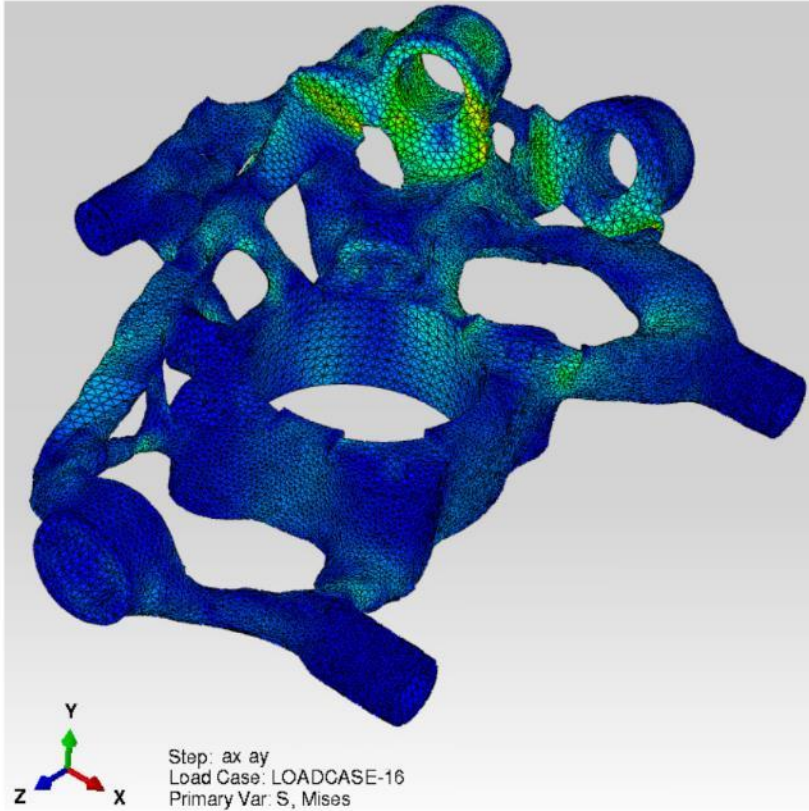


Figure 6-45 Stress results: ax+ay 2

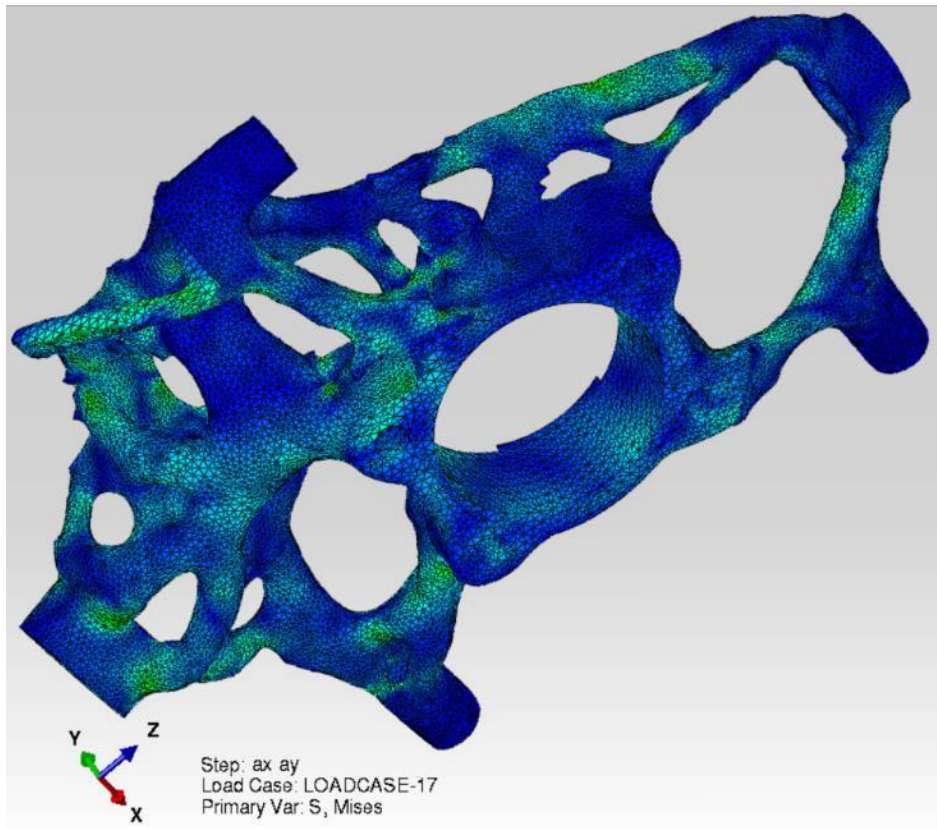
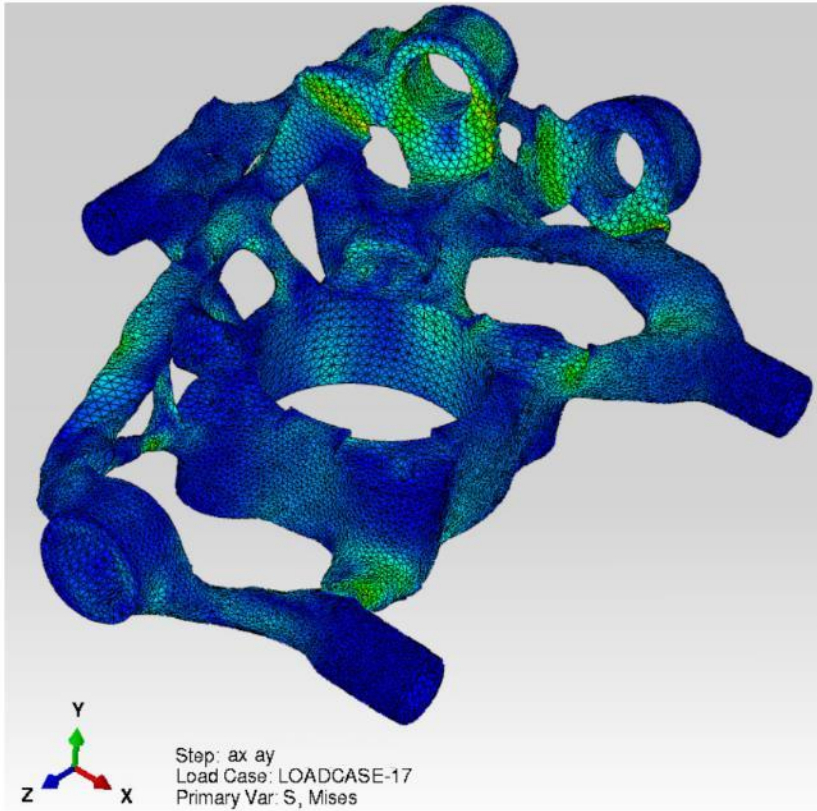


Figure 6-46 Stress results: ax+ay 3

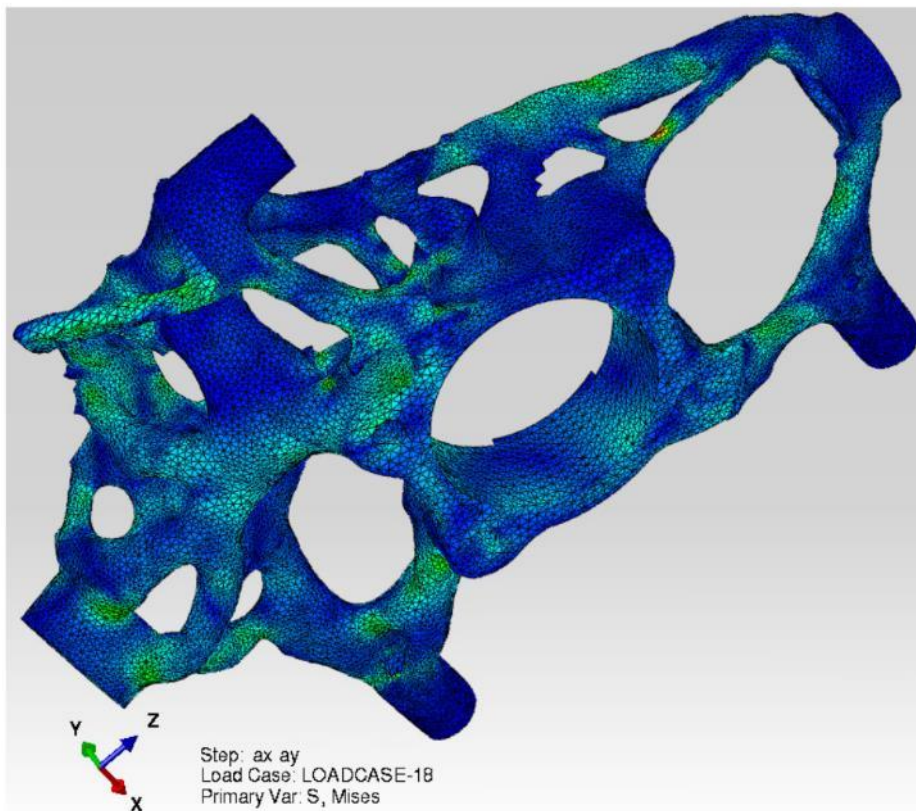
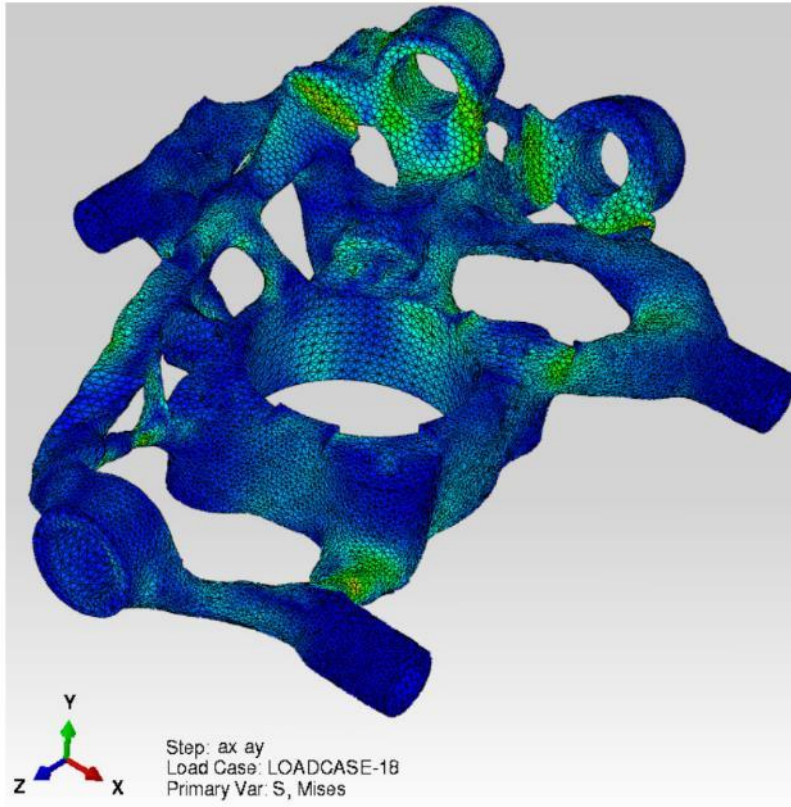


Figure 6-47 Stress results: ax+ay 4

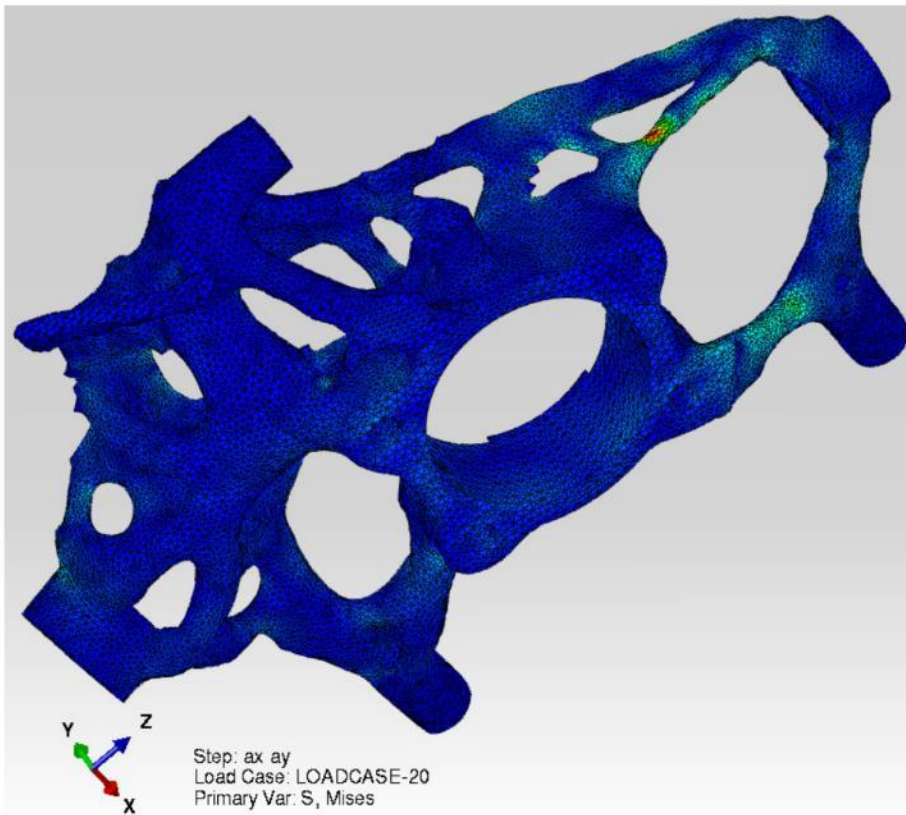
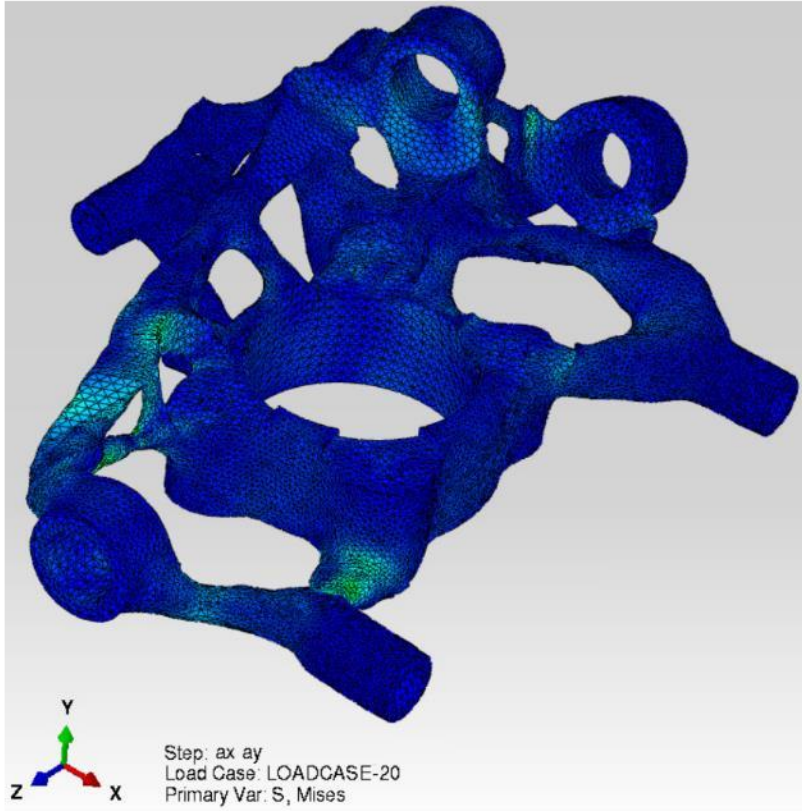


Figure 6-48 Stress results: ax+ay 5

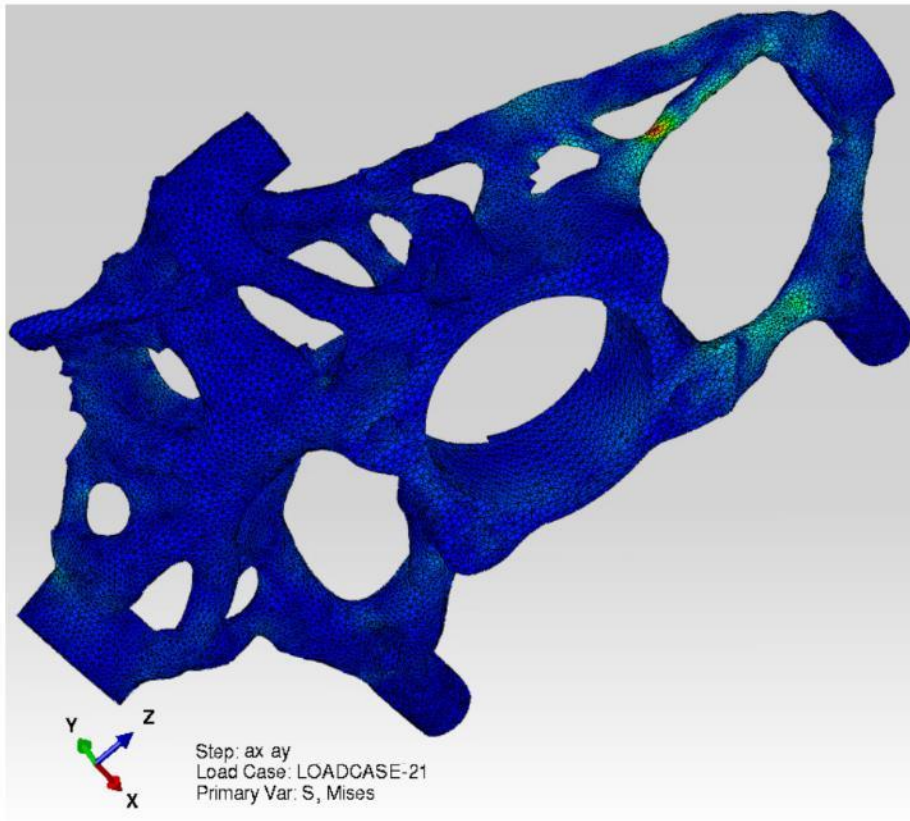
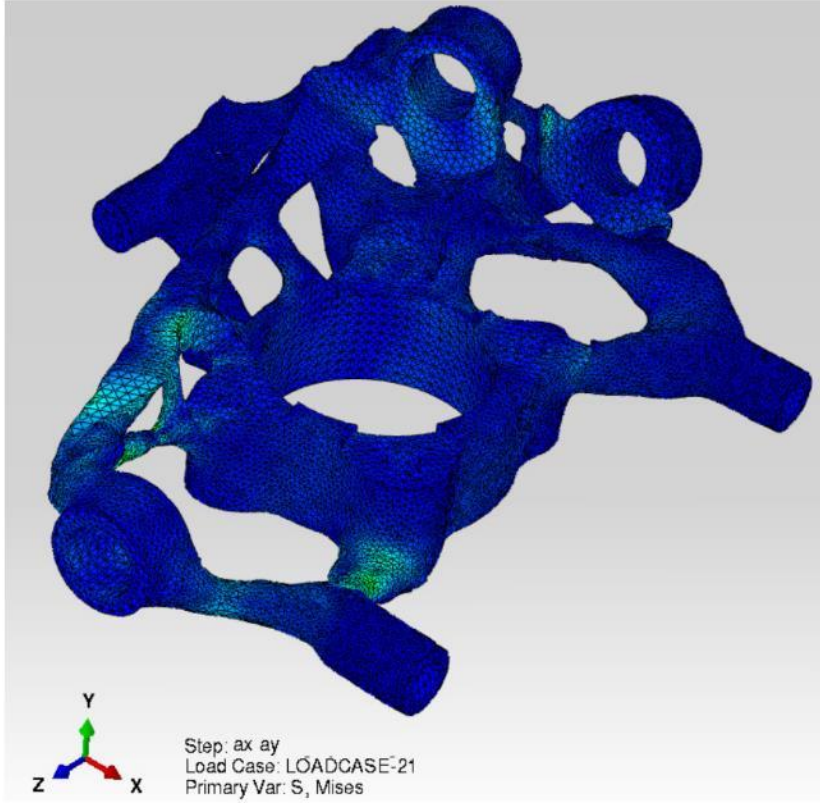


Figure 6-49 Stress results: ax+ay 6

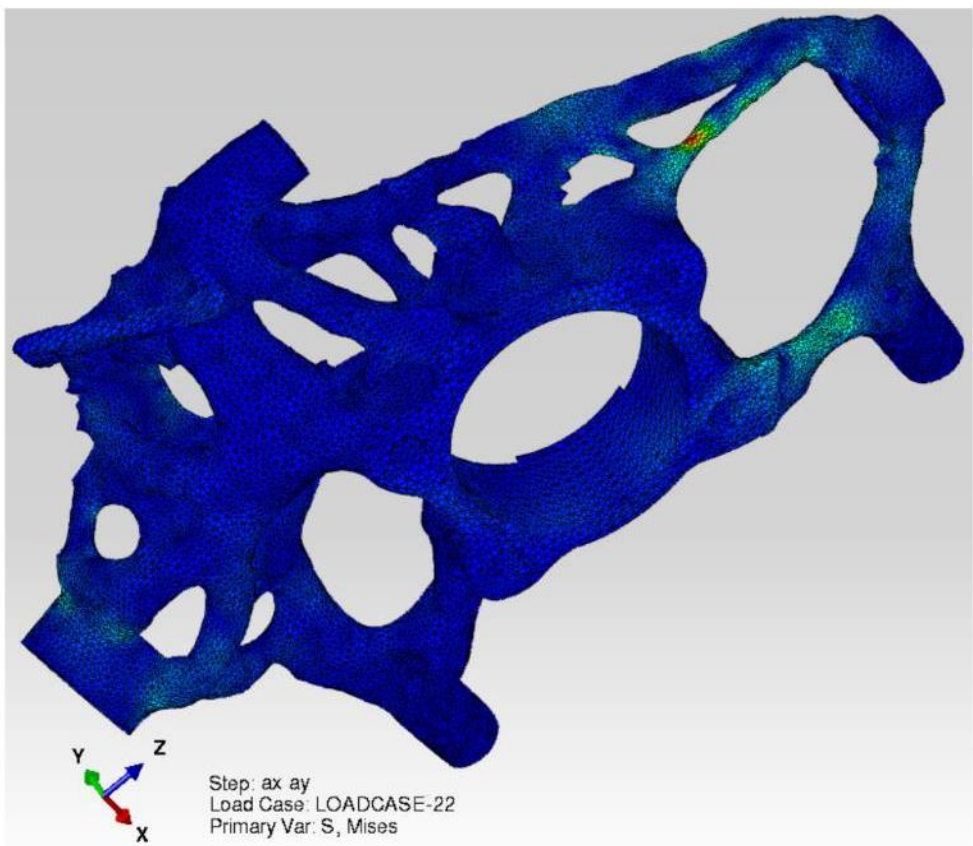
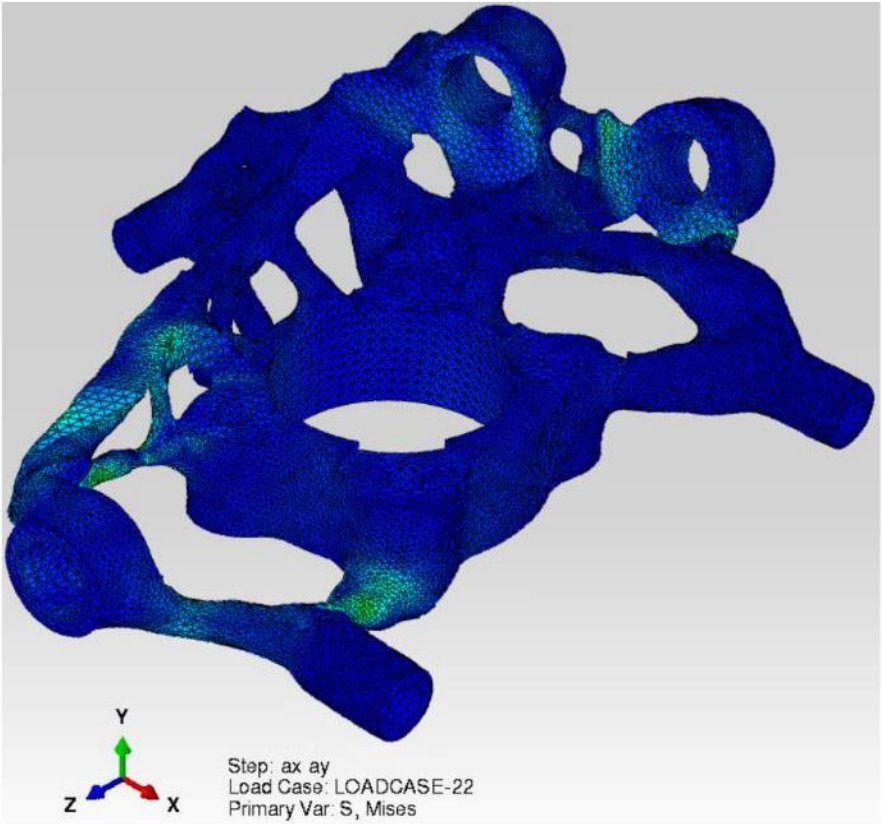


Figure 6-50 Stress results: ax+ay 6

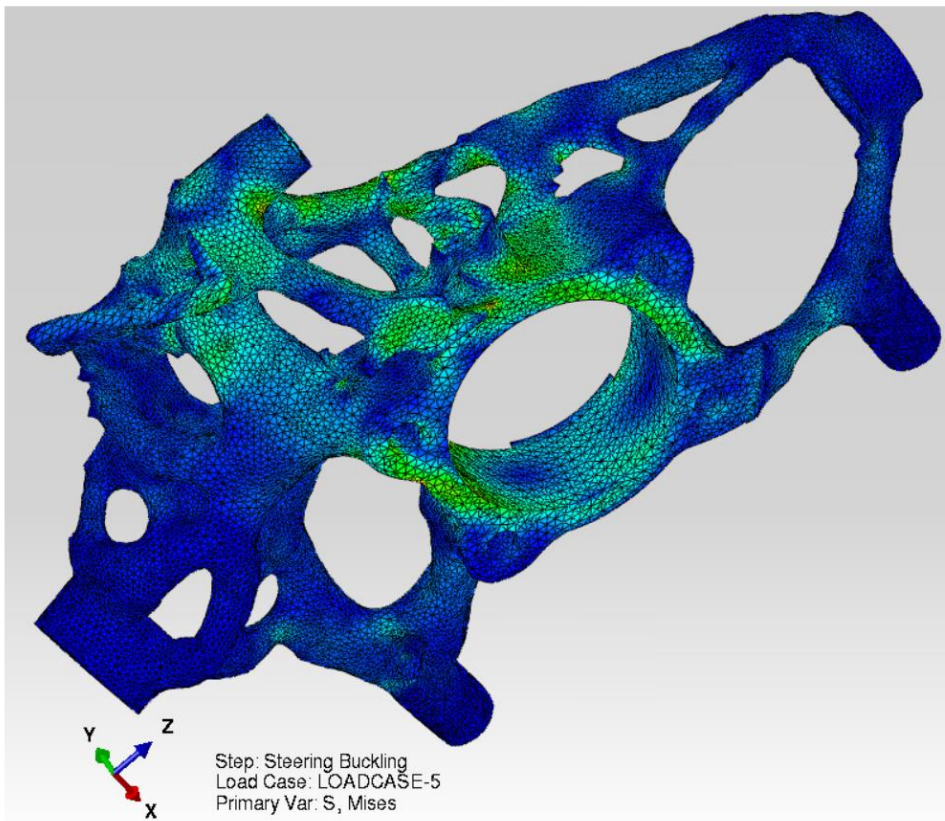
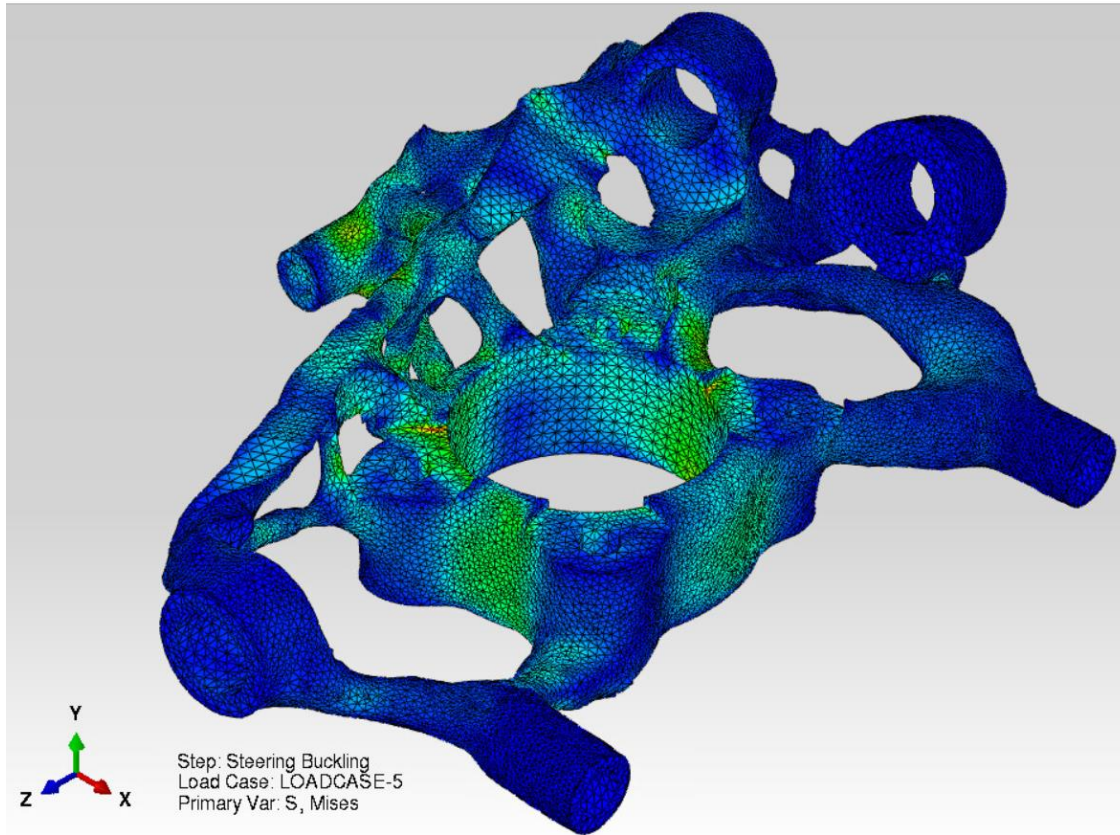


Figure 6-51 Stress results: Buckling steering

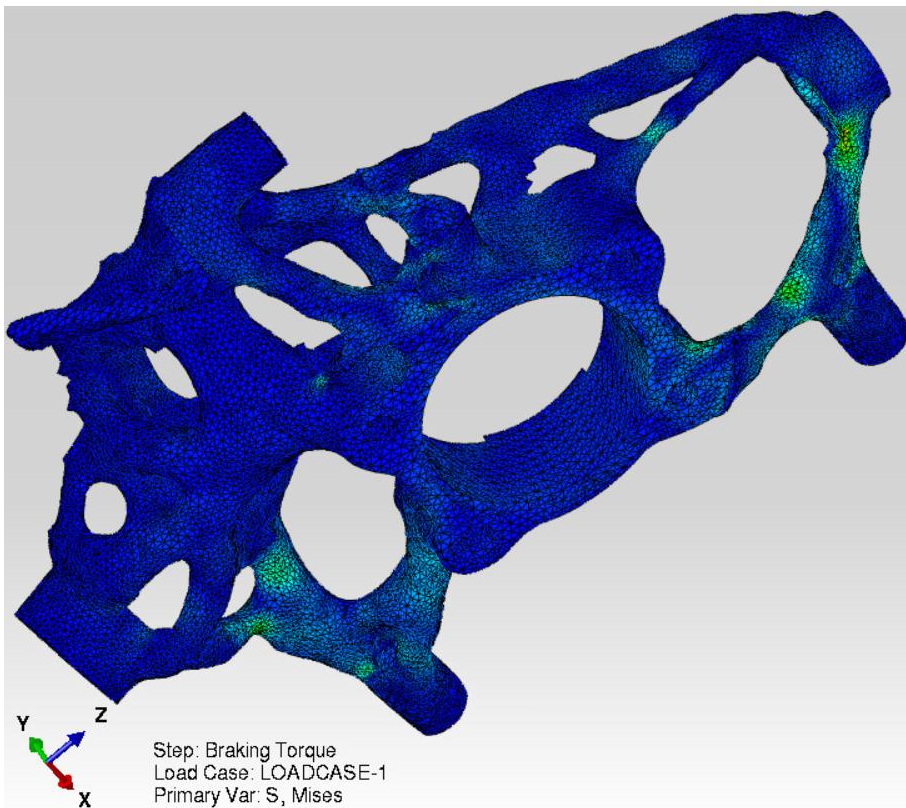
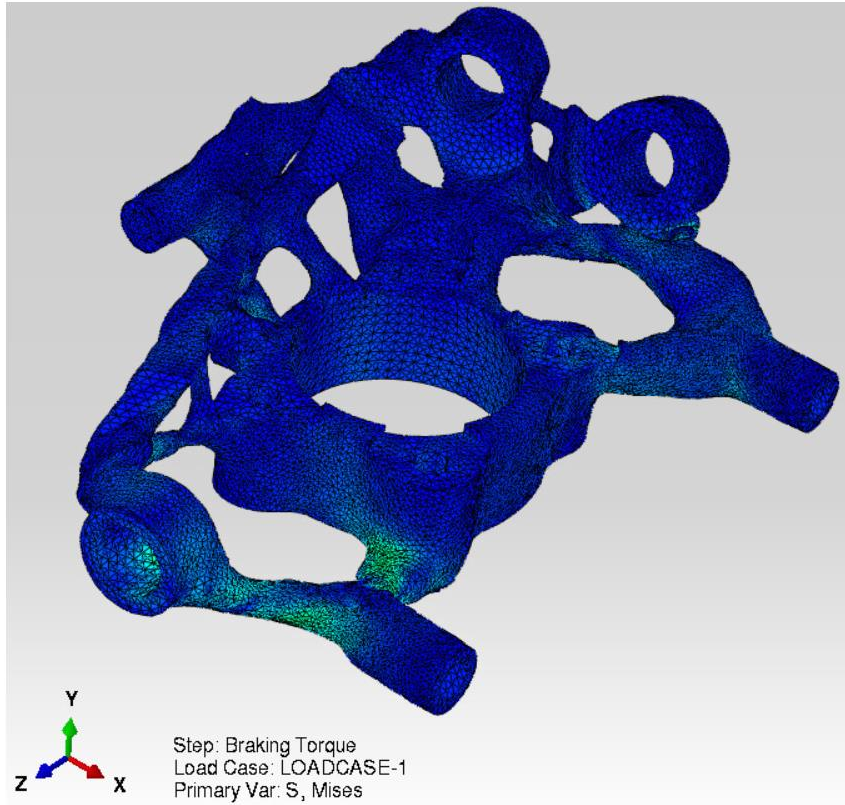


Figure 6-52 Stress results: Braking torque

6.14 Printing operation

Considering the positive results that the FE verification gave for the optimized component, as the stress was under the prescribed limits with a certain margin of safety the part can be considered ready for the printing operation.

The optimized steering knuckle has large dimensions for the Additive Manufacturing technology standard. In fact, the maximum dimensions of the part are around 360x280x190 mm. Due to this, it has not been possible to manufacture the component in the EOS M280 DMLS machine, available in the laboratory of the McMaster University. The building volume of this machine's chamber is 250 x 250 x 300 mm, so it is not possible to build the component in this machine.

In order to fabricate the component, it had been necessary to use a larger machine, like the EOS M400 whose chamber has the building volume of 400 x 400 x 400 mm. It has been found a supplier that owns this machine and that fabricated the component. The whole process of fabrication has been followed by the engineers and technicians of this company, so this thesis work will not treat in detail this phase of the project.



Figure 6-53 Support removal process on the optimized component

7 Conclusions

This thesis work describes the process adopted to redesign the steering knuckle of an automobile, to be fabricated with Additive Manufacturing technology. It has been presented the mechanical components and its unifying role of the steering, suspension and braking systems of the vehicle and the importance in its weight loss, to reduce the fuel consumption and to improve comfort and handling.

In order to achieve this improvement, it has been decided to verify the potential of the Additive Manufacturing technology. In the last years, this technology is dramatically increasing its use and applications, but the technology is still at its dawn, and much further advancement are necessary to allow AM to compete to the traditional manufacturing processes, especially in the large-scale production. Numerous companies, in different industrial sectors are investing in this technology, but the number of direct applications is still limited, as the main activities are nowadays related to prototyping, mainly to verify which is the real potential of the AM, always keeping in consideration its limitations and high cost.

This project, in collaboration with Politecnico di Torino, McMaster University and Fiat Chrysler Automobiles is exactly part of this industrial research, which evaluates the benefits that AM can provide in the construction of a complex metallic component.

The original steering knuckle is made in an aluminum alloy and weights 4,1 kg. Differently from most of the previous researches in the AM field, for which it has been quite common to choose a lighter material for the redesigned component to enhance the weight reduction, for this project it has been chosen to take a counter-trend path, by using a heavier material like the Maraging steel. This has been done because the company was interested in the real capability of the Additive Manufacturing technology, whose benefits in some cases can be hidden by the utilization of a lighter material. Moreover, this thesis has been developed in parallel with another study, for which the same component had to be redesigned, but in this case using an aluminum alloy. Consequently it will be also possible to compare the two results, to verify which metallic powder is more convenient.

The fundamental tool, that has been used to obtain the lightest possible result is the Topology Optimization. In several CAE software have been implemented a Topology Optimization module, and this is by used always more, thanks to the development of AM. Despite this, these softwares generally have not already implemented the constraints that may be useful for AM.

For the optimization simulations and FE analyses has been used the software Abaqus CAE-Tosca. After importing the space design, constructed with the CAD NX Siemens, an initial Finite Elements Analysis has been conducted, in order to verify the correct definition of the model and to check which are the most demanding loading conditions. In fact, because of the large number of loading conditions that has been necessary to analyze, it has been decided to include in the topology optimization only the most demanding loading cases, in order to reduce the really high computational cost.

The optimized part in Maraging steel reached a weight of 4,2 kg. So even if the material used for the re-designed part has a density which is the triple of the original one, its weight is almost the same. It must be considered that for the new part, most of the weight is taken by the non-design

areas, which are the part of the component that cannot be modified, being the connecting elements with the other suspension and braking systems. The application of this kind optimization would have given an even better result, if the non-design spaces were smaller.

Moreover, this component has been optimized, considering the as-built material properties. A more efficient solution (a lighter component) could have been obtained by submitting the component to an ageing heat treatment, which would lead to a doubling of the yield limit of Maraging steel.

The initial optimized part, which had a really rough and discontinuous surface, has been subjected to a smoothening process with the software Tosca. The complex STL file that was produced after the smoothening procedure has been reimported in Abaqus and transformed into a geometry, in order to validate the optimized steering knuckle with a final FEA with all the loading conditions, included those loading cases that have been initially excluded from the optimization.

Because of the large dimensions of the component, the printing operation had to be done in the largest machine available in the market, the EOS M400, which was not available in the laboratories of the McMaster University, so the component has been manufactured by an external supplier.

With this project, it has been possible to evaluate the real power of the Additive Manufacturing technology, demonstrating that it is possible to fabricate end-usable large metallic components. Of course, the dimension is still an important restriction, but in the future the building chambers are going to increase in size.

This production method is continuously spreading in different markets, but its utilization is still scarce because of the several limitations, above all the high cost of the machines and of the powders.

In addition, the printed parts sometimes have several defects, including microcracks and porosity and a fabrication free of defects is still difficult to be achieved. This is also caused by the lack of information regarding the optimal calibration of the machine, which can considerably variate depending on the activity.

Several progresses are still also necessary with regards to the Topology Optimization softwares, which are still not effectively connected to the AM sector, as generally they do not have the manufacturing restrictions that this fabrication method requires.

Finally, a fundamental boost to the Topology Optimization in combination with AM, can be achieved if in the CAD programs, the reconstruction of the component would be simpler, with a more automatic process. In fact, usually the results of the topology optimizations have really complex shapes, and most of the time may be taken using the CAD, reconstructing the optimized part into a geometry.

8 References

- [1] "REGULATION (EU) 2019/631 OF THE EUROPEAN PARLIAMENT AND OF THE COUNCIL setting CO2 emission performance standards for new passenger cars and for new light commercial vehicles," *Official Journal of the European Union*, 2019.
- [2] J. Barkenbus, "Our electric automotive future: CO2 savings through a disruptive technology," *Policy and Society*, no. 27, p. 399–410, 2009.
- [3] A. Serrenho, J. Norman and J. Allwood, "The impact of reducing car weight on global emissions: the future fleet in Great Britain," 2017.
- [4] "Alpine performance - Maserati Quattroporte Ghibli right rear spindle knuckle #5766," [Online]. Available: www.alpineperformance.com/maserati-quattroporte-ghibli-right-rear-spindle-knuckle-5766.
- [5] P. Dumbre, A. Mishra, A. Aher and S. Kulkarni, "STRUCTURAL ANALYSIS OF STEERING KNUCKLE FOR WEIGHT REDUCTION," *Int. J. Adv. Eng. Res. Studies*, no. 3, 2014.
- [6] SKF, "The next generation of hub units - Generation 3 hub bearings".
- [7] "Front Wheel Bearing Hub Assembly," [Online]. Available: www.alliedautoonline.com.au/front-wheel-bearing-hub-assembly-for-hyundai-i30-g.
- [8] J. C. Dixon, *Suspension Geometry and Computation*, Wiley, 2009.
- [9] W. Milliken and D. Milliken, *Race Vehicle Dynamics*, SAE, 1995.
- [10] V. Sivananth and S. S. Vijayarangan, "Fatigue life analysis and optimization of a passenger car steering knuckle under operating conditions," *International Journal of Automotive and Mechanical Engineering*, vol. 11, pp. 2417-2429, 2015.
- [11] "Alfa Romeo Giulia: sospensioni," January 2019. [Online]. Available: www.autotecnica.org/giulia-la-regina-dellhandling/.
- [12] T. Raiciu, "How Multi-Link Suspension Works," [Online]. Available: www.autoevolution.com/news/how-multi-link-suspension-works-7804.html.
- [13] G. Triantafyllidis, A. Antonopoulos, A. Spiliotis, S. Fedonos and D. Repanis, "Fracture Characteristics of Fatigue Failure of a Vehicle's Ductile Iron Steering Knuckle," *ASM International*, 2009.

- [14] M. Guiggiani, *The Science of Vehicle Dynamics: Handling, Braking, and Ride of Road and Race Cars*, Springer, 2018.
- [15] "Incidenza della diminuzione delle masse non sospese sull'handling del veicolo," [Online]. Available: www.staccone-engineering.com/articoli-tecnici/incidenza-della-diminuzione-delle-masse-non-sospese-sullhandling-del-veicolo/.
- [16] "Massa non sospesa, dinamica del veicolo," [Online]. Available: www.staccone-engineering.com/articoli-tecnici/masse-non-sospese/.
- [17] D. Hrovat, "Influence of unsprung weight on vehicle ride quality," *Journal of Sound and Vibration*, no. 124, pp. 497-516, 1988.
- [18] D. Pujari and R. Yerrawar, "Design And Experimental Evaluation of Steering Knuckle Arm For Stiffness," *IOSR Journal*, vol. 15, pp. 34-43, 2018.
- [19] S. Srivastava, S. Salunkhe, S. Pande and B. Kapadiya, "Topology optimization of steering knuckle structure," *Int. J. Simul. Multidisci. Des. Optim.*, vol. 11, no. 4, 2020.
- [20] V. Sivananth and S. Vijayarangan, "FATIGUE LIFE ANALYSIS AND OPTIMIZATION OF A PASSENGER CAR STEERING KNUCKLE UNDER OPERATING CONDITIONS," *IJAME*, vol. 11, pp. 2417-2429, 2015.
- [21] P. Tagade, A. Sahu and H. Kutarmare, "Optimization and Finite Element Analysis of Steering Knuckle," in *ICQUEST*, 2015.
- [22] S. Reddy, V. Maranan and T. Simpson, "APPLICATION OF TOPOLOGY OPTIMIZATION AND DESIGN FOR ADDITIVE MANUFACTURING GUIDELINES ON AN AUTOMOTIVE COMPONENT," in *ASME International Design Engineering Technical Conferences*, 2016.
- [23] B. Berman, "3-D printing: The new industrial revolution," 2012.
- [24] ASTM International, "ASTM Additive Manufacturing Technology Related Standards".
- [25] "Google Trends," [Online]. Available: <https://trends.google.it/>.
- [26] "Croft Additive manufacturing," [Online]. Available: <https://www.croftam.co.uk/>.
- [27] I. Gibson, D. Rosen and B. Stucker, *Additive Manufacturing Technologies: 3D Printing, Rapid Prototyping, and Direct Digital Manufacturing*, Springer, 2015.
- [28] D. Cooper, M. Stanford, K. Kibble and G. Gibbons, "Additive Manufacturing for product improvement at Red Bull Technology," 2012.

- [29] M. Mehrpouya, A. Dehghanghadikolaei, B. Fotovvati, A. Vosooghnia, S. Emamian and A. Gisario, "The Potential of Additive Manufacturing in the Smart Factory Industrial 4.0: A Review," 2019.
- [30] E. Goulart, L. de-Caires, T.-S. K. B. Araujo, S. Rocco, M. Sforca, I. de-Sousa, G. Kobayashi, C. Musso, A. Assoni, D. Oliveira, E. Caldini, S. Raia, P. Lelkes and M. Zatz, "3D bioprinting of liver spheroids derived from human induced pluripotent stem cells sustain liver function and viability in vitro," 2019.
- [31] A. Paolinia, S. Kollmannsberg and E. Rank, "Additive manufacturing in construction: A review on processes, applications, and digital planning methods," 2019.
- [32] Cadalyst, "Wholers Reports on Additive Manufacturing," 2017. [Online]. Available: www.cadalyst.com/hardware/3d-printers/wohlers-report-finds-slower-overall-growth-more-competition-3d-printing-space.
- [33] E. P. Design. [Online]. Available: <http://engineeringproductdesign.com/additive-manufacturing-process-steps/>.
- [34] All3DP, "STL File Format (3D Printing)," [Online]. Available: all3dp.com/what-is-stl-file-format-extension-3d-printing/.
- [35] Materialise, MAGICS Print Metal - User Manual.
- [36] B. Leutenecker-Twelsieka, C. Klahnb and M. Meboldt, "Considering Part Orientation in Design for Additive Manufacturing," no. 50, pp. 408-413, 2016.
- [37] P. Das, "Optimum Part Build Orientation in Additive Manufacturing for Minimizing Part Errors and Build Time," 2016.
- [38] EOS, "MaragingSteel MS1 - Material data sheet".
- [39] P. Jacobs, Rapid Prototyping & Manufacturing: Fundamentals of Stereolithography, Society of Manufacturing Engineers, 1993.
- [40] K. Wegener, "Vorwort "Additive Fertigung"," in *SWISS RaPiD Forum*, 2010.
- [41] G. Moroni, W. Syam and S. Petrò, "Functionality-based part orientation for additive manufacturing," *Procedia CIRP*, no. 36, pp. 217-222, 2015.
- [42] S. Ford and M. Despeisse, "Additive manufacturing and sustainability: an exploratory study of the advantages and challenges," *Journal of Cleaner Production*, vol. 137, pp. 1573-1587, 2016.

- [43] H. Taheri, M. Shoaib, L. Koester and T. Bigelow, "Powder-based additive manufacturing – a review of types of defects, generation mechanisms, detection property evaluation and metrology," 2017.
- [44] L. Wang, S. Wang and X. Hong, "Pulsed SLM-manufactured AlSi10Mg alloy: mechanical properties and microstructural effects of designed laser energy densities," *Journal of Manufacturing Processes*, no. 35, p. 492–499, 2018.
- [45] Wikipedia, "Selective Laser Melting," [Online]. Available: en.wikipedia.org/wiki/Selective_laser_melting.
- [46] A. Fagali-de-Souzaa, K. Al-Rubaie, S. Marques and B. Zluhand, "Effect of laser speed, layer thickness, and part position on the mechanical properties of maraging 300 parts manufactured by selective laser melting," *Materials Science & Engineering A*, 2019.
- [47] S. Cacace and Q. Semeraro, "About Fluence and Process Parameters on Maraging Steel Processed by Selective Laser Melting: Do They Convey the Same Information?," *INTERNATIONAL JOURNAL OF PRECISION ENGINEERING AND MANUFACTURING*, vol. 19, no. 12, pp. 1873-1884, 2018.
- [48] P. Nezhadfar, A. Soltani-Tehrani, A. Sterling, N. Tsolas and N. Shamsaei, "The Effects of Powder Recycling on the Mechanical Properties of Additively Manufactured 17-4 PH Stainless Steel," in *Solid Freeform Fabrication 2018: 29th Annual International Solid Freeform Fabrication Symposium*, 2018.
- [49] G. Jacob, C. Brown, A. Donmez and S. Watson, "Effects of powder recycling on stainless steel powder and built material properties in metal powder bed fusion processes," 2017.
- [50] "Arcam AB (General Electric)," [Online]. Available: <https://www.ge.com/additive/who-we-are/about-arcam>. [Accessed 13 4 2020].
- [51] R. Lancaster, G. Davies, H. Illsley, S. Jeffs and G. Baxter, "Structural Integrity of an Electron Beam Melted Titanium Alloy," *Materials — Open Access Journal*, 2016.
- [52] G. Casalino, S. Campanelli, N. Contuzzi and L. A., "Experimental investigation and statistical optimisation of the selective laser melting process of a maraging steel," *Optics & Laser Technology*, vol. 65, pp. 151 - 158, 2015.
- [53] D. Apparao and M. Jagannadha-Raju, Experimental investigation on hardness, microstructure and surface roughness of Maraging steel parts produced by DMLS technique, 2018.

- [54] "Roughness parameters," Rubert & Co, [Online]. Available: rubert.co.uk/faqs/roughness-parameters/.
- [55] G. Meneghetti, D. Rigon, D. Cozzi, W. Waldhauser and M. Dabalà, "Influence of build orientation on static and axial fatigue properties of maraging steel specimens produced by additive manufacturing," in *3rd International Symposium on Fatigue Design and Material Defects*, Lecco, Italy, 2017.
- [56] C. Tan, K. Zhou, X. Tong, Y. Huang, J. Li, M. Wenyong, F. Li and T. Kuang, "Microstructure and Mechanical Properties of 18Ni-300 Maraging Steel Fabricated by Selective Laser Melting," in *ICADME 6th*, 2016.
- [57] D. Croccolo, M. DeAgostinis, S. Fini, G. Olmi, S. Ciric'-Kostic' and A. Vranic', "Influence of the build orientation on the fatigue strength of EOS maraging steel produced by additive metal machine," 2015.
- [58] Y. Bai, Y. Yang, D. Wang and Z. M., "Influence mechanism of parameters process and mechanical properties evolution mechanism of maraging steel 300 by selective laser melting," *Materials Science & Engineering*, vol. A, 2017.
- [59] D. Croccolo, M. DeAgostinis, S. Fini, G. Olmi, F. Robusto, S. Kostic', A. Vranic' and B. N., "Fatigue Response of As-Built DMLS Maraging Steel and Effects of Aging, Machining, and Peening Treatments," 2018.
- [60] A. I. T. M. I. Company, "ASM Handbook Vol. 4 Heat Treating," 1991, pp. 528-548.
- [61] J. Mutua, S. Nakata, T. Onda and C. Z., "Optimization of selective laser melting parameters and influence of post heat treatment on microstructure and mechanical properties of maraging steel," *Materials & Design*, 2017.
- [62] M. Nozar, I. Zetková and O. Hronek, "Searching for favourable power bed fusion settings in sintering of Maraging steel MS1," *29th DAAAM International Symposium*, pp. 777-785, 2018.
- [63] K. Kempen, E. Yasa, L. Thijs, J. Kruth and V.-H. J., "Microstructure and mechanical properties of Selective Laser Melted 18Ni-300 steel," *Physics Procedia*, vol. 12, no. 255–263, 2011.
- [64] "Standard Test Methods for Tension Testing of Metallic Materials - E8," ASTM International.
- [65] Treatstock, "EOS INT M280," [Online]. Available: treatstock.com/machines/item/220-eosint-m-280.

- [66] E. Gmbh, "EOS INT M280 technical data brochure".
- [67] L. J. Schmit, "Recent Advances in Matrix Methods of Structural Analysis and Design," in *Structural synthesis 1959–1969: A decade of progress*, 1971, p. 565–634.
- [68] M. Bendsøe and N. Kikuchi, "Generating optimal topologies in structural design using a homogenization method," in *Computer Methods in Applied Mechanics and Engineering*, 1988, pp. 197-224.
- [69] A. Sciacovelli, F. Gagliardi and V. Verda, "Maximization of performance of a PCM latent heat storage system with innovative fins," in *Applied Energy*, 2015, pp. 137, 707–715.
- [70] A. Arvay, J. French, J.-C. Wang, X.-H. Peng and A.-M. Kannan, "Nature inspired flow field designs for proton exchange membrane fuel cell," *International Journal of Hydrogen Energy*, pp. 38(9), 3717–3726, 2013.
- [71] M. Bendsøe and O. Sigmund, *Topology Optimization: Theory, Methods, and Applications*, Springer, 2004.
- [72] N. Olhoff and A. Eschenauer, "Topology optimization of continuum structures: A review," 2001.
- [73] A. Olason and D. Tidman, "Methodology for topology and shape optimization in the design process," 2010.
- [74] N. Rozvany, "Aims, scope, methods, history and unified terminology of computer-aided topology optimization in structural mechanics," *Structural Multidisciplinary Optimization* 21, pp. 90-108, 2000.
- [75] G. Rozvany and T. Birker, "On singular topologies in exact layout," *Structural Multidisciplinary Optimization* 8, p. 228–235, 1994.
- [76] M. Bendsøe and O. Sigmund, "Material interpolation schemes in topology optimization," *Archive of Applied Mechanics* 69, p. 635–654, 1999.
- [77] S. Amstutz, "Connections between topological sensitivity analysis and material interpolation schemes in topology optimization," *Structural Multidisciplinary Optimization* 43, p. 755–765, 2011.
- [78] D. Yang, H. Liu, W. Zhang and L. Shi, "Stress-constrained topology optimization based on maximum stress measures," 2018.

- [79] J. T. Pereira, E. A. Fancello and S. Barcellos C., "Topology optimization of continuum structures with material failure constraints," *Structural Multidisciplinary Optimization* 26, pp. 50-66, 2004.
- [80] E. Holmberg, B. Torstenfelt and A. Klarbring, "Stress constrained topology optimization," 2013.
- [81] C. Le, J. B. T. Norato, C. Ha and D. Tortorelli, "Stress-based topology optimization for continua," *Structural Multidisciplinary Optimization* 41, pp. 605-620, 2010.
- [82] I. Ferguson, M. Frecker, T. Simpson and C. Dickman, "Topology optimization software for additive manufacturing: A review of current capabilities and a real-world example," in *ASME International Design Engineering Technical Conferences and Computers and Information in Engineering Conference*, 2016.
- [83] Simulation, Netfabb Local - User manual 18.3, Autodesk, 2018.
- [84] Hyperworks, Optistruct userguide 2019.1, Altair Engineering, 2019.
- [85] Ansys, User's Guide 12.0.
- [86] "NASTRAN," MSC Software, [Online]. Available: www.mscsoftware.com/product/msc-nastran.
- [87] 3. - D. Systemes, "Abaqus FEA," [Online]. Available: <https://www.3ds.com/products-services/simulia/products/abaqus/>.
- [88] V. Shobeiri, "Structural Topology Optimization Based on the Smoothed Finite Element Method," *LAISS*, 2016.
- [89] C. Obbink-Huizer, "<https://info.simuleon.com/blog/units-in-abaqus>," [Online].
- [90] Dassault Systemes - Simulia, Abaqus/CAE User's Guide 6.13.
- [91] R. Budynas and K. Nisbett, in *Shigley's Mechanical Engineering Design*, 2014, pp. Paragraph 6-15.
- [92] Y. Saadlaouia, J. Milanb, J. Rossib and P. Chabrand, "Topology optimization and additive manufacturing: Comparison of conception methods using industrial codes," 2017.
- [93] Dassault Systemes - Simulia: Tosca structure guide, 2014.
- [94] EOS, AlSi10Mg material datasheet.
- [95] K. Wong and A. Hernandez, "A Review od Additive Manufacturing," 2012.

- [96] D. Santos-Gonzalez and A. Gonzalez-Alvarez, "ADDITIVE MANUFACTURING FEASIBILITY STUDY & TECHNOLOGY DEMONSTRATION," European Defence Agency, 2018.
- [97] A. Salmi, Additive manufacturing - lectures, 2018.
- [98] D. Schramm, M. Hiller and R. Bardini, Vehicle Dynamics: Modeling and Simulation, Springer, 2018.